N 70 16657
NASA CR 102[illegible]

LAMONT-DOHERTY GEOLOGICAL OBSERVATORY
of Columbia University
Palisades, New York

QUARTERLY PROGRESS REPORT NO. 1

Reporting Period July-Sept. 1969

CASE FILE
COPY

Work performed under NAS 9-6037

Development of a Lunar Heat Flow Experiment
for ALSEP

Marcus G. Langseth, Jr.
Principal Investigator

NASA CR 102080

LAMONT-DOHERTY GEOLOGICAL OBSERVATORY
of Columbia University
Palisades, New York

QUARTERLY PROGRESS REPORT No. 1

Reporting Period July-Sept. 1969

Work performed under NAS 9-6037

Development of a lunar Heat Flow Experiment
for ALSEP

Marcus G. Langseth, Jr.
Principal Investigator

QUARTERLY PROGRESS REPORT JULY-SEPTEMBER 1969

ON CONTRACT NAS 9-6037

Development of a Lunar Heat Flow Experiment for ALSEP

Summary: During the report period the main effort at Lamont-Doherty Geological Observatory has been to complete preparations for real time data reduction at MSC. Two documents have been submitted to MSC: 1) describing the reduction of ALSEP data in terms of temperatures and temperature differences as a function of time, 2) describing the reduction and interpretation of the conductivity data in real time at MSC.

We have continued theoretical investigations of possible disturbances of the steady-state thermal field in the lunar surface layer where the experiment is to be set up. There are three main areas of investigation:

1) the decay from initial conditions:

2) the downward propagation of surface disturbances such as the temperature cycle of a lunation and changes in average temperature and thermal properties at the surface when the experiment is set up;

3) the effect of the fiber glass casing on the downward propagation of transient surface effects.

Under subcontracts, scientists at ADL are continuing on two important programs:

1) the extended testing of the conductivity experiments of the HFE;

2) mathematical modeling of the thermal conductivity experiment.

Lastly, we have continued to monitor the development of flight hardware for the ALSD and to study the most recent results from the Apollo 11 mission in view of the problems of drilling the lunar soil and conducting heat-flow measurements.

Data Reduction Procedures:

Real time data reduction of temperature and temperature difference measurements:

Formulation of real time data requirements for the ALSEP HFE were completed during this period. A data reduction procedure was developed, tested and submitted to the Manned Spacecraft Center for implementation. The analysis programs developed at MSC are currently being tested by the Experiments Office using data supplied by the Lamont-Doherty Geological Observatory.

The document, "Real Time Data Requirements for the ALSEP Lunar Heat Flow Experiment," L-DGO Technical Report #2-1969, is appended to this report, The method of data reduction proposed in this document differs somewhat from that used earlier by ADL and Bendix in test data reduction.

To speed the reduction process, temperature and temperature difference are calculated using third and fourth order 2-dimensional polynomial functions with the total resistance of the bridge and the voltage ratio as independent variables. The technique has been thoroughly tested at L-DGO.

Real Time Interpretation of the Lunar Conductivity Experiments:

Conductivity experiments at eight locations on the heat flow probes will be run during the first 45-day real time observation period on the moon. Initially, the heat flow team planned to reduce the data of these experiments and interpret the results in terms of conductivity of the lunar soil using a computer facility outside of MSC. However, it is now clear that the interpretation of the results of these experiments is essential to the efficient execution of the experiments, particularly to the commanding sequence. Thus it was decided that the conductivity experiments would be reduced and inter-

preted in real time using the MSC computing facility.

During August we developed a preliminary procedure for the real time data reduction of the conductivity experiments and delivered this procedure as a supplement to our "Real Time Data Requirements for the ALSEP Lunar Heat Flow Experiment." This supplement is appended to this report.

The suggested reduction procedure consists of two parts:

Part one is analysis of the time variations of the temperature difference at the sensor location where the experiment is to be run. This analysis is aimed at predicting the time variations during the period when the heater is turned on and will be based on data from the first 100 hours of lunar operation. Data sampled at one hour intervals at each bridge will be least square fitted to theoretical expressions describing the decay from initial conditions and accounting for the lunation cycle temperature variations in the soil.

However, subsequent to submittal of the above document, further investigation of the problem of transient temperature variation during the conductivity measurements reveals that at least 500 hours of data are required to reliably predict temperature variations. The need for this additional observation time results from the periodic nature of the variations. The period of the lunation cycle is about 700 hours and at least one-half period of observation is required to establish the amplitude and phase of the variation at the depth of interest.

In the 45-day real time data analysis period there are approximately 1080 hours of data acquisition time available. In Table 1 we show how this time might be divided between trend analysis and conductivity measurement so as to complete the measurements in that time frame.

Further Investigations:

Within the next month, October 1969, we will provide NASA with a revised procedure for interpreting the conductivity experiment data.

Computer modeling of the heat flow experiment continues at ADL and the results of this study will be used to provide coefficients for functions described in the supplemental document. These coefficients will be provided on about January 1970.

TABLE 1: Estimates of the times required for HFE conductivity measurement as a function of lunar soil conductivity.

Soil Conductivity Range watts/cm°C	Mode	Time/Experiment Hours	Time for Trend Analysis Hours
5×10^{-6}-5×10^{-5}	2	58	500 [1]
5×10^{-5}-5×10^{-4}	2/3	42	660 †
5×10^{-4}-5×10^{-3}	3	34	740 [2]

† This the most likely range of lunar soil conductivity exclusive of isolated blocks of dense rock.

[1] In the low conductivity range the principal transient disturbance is due to the very slow cool down from transient conditions.

[2] In the high conductivity range the principal transient disturbances result from downward propagation of the lunation temperature cycle.

Theoretical Investigations of Transient and Steady-State Heat Flow in the Lunar Soil Layer:

These investigations were principally aimed at determining the magnitude of certain transient disturbances seen by the heat flow probes in the lunar soil as a function of depth and time. Functions describing these anticipated effects were derived for use in the transient analysis just described. A large part of this work was carried out by Stephen Keihm, a

graduate student, working on the program during the summer.

1. The rate of change of temperature as a function of depth due to downward propagation of a lunation cycle.

The objective of this calculation is to determine the rate of change of temperature with time in °C/hour at various depths below the lunar surface. These results give the order of change anticipated for trend analysis calculations.

For simplicity it is assumed that the lunar soil is homogeneous and isotropic. Of course this may not be the actual case. More than likely the soil layer has a conductivity that increases rapidly with depth in the upper several centimeters and is more uniform at depth. However, this situation causes an even greater attenuation of the surface variations than a homogeneous medium with a conductivity of that at depth. The results presented in Figure 1 give the maximum gradients expected from the downward propagation of the lunation cycle into the lunar soil whose average conductivity is K.

Rates of change of temperature of 10^{-4} °C/hours must be accounted for in the reduction of the conductivity experiment. It is clear that at depths below 200 cm (the normal depth of the uppermost heater location) the effect is not appreciable unless the conductivity is greater than 8×10^{-4} watt/cm °C. This value is somewhat higher than that usually measured in evacuated powders.

2. The downward propagation of a surface change in temperature or surface thermal properties caused during emplacement of the experiment.

It has long been realized that the activity of the astronaut around the heat flow borehole can result in a change in the average temperature

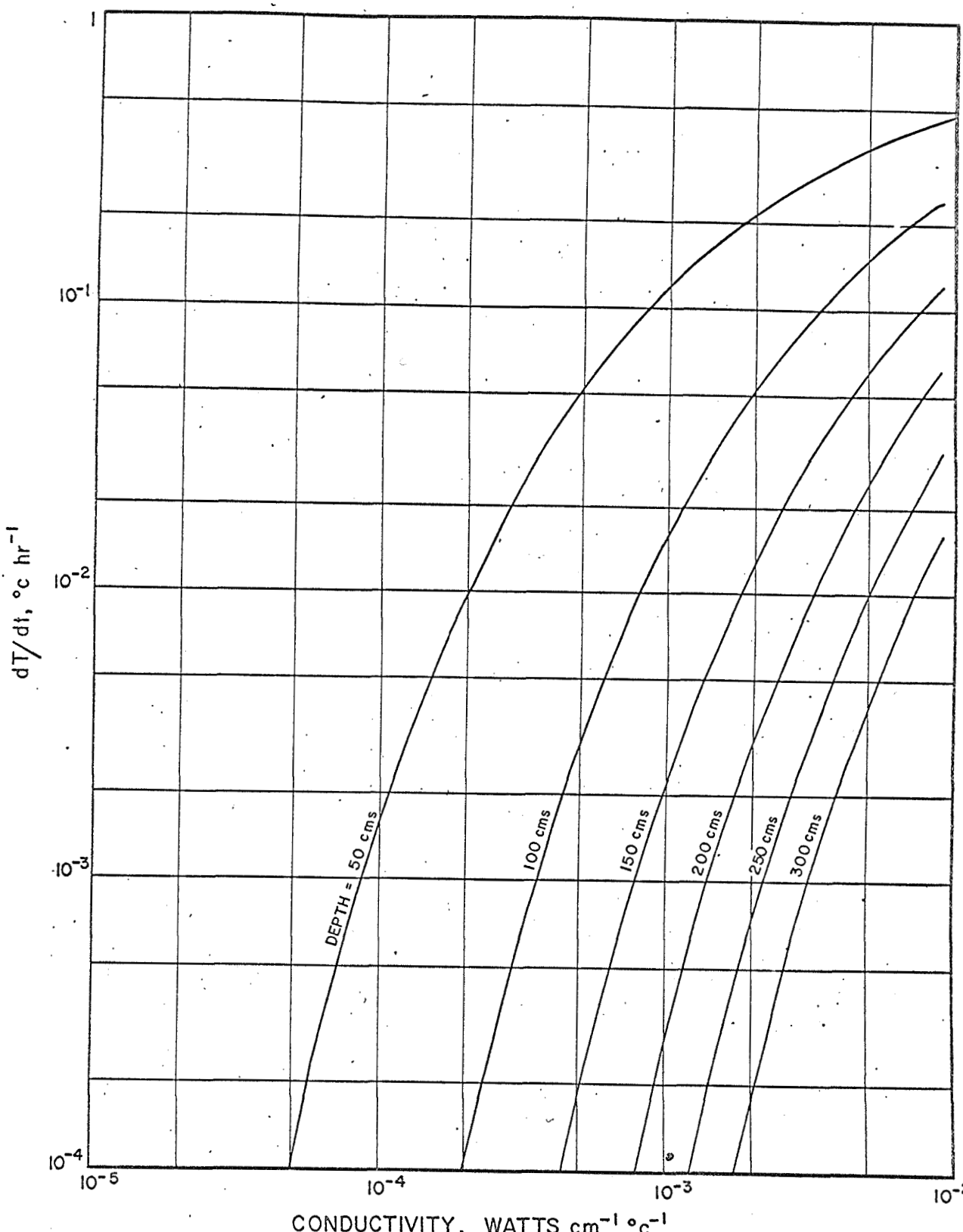

FIGURE 1: The maximum rate of temperature change at six depths below a plane surface is plotted as a function of conductivity.

The temperature of the surface varies periodically with an angular frequency of 9.04×10^{-3} hr^{-1} and a peak to peak amplitude of 200° C. For the semi-infinite solid $\rho c = 1.34$ watts $°C^{-1}$ cm^{-3}.

of the area where he had made footprints or in the thermal properties of the surface layer. These changes would ultimately cause a disturbance in heat flow at depth, (these effects were reviewed in the ADL study report, Design Definition of the Heat Flow Probe). However the disturbance takes a finite time, dependent on the diffusivity, to propagate to a given depth and can therefore induce a rise or fall of temperature with time which should be accounted for in the conductivity analysis. Again changes greater than 10^{-4} °C/hr are of interest.

The results of Lachenbruch* are used. The results given in Figure 2 apply to a point 200 cm below the surface. It is assumed that a circular area 200 cm in radius (or 136 sq. ft.) has had a change in average surface temperature B in °C above the surface temperature of the surrounding undisturbed area. Note: The area of 136 sq. ft. is considerably larger than the astronaut would be expected to disturb; however, the effect at a given depth is roughly proportional to the surface area disturbed. The results are shown as the ratio of the temperature disturbance T(+) and B. For example in Figure 2 for a conductivity of $K = 3 \times 10^{-4}$, the density $\rho = 1.6$ and heat capacity C = 0.8 watts/gm°C, the temperature at a point 200 cm below the surface has risen 0.1% of the change in surface temperature 2200 hrs. (2½ months) after the probe is emplaced. For a conductivity of 3×10^{-4}, such an effect would not be important to the conductivity measurement. However, it would be if the conductivity is as high as 6×10^{-4}.

This effect will be further examined in terms of the temperature difference over each probe section and for different areas.

3. Decay of the temperature distribution caused by emplacement of the heat flow probe and hole casing.

*Three-dimensional Heat Conduction in Permafrost Beneath Heated Buildings - A. H. Lachenbruch. Geological Survey Bulletin, 1052-B, 1957.

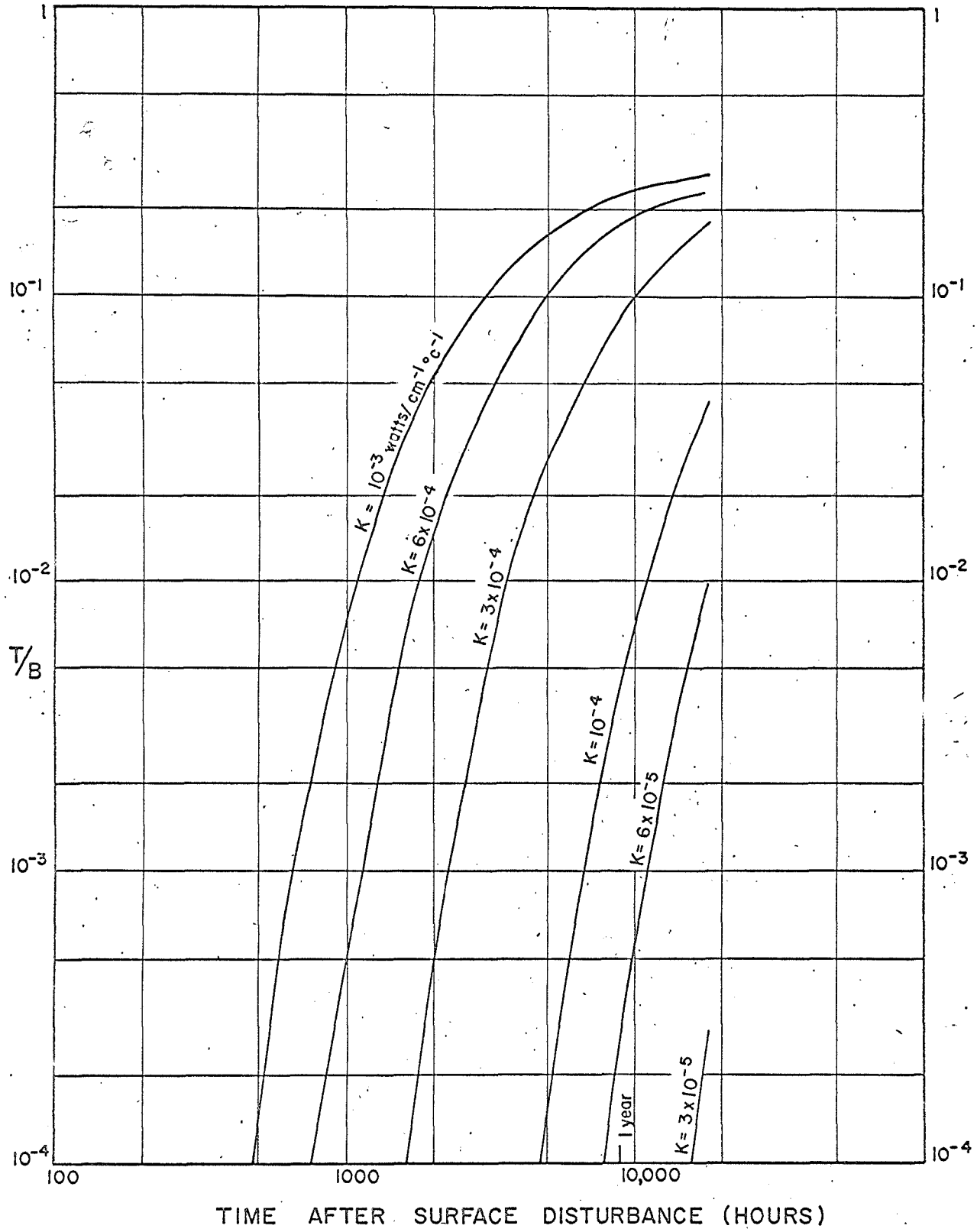

FIGURE 2: The temperature as a function of time at a depth of 200 cm resulting from a sudden change in surface temperature by an amount B inside a circular region 400 cm in diameter. The temperature is given as a fraction of B. ρc = 1.34 watts $°C^{-1}$ cm^{-3}.

A preliminary analysis has been completed of the transients associated with the temperature decay of the heat flow probe and the borehole casing in possible lunar materials. Primarily the results of Blackwell* were used. Two types of models were examined:

1. The probe and borehole casing were modeled as an infinite cylinder which is perfectly conducting in an infinite medium. The cylinder is assumed to have initial uniform temperatures to above that of the surrounding medium.

2. The model was the same as the first except the probe has a finite conductivity.

Since the length of the borehole casing is nearly 100 times the diameter, modeling the casing as an infinite cylinder will produce useful results.

As the transients of interest will be observed beyond 100 hours after probe emplacement, the long-term solutions should suffice.

For Model (1)

$$T(t)/T_o \doteq \frac{1}{2\alpha\tau} - \frac{1}{4\alpha^2\tau^2}\left[\alpha + (\alpha - 2)\left(\ln \frac{4\tau}{1.7811} - 1\right)\right] \quad (1)$$

τ and α are two important and useful parameters.

τ is a dimensionless time equal to $Kt/\rho ca^2$.

K, ρ and c are the conductivity, density and heat capacity of the medium outside the cylinder, t is time in seconds, and a is the radius of the cylinder in centimeters. α is the ratio of the thermal mass of the lunar medium to that of the probe, and is equal to $\rho c/\rho' c'$ where ρ' and c' are the density and heat capacity of the cylinder representing the probe.

*Blackwell, Journal of Applied Physics, 1954.

For Model (2):

$$T(t)/T_o = \frac{1}{2\alpha\tau} - \frac{1}{2\alpha^2\tau^2} + \ln\left(\frac{4\tau}{c}\right)\left\{\frac{1}{2\alpha^2\tau^2} - \frac{1}{4\alpha\tau^2}\right\} + \frac{K_2}{\alpha^2\tau^2 K_1}\left\{3/8 - \tfrac{1}{4}\left(\frac{r}{a}\right)^2\right\} \text{ for } r < a. \quad (2)$$

The ratio K_2/K_1 is the ratio of conductivities of the lunar medium to the probe, and the remaining variables have the definitions given for Model (1).

The borehole casing with the probe inside is, of course, not a solid cylinder to which these solutions apply. The casing is thin walled (0.060") and the thermal mass of the probe varies greatly along its length. The best value for α appears to be about 60.

In Figure 3 the ratio T/T_o is plotted as a function of τ and α as a parameter. The long term solutions are quite valid for $\tau = 6$ and greater. For lunar type soils we anticipate that $K \cong 2 \times 10^{-4}$ watt cm^{-1} $°C^{-1}$, $\rho c = 1.6 \times 0.84 = 1.28$ watt-sec cm^{-3} $°C^{-1}$, and $a \cong 1$ cm. Since $t = \frac{\tau \rho c a^2}{K}$; $t = 6.4 \times 10^3\ \tau$ in seconds. Thus the solutions become valid for times greater than 3.84×10^4 seconds or a little over 100 hours.

The form of the expressions in equations (1) and (2) will be used in the real time trend analysis to fit the decay from initial conditions. The values of the coefficients will give us our first indication of the conductivity of the lunar material.

In the next few months we plan to improve this theoretical work by using the detailed model developed at ADL under Subcontract #8 to investigate the decay from intial conditions. This work will probably be done by MIT under the auspices of M. G. Simmons.

Report on Work Being Done Under the Subcontracts:

Subcontract #6 - This subcontract with Arthur D. Little, Inc. (ADL) covered the development and fabrication of prototype models of the boron

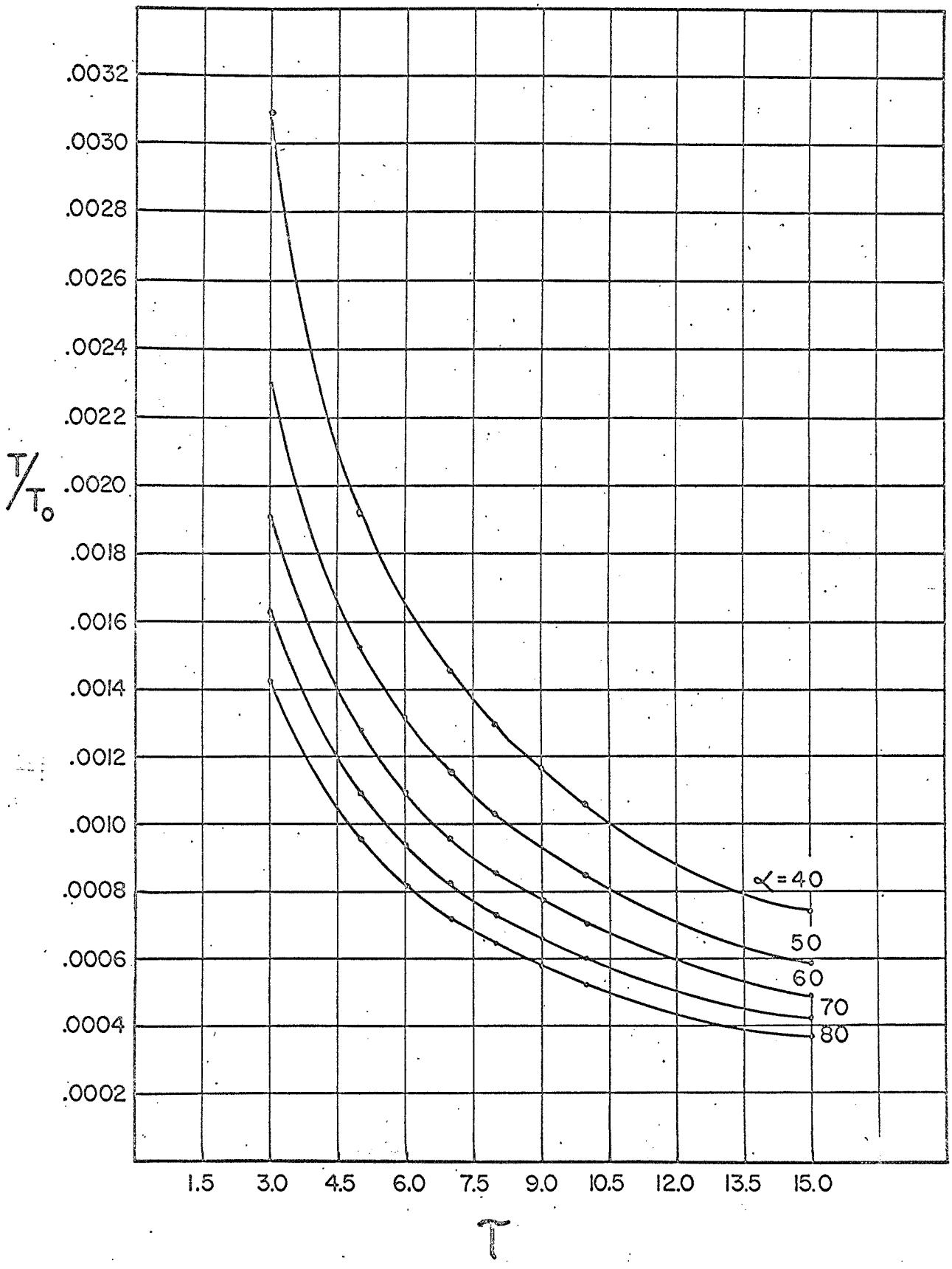

FIGURE 3: Decay of temperature in an infinite cylinder which had a uniform initial temperature of T_o. The cylinder is embedded in an infinite isotropic homogeneous medium of conductivity K. $\tau = Kt/\rho ca^2$ (see text for definition of terms).

reinforced epoxy drill stem. Although these items were delivered to the Martin Marietta Company in May and early June, there remained, as part of the subcontract, measurements of the thermal conductance of a piece of the drill stem. These measurements were completed in July and are reported on in the ADL report attached as Appendix A.

A final report on the development of the boron reinforced drill stem is nearing completion and it will contain more information relative to these measurements.

Subcontract #7 - This subcontract covers the additional experiments on the HFE conductivity experiments. As of this date all of the prescribed tests have been completed and the data is being analyzed. A recent progress report for August 25 on this subcontract is attached as Appendix B.

Several developments during the past month are of concern. 1) Tests have been run both in Mode 2 and Mode 3 with the bead tank at 43 μ of N_2 gaseous pressure. These measurements were made to compare the results of the modes at the same conductivity. However, the absolute value of the conductivity at this pressure is unknown except from extrapolation and interpolation of data at the other gas pressures. It is well-known that the conductivity is <u>not</u> a linear function of gas pressure in this region of pressures, therefore it would be of great value to make independent absolute measurements of the conductivity with the 43 μ pressure.

I have discussed with the thermophysics group at Marshall Space Flight Center in Huntsville, Alabama, the possibility of using their facility to make these measurements. This group, headed by Mr. Billy P. Jones, has done considerable work on the measurement of the conductivity of evacuated powders. During a recent visit we agreed on a plan and procedure for

carrying out conductivity tests at Huntsville. A sample of the glass beads used in the K apparatus at ADL have already been sent for these measurements.

2) Recent measurements in the conductivity test tanks at ADL give strong evidence that there is a gradient in conductivity from the top to the bottom of the tank. Our preliminary analysis suggests that this gradient results from improvement of thermal contacts and a slight decrease in porosity as a result of increased loading with depth in the tank. It would be important to determine the existence and value of such a gradient in the tanks. Therefore we have suggested to Huntsville that their measurement might also include measurements of conductivity as a function of static loads up to 7 psi. Alternately, direct measurements of conductivity as a function of depth in the tank can be attempted. These possibilities will be more fully examined in the next few months.

The period of performance of this contract has been extended through November 28, 1969. Additional funds of $2,709 have been granted for the added tests under revision H of the test procedures.

Lastly, the disposition of the test apparatus at ADL must be decided. The Principal Investigator recently sent a letter to NASA Headquarters proposing that the calibration apparatus be maintained in an operating condition on a year-to-year basis by means of a contract directly from NASA Headquarters. This would allow this facility to be used in the future development of thermal experiments for the lunar mission. The accuracy and stability of this equipment would be very difficult to duplicate on short notice.

Subcontract #8 - This subcontract with ADL is for the development of

a detailed math-model of the heat flow probes in the lunar medium. This work had proceeded to the point that the models of the probe and the lunar medium are complete. Numerous test runs have been made in a simulation of the probes in isothermal conditions which validate the accuracy of the model. Two progress reports, numbers 1 and 2, are attached to this report as Appendix C.

During September we decided to extend the scope of this subcontract to have ADL make computer runs using these models for establishing the inversion functions to be used in the real time data analysis at MSC. We have asked ADL to propose on this additional work and their proposal is now under review. As part of this proposal the performance period of this subcontract would be extended through February 1970.

At L-DGO we are continuing to monitor with interest and advise where possible the final fabrication, testing and training with the ALSD modified to use the fiber glass drill stem. This work has included attending design reviews and testing. Active support of the astronaut training sessions and briefings. This work is largely being carried forward by Richard Perry.

Programmatical Changes:

In April 1969 Dr. John Chute, a recent Ph. D. recipient from Columbia University, joined the program. His principal duties have been in the area of HFE data reduction and certain theoretical studies to interpret the data.

During the summer months Steven Keihm, a graduate of the Columbia Engineering School and a scholarship graduate student at Stanford, worked on theoretical problems associated with interpreting HFE data. He terminated his work here September 4 to continue school.

Miss Susan Kaghan was added to the staff during the summer months on an hourly basis to assist in drafting and data processing work associated with the HFE.

Kevin McDermott, project engineer, left the program August 15, 1969. There are no plans to hire a replacement engineer.

Co-Investigator Efforts:

Proposals have been received from both Sydney P. Clark at Yale and Gene Simmons at MIT to extend their efforts in parallel on the Lunar Heat Flow Experiment Program through December 1970. Professor Clark's proposal was submitted to MSC for consideration and Professor Simmons' proposal was forwarded on October 8.

It is our hope that these proposals will be funded in the near future.

REAL TIME DATA REQUIREMENTS FOR THE ALSEP LUNAR HEAT FLOW EXPERIMENT

-o-

Marcus G. Langseth, Jr.
Principal Investigator

May 1969

-o-

Lamont-Doherty Geological Observatory
of Columbia University
Palisades, New York

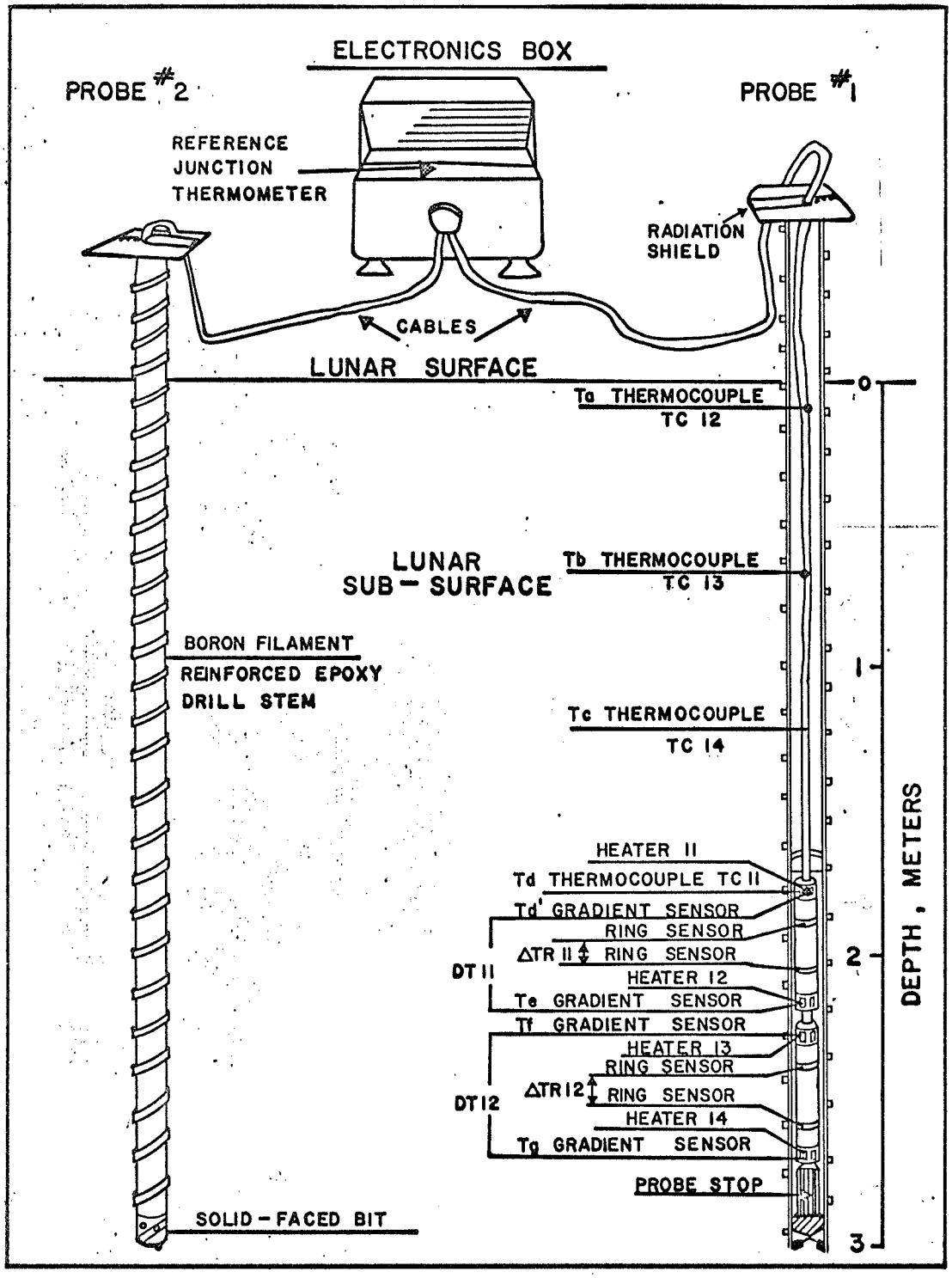

SCHEMATIC DRAWING OF THE ALSEP LUNAR HEAT FLOW EXPERIMENT

REAL TIME DATA REQUIREMENTS FOR THE ALSEP LUNAR HEAT FLOW EXPERIMENT

Scope:

This document defines the Principal Investigator's requirements for data acquisition and reduction in real time at the Manned Spacecraft Center in Houston, Texas.

This document supersedes two preliminary documents submitted by the Principal Investigator on March 25, 1969 and March 22, 1967.

Requirements:

Reduction of the ALSEP Lunar Heat Flow Experiment data in near real-time is required to:

1. Verify performance of the experiment after initial turn on.
2. Verify receipt of commands.
3. To monitor the initiation of the conductivity experiments to select the optimum mode of operation and to monitor the decay mode of the conductivity experiments.
4. To rapidly analyze the results of the conductivity experiment to determine the validity of the completed experiment and to determine the optimum strategy for the remainder of the tests.

Command and Performance Verification:

Requirements 1 and 2 can be met by presentation on a high-speed printer of bridge temperatures and temperature differences, reference bridge temperatures, thermocouple temperatures and experiment ID words for one complete sequence (7.25 minutes of data). (Definitions of a complete sequence, measurement parameters and other information pertinent to the interpretation

of data from the HFE are given in the Appendix attached to this document.) The above measurements are correlated with the time of receipt of the first ALSEP word of the eight required to calculate one parameter. For optimum operation a full 7.25 minutes of data, which is stored in buffer, would be printed out on command from the flight director. At every 90th frame mark (∿54 seconds), two of the parameters are up-dated; this represents the minimum time between print-outs.

Monitoring Conductivity Experiments:

Requirement three necessitates display of the heat flow measurement parameters for a longer period. Before initiating a conductivity experiment, the temperature and temperature difference at the bridge to be used for the experiment will be sampled at regular intervals to determine the rate of change of these parameters. Each conductivity experiment is always initiated in Mode 2. After an observation period of approximately one hour, a decision is made based on the rate of rise of temperature whether to stay in Mode 2 or switch to Mode 3. An additional one hour of data is required after the switch to Mode 3 to assure proper operation in Mode 3.

Decay Mode Operation:

After completion of a conductivity experiment in Mode 3, much additional information can be gained about the thermal properties of the surrounding lunar medium by observing the temperature decay at other sensors near to the heater. This can be accomplished by periodically sampling the appropriate bridges either in Mode 1 or Mode 3, with the heater off. This operation will require constant monitoring of the data during a 12-hour period.

A practical display for both the initiation of the conductivity experiment and monitoring the decay mode would be a print-out of all data after

the completion of two complete sequences (14.5 minutes).

Preliminary Analysis of the Conductivity Experiments:

The heat-flow experiment has eight independent conductivity experiments each of which can be operated in two modes. These experiments will be run during the first 45 days that the ALSEP is on the lunar surface. During this period the bore holes and probes will be equilibrating to the lunar subsurface temperatures. The conductivity experiments, which also disturb subsurface temperature, would least effect the subsequent gradient measurements if run during this period. It is strongly recommended that a second series of conductivity experiments be run after a ten-month observation period if sufficient gradient measurements have been obtained by that time.

The eight experiments will be run consecutively. The duration of each experiment depends on the conductivity of the lunar subsurface and in which mode the experiment is run.

From laboratory experiments we know that the Mode 2 operation will take anywhere from 24 to 72 hours and the Mode 3 experiments require from 10 to 20 hours. A typical schedule of conductivity tests showing the required switching of heater states and modes is shown in Figure 1 in the Appendix.

To most effectively utilize the conductivity experiments in an unknown medium it is essential that the data from the experiment (temperature versus time) be analyzed rapidly. The maximum "turn-around" time for this data analysis should be about 24 hours. This reduction would include trend analysis of temperatures prior to initiation of the experiment, accurate determination of the slope (dT/dt) at long times, and theoretical extrapolation

of temperature histories to equilibrium.

Our recommendation is that the above analysis be carried out by the principal investigator using a computer facility outside of Mission Control. To obtain the 24-hour turn around it is essential that the data for the HFE be in a form (card or tape) that is compatible with other computers such as punch card or magnetic. Proposed card formats are outlined in the format section.

In addition it is desirable to have a systematic print-out of all heat flow data in two-hour blocks (16 complete sequences). This data would be grouped by parameter. A print-out format is suggested in the format section that follows.

Data Formats:

Format A: This format is for printing out data in two-hour time blocks. The 16 cycles of data are grouped by parameter. Each parameter group is printed on a single sheet. Five sheets are required to print out the two-hour data block.

Sheet #	Grouped Parameter
1	Temperature difference high sensitivity.
2	Temperature difference low sensitivity.
3	Absolute temperature of gradient bridges.
4	Thermocouple temperatures and reference bridge temperatures.
5	Housekeeping data.

Housekeeping Data:

The ALSEP samples the housekeeping data far more frequently than is

required for our needs; therefore, we recommend printing and storing housekeeping data every 8th 90-frame mark. We see no need for housekeeping data being displayed on TV monitors.

Format A:

Data print-out in two-hour blocks, separate parameters are grouped on a page. (Mode 1 and Mode 2.)

Page 1

ALSEP NO._ _ SER. NO. _ _ REDUCTION DATE _ _ MODE_ _ HEATER _ _

Temperature difference high sensitivity

Time	DTH 11	DTH 12	DTH 21	DTH 22
t_1	1	2	3	4
:	:	:	:	:
t_{16}	1	2	3	4

Page 2

Temperature difference low sensitivity

Time	DTL 11	DTL 12	DTL 21	DTL 22
t_1	5	6	7	8
:	:	:	:	:
t_{16}	5	6	7	8

Page 3

Absolute Temperature Gradient Bridge

Time	T 11	T 12	T 21	T 22
t_1	9	10	11	12
:	:	:	:	:
t_{16}	9	10	11	12

Page 4

Thermocouple Temperature

PROBE 1 REF TEMP 17 GAIN ____ OFFSET ___

Time	TC 11	TC 12	TC 13	TC 14
t_1	13	14	15	16
:	:	:	:	:
t_{16}	13	14	15	16

PROBE 2 REF. TEMP. 22 GAIN____ OFFSET ____

t_1	18	19	20	21
:	:	:	:	:
t_{16}	18	19	20	21

Page 5

Housekeeping Data Format:

Housekeeping Data

Time	+5Y	-5Y	+15Y	-15Y	Low K	High K
t_1	HF1	HF2	HF3	HF4	HF5	HF6
:	:	:	:	:	:	:
t_{16}	HF1	HF2	HF3	HF4	HF5	HF6

Notes:

1. Out of Specification data will be flagged.

Format B: This data format is intended for HFE Mode 3. In Mode 3 a complete cycle requires only 54.4 seconds. A data record consists of 16 cycles of data (32 data points) and two lines of housekeeping data at the bottom of each block. We prefer to have two records per sheet.

B. Continuous, in-line, real-time data format for Mode 3 (high conductivity).

ALSEP No.	Serial No.	Reduction Date	Mode	Heater St.
_ _ _	_ _ _	_ _ _	_ _ _	_ _ _

Time - Day Hr Min Sec	Temp. Diff °K	Abs. Temp.
t_1	DTR 13	TR 13
:	:	:
t_8	1	2

Housekeeping Data:

Time _ _ _ _ +5V _ _ -5V _ _ +15V _ _ -15V _ _ Low K _ _ High K _ _

Notes:

1. This data block comprises one record.
2. Two records per page.
3. Time t_1 refers to time of receipt of first ALSEP word of temperature difference measurement.

Flagging Data:

Heat-flow data points that have out-of-tolerance conditions should be flagged. Four types of out-of-tolerance conditions should be discriminated.

1. Out-of-tolerance housekeeping data. Place asterisk (or other distinctive mark) next to time entry.

2. Number exceeds the dynamic range of measurement. Place one asterisk

next to parameter value.

3. The calculated amplifier gain or offset is out-of-tolerance. Place two asterisks next to parameter value.

4. Sequencing error or invalid programmer state. Parameter is marked with an approporiate mark and bit or bits in error are indentified on the same line.

Card format for real time output:

Full sequence (7.25 min.), Mode 1

Column	Word	Card 1,	2,	3,	4,	5,	6
1 - 12	Time	✓	✓	✓	✓	✓	✓
13 - 14	Mode	✓	✓	✓	✓	✓	✓
15 - 16	Para ID	✓	✓	✓	✓	✓	✓
17 - 26	Para	ΔTH_{11}	ΔTH_{21}	T_{11}	T_{21}	TCR	TCR
27 - 28	Para ID	✓	✓	✓	✓	✓	✓
29 - 38	Para	ΔTH_{12}	ΔTH_{22}	T_{12}	T_{22}	TC_{11}	TC_{21}
39 - 40	Para ID	✓	✓	✓	✓	✓	✓
41 - 50	Para	ΔTL_{11}	ΔTL_{21}	HF2	HF2	TC_{12}	TC_{22}
51 - 52	Para ID	✓	✓	✓	✓	✓	✓
53 - 62	Para	ΔTL_{12}	ΔTL_{22}	HF3	HF3	TC_{13}	TC_{23}
63 - 64	Para ID	✓	✓	✓	✓	✓	✓
65 - 74	Para	HF1	HF1	HF4	HF4	TC_{14}	TC_{24}
75 - 79	Par	HF6	HF6	HF7	HF7	SPARE	SPARE
80	Card #	✓	✓	✓	✓	✓	✓

Probe 1 only, use cards 1, 3, 5.

Probe 2 only, use cards 2, 4, 6.

Mode 3 Operation

Use cards 1, 2, 3, 4.

with ring bridge data replacing gradient bridge data

Equipment Requirements for Real-Time Data Analysis at MSC:

Real time data analysis of the HFE will be of two types: 1) that done manually, 2) that done by PI utilizing computer facilities in MSC area.

Type 1 Requirements

a. A light table at least 5' x 3'.

b. A hanging chart rack for convenient filing of plotted work.

c. A six-foot x 2 foot deep shelf.

d. Access to Xerox copying machine.

e. Standard working desk with telephone.

f. Small desk calculator (PI can supply).

Type 2 Requirements

a. Access to an IBM keypunch.

b. Storage space for 20 computer tapes.

c. Storage space for 40 boxes (80,000 units) computer cards.

d. Access to a computer equivalent to IBM 1130 or 1800 series, with facility for computer plotting on hard copy (not film).

APPENDIX

Definitions:

The following parameters are determined for a full sequence (Mode 1, 2).

DTH(IJ)	I = 1, 2	J = 1, 2	Temp Diff for High sensitivity gradient bridge measurement Probe I, section J.
DTL(IJ)	I = 1, 2	J = 1, 2	Temp Diff for low sensitivity gradient bridge measurements Probe I, Section J.
T(IJ)	I = 1, 2	J = 1, 2	Average Temp of gradient bridges Probe I, Section J.
TREF			Reference bridge temperature.
TC(IJ)	I = 1, 2	J = 1, 4	Thermocouple temperature Probe 1, Thermocouple J.

The following Parameters are determined for conductivity Mode 3.

DTR(IJ)	I = 1, 2	J = 1, 2	Ring bridge temperature difference Probe I, section J.
TR(IJ)	I = 1, 2	J = 1. 2	Average temperature of ring bridges Probe I, section J.

The following Parameters are used for housekeeping.

Voltage +5 volt supply	HF1
Voltage -5 volt supply	HF2
Voltage +15 volt supply	HF3
Voltage -15 volt supply	HF4
High conductivity heater volts	HF6
Low conductivity heater volts	HF7

FLOW CHART FOR HFE DATA REDUCTION

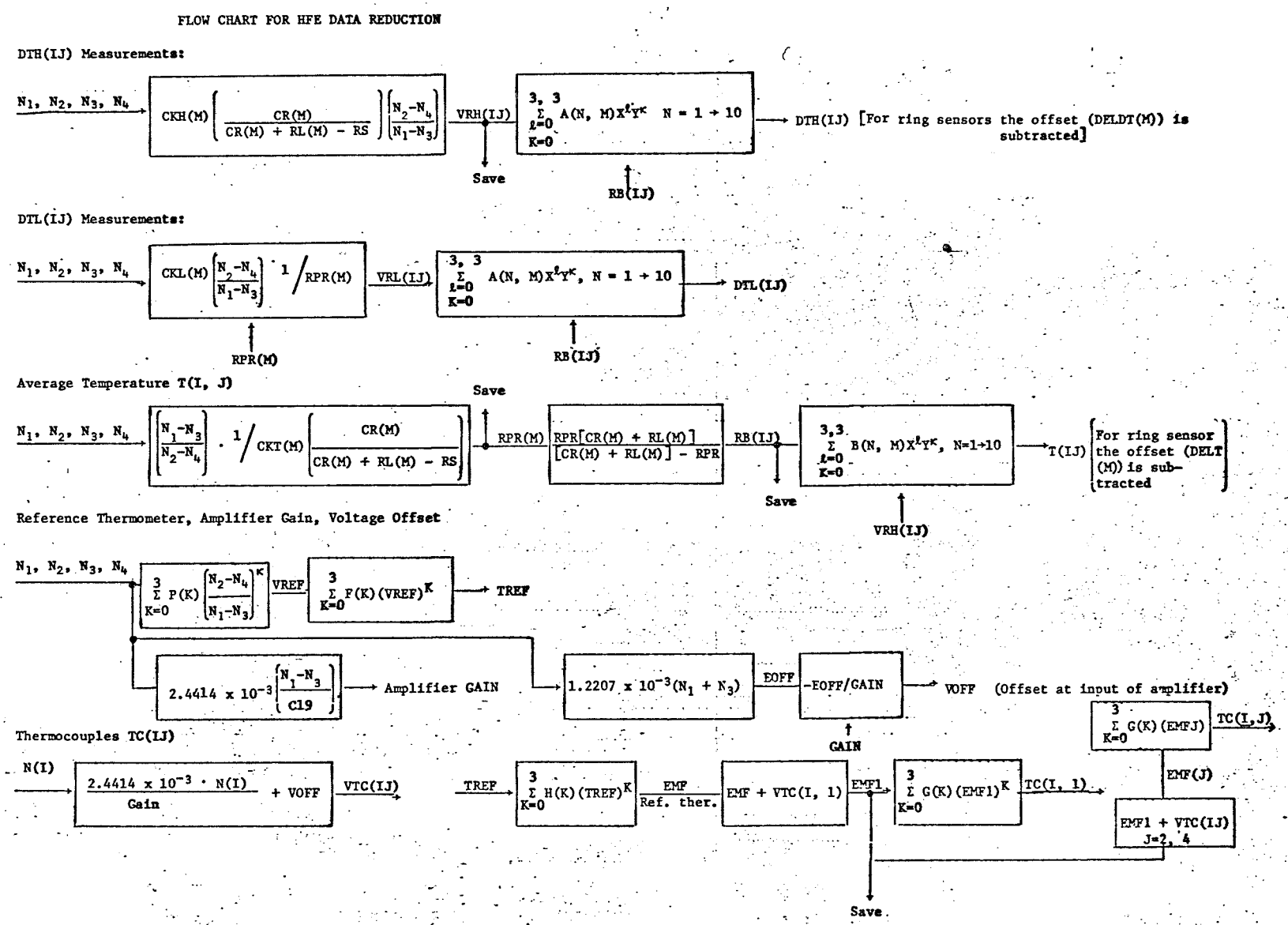

Flow chart to compute HFE parameters from heat flow words with list of variable names and symbols:

List of variable Names and Symbols:

I. Heat flow data parameters.

A. Normal sequence (Mode 1, 2).

	Parameter Name	Mnemonic
1.	High sensitivity temperature difference on Probe I, Section J	DTH(IJ)
2.	Low sensitivity temperature difference on Probe I, Section J	DTL(IJ)
3.	Average temperature Probe I, Section J	T(IJ)
4.	Voltage ratio high sensitivity, Probe I, Section J	VRH(IJ)
5.	Voltage ratio low sensitivity Probe I, Section J	VRL(IJ)
6.	Total bridge resistance Probe I, Section J	RB(IJ)
7.	Reference bridge temperature	TREF
8.	Reference bridge voltage ratio	VREF
9.	Thermocouple temperature Probe I, Thermocouple J	TC(IJ)
10.	Gain of amplifier	GAIN
11.	Voltage offset of amplifier	VOFF

B. Conductivity modes (Modes 2, 3).

1.	Heater state NN, NN = 1 → 16	HTR(NN)
2.	Ring bridge temperature difference Probe I, Section J	DTR(IJ)
3.	Average ring bridge temperature Probe I, Section J	TR(IJ)
4.	Voltage ratio, Probe I, Section J	VRR(IJ)
5.	Bridge resistance, Probe I, Section J	RBR(IJ)

Parameter Name	Mnemonic
C. Housekeeping Data	
1. Voltage +5 volt supply	HF1
2. Voltage -5 volt supply	HF2
3. Voltage +15 volt supply	HF3
4. Voltage -15 volt supply	HF4
5. High conductivity heater volts	HF6
6. Low conductivity heater volts	HF7

II. Calibration Constants

A. Sensor and bridge calibration constants*

1. Coefficients of polynomial relating DTH(IJ) and DTL(IJ) to VRH(IJ) and RBR(IJ) for bridge K. K = 2(I-1) + J (see definition of I and J above)	A(L, K)[1]
2. Coefficient of polynomial relating T(IJ) to VRH(IJ) and RBR(IJ) for bridge K. K = 2(I-1) + J	B(L, K)[1]
3. Coefficient of polynomial relating DTR(IJ) to VRR(IJ) and RBR(IJ) for bridge, K.	C(L, K)[1]
4. Coefficient of polynomial relating TR(IJ) to VRR(IJ) and RBR(IJ) for bridge K	D(L, K)[1]
5. Coefficient of polynomial relating reference bridge temperature, TREF, to voltage ratio, VREF	F(K)[(2)]
6. Coefficient of polynomial relating thermocouple temperatures to EMF's	G(K)[(3)]
7. Coefficient of polynomial relating EMF to temperature of reference thermometer TREF	H(K)[(4)]

*These are the constants derived at Lamont-Doherty Geological Observatory from calibrations at Rosemount Engineering Company.

B. Electronics Box (Gulton document: Instruction Manual).

	Parameter Name	Mnemonic
1.	Excitation voltage attenuation factor for gradient and ring bridges . . . . . M = 2(I-1) + J for gradient bridges, I, J. M = 4 + 2(I-1) + J for ring bridges.	CKH(M)
2.	Series resistor for DTL(IJ) measurement. Where M has the same meaning as above	CKL(M)
3.	Attenuation factor for absolute temperature measurement accounting for series resistor for current measurement. M has the same meaning as above . .	CKT(M)
4.	Attenuation resistors, M has the same meaning as above	CR(M)
5.	Simulator lead resistance	RS
6.	Effective resistance of bridge as seen at amplifier input	RPR(M)
7.	Coefficient of polynomial of computing VREF . . .	P(K)(5)
8.	Factor for converting excitation voltage of reference bridge to amplifier gain	C19

C. Probe calibration factors

1.	Excitation voltage lead resistance M = 2(I-1) + J for gradient bridge in Probe 1 and Section J . . . M = 4 + 2(I-1) + J for ring bridge in Probe I Section J.	RL(M)
2.	Ring bridge temperature offset M = 2(I-1) + J	DELT(M)
3.	Ring bridge temperature difference offset, M = 2(I-1) + J	DELDT(M)

Equations:

1. $DTH(IJ) = A(1, K)\, X^3\, Y^o + A(2, K)\, X^2\, Y^o + A(3, K)\, X^2\, Y^1$

$+A(4, K)\, X^1\, Y^o + A(5, K)\, X^1\, Y^1 + A(6, K)\, X^1\, Y^2 + A(7, K)$

$+A(8, K)\, X^0\, Y^1 + A(9, K)\, X^o\, Y^2 + A(10, K)\, X^o\, Y^3$

$X = RB(IJ) \qquad Y = RB(IJ) \times VRH(IJ)$

Equations (Cont.)

2. $TREF = F(0) + F(1)\ VREF + F(2)(VREF)^2 + F(3)(VREF)^3$

3. $TCIJ = G(0) + G(1)\ EMF + G(2)(EMF)^2 + G(3)(EMF)^3$

4. $EMF = H(0) + H(1)(TREF) + H(2)(TREF)^2 + H(3)(TREF)^3$

5. $$VREF + P(0) + P(1)\left(\frac{N_2-N_4}{N_1-N_3}\right) + P(2)\left(\frac{N_2-N_4}{N_1-N_3}\right)^2 + P(3)\left(\frac{N_2-N_4}{N_1-N_3}\right)^3$$

List of commands and their function:

Command #		Function
C1		Place in Mode 1
C2		Place in Mode 2
C3		Place in Mode 3
C4		Full sequence of measurements
C5		Probe 1 only
C6		Probe 2 only
C7	C7 → ΔTH	H(P-Bits = 0)
C8	C7 & C8 → ΔTL	L(2nd P-Bit = 1)
C9	C7 & C9 - ΔT	(1st + P-Bit = 1)
	C8 & C9 - TC	
C10		Advance Heater

List of Heater States

State No.	Heater Loc.	K Bridge	On	Off
1	12	ΔTR11		X
2	12	ΔTR11	X	
3	14	ΔTR12		X
4	14	ΔTR12	X	
5	11	ΔTR11		X
6	11	ΔTR11	X	
7	13	ΔTR12		X
8	13	ΔTR12	X	
9	22	ΔTR21		X
10	22	ΔTR21	X	
11	24	ΔTR22		X

List of Heater States (Cont.)

State No.	Heater Loc.	K Bridge	On	Off
12	24	ΔTR22	X	
13	21	ΔTR21		X
14	21	ΔTR21	X	
15	23	ΔTR22		X
16	23	ΔTR22	X	

*First digit gives the probe number, the second the heater location starting from the top of the probe.

1: Table of possible operating states of the Lunar Heat Flow Experiment in Mode 1

Parameter / Probe	1 ΔTH	2 ΔTL	3 T	4 TC & RT	5 Full Sequence
a P1	C5, C7*	C5, C7, C8*	C5, C7, C9*	C5, C8, C9*	C5
b P2	C6, C7*	C6, C7, C8*	C6, C7, C9*	C6, C8, C9*	C6
c P1&P2	C7*	C7, C8*	C7, C9*	C8, C9*	C4

*These states will probably not be used on the moon.

The commands required to put the experiment in one of the above states are given in each box.

Other commands are:

C1 - Mode 1

C2 - Mode 2

C3 & C7 - Mode 3

C10 - Advance heater state (see heater state table on next page).

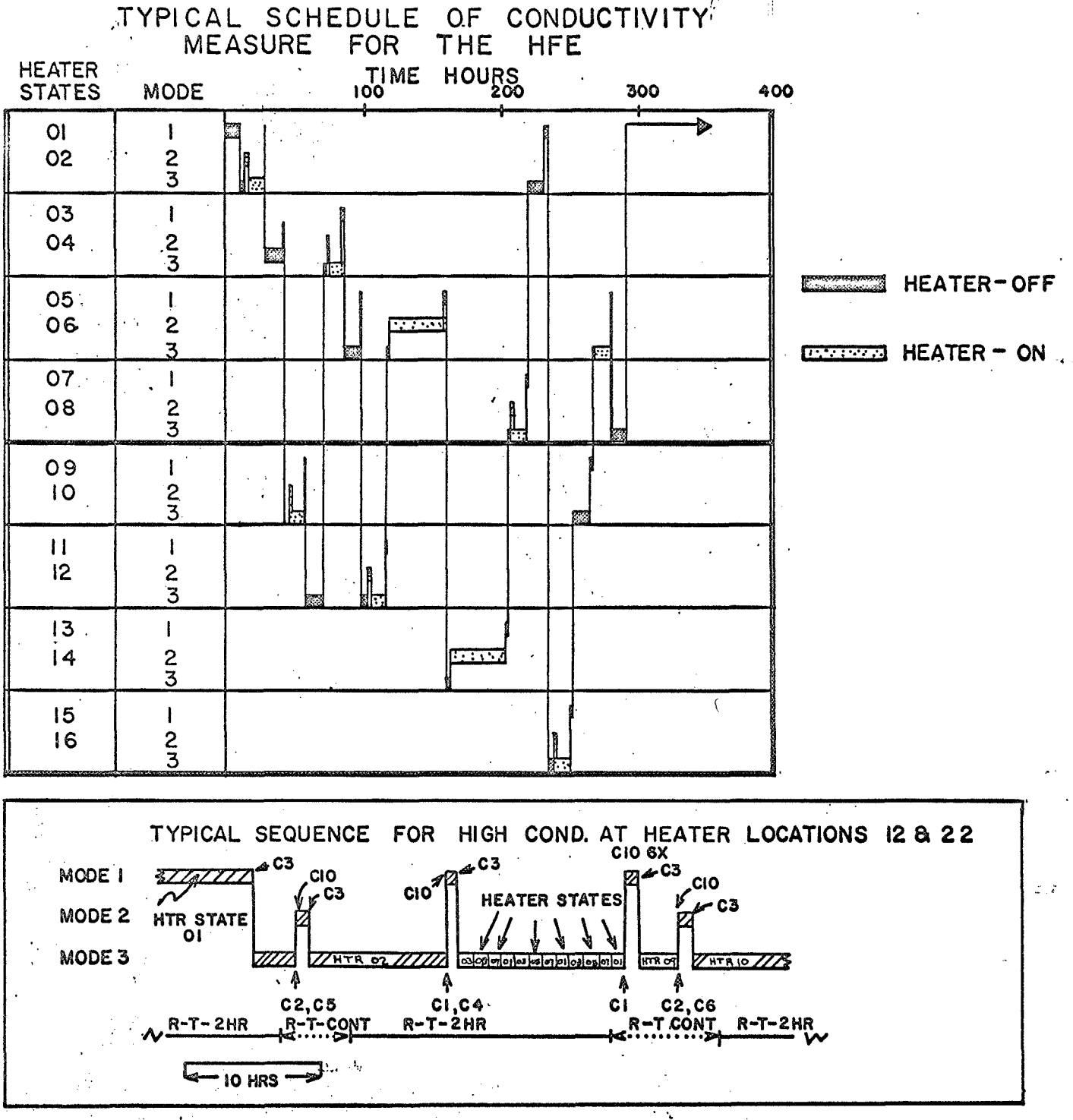

Appendix Figure 1

Outline of

DATA REDUCTION PROCEDURE

FOR THE ALSEP LUNAR HEAT FLOW EXPERIMENT*

with

HFE S/N-5 Coefficients

July 18, 1969

Lamont-Doherty Geological Observatory

of Columbia University

Palisades, New York

*This document is an amendment to "Real Time Data Requirements for the ALSEP Lunar Heat Flow Experiment."

FLOW CHART FOR HFE DATA REDUCTION

DTH(IJ) Measurements:

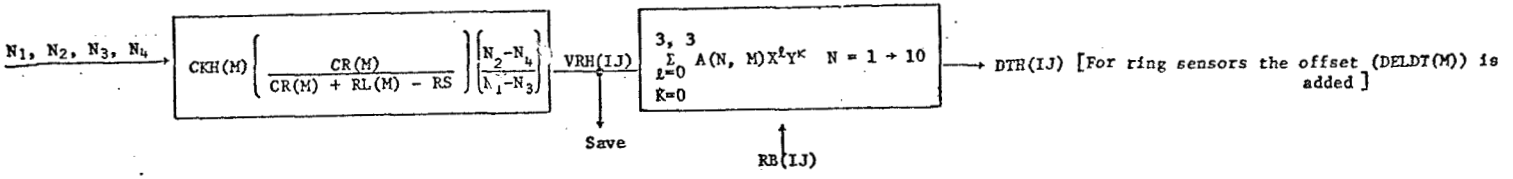

DTL(IJ) Measurements:

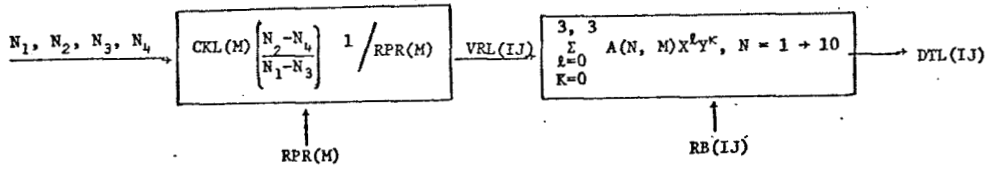

Average Temperature T(I, J)

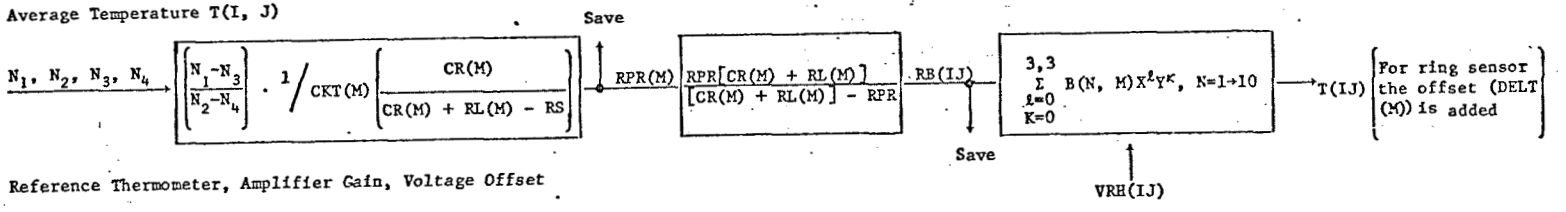

Reference Thermometer, Amplifier Gain, Voltage Offset

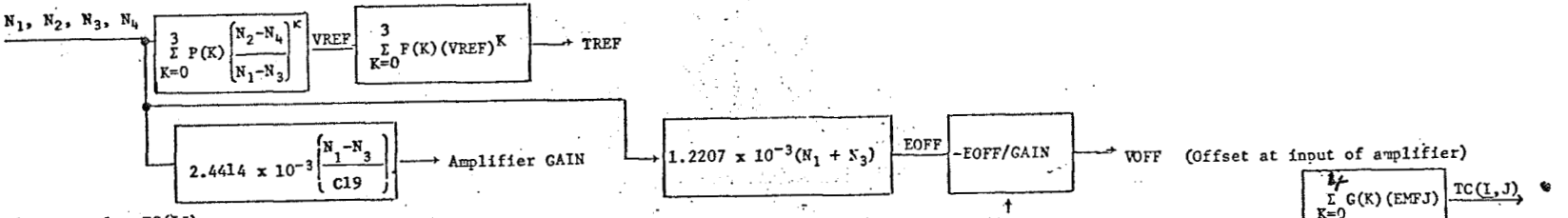

Thermocouples TC(IJ)

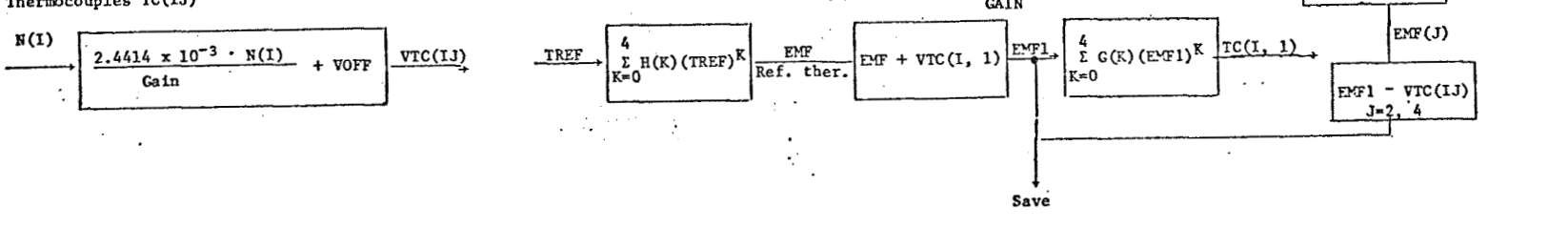

Equations:

1. $DTH(IJ) = A(1, K)\ X^3\ Y^0 + A(2, K)\ X^2\ Y^0 + A(3, K)\ X^2\ Y^1$
$+A(4, K)\ X^1\ Y^0 + A(5, K)\ X^1\ Y^1 + A(6, K)\ X^1\ Y^2 + A(7, K)$
$+A(8, K)\ X^0\ Y^1 + A(9, K)\ X^0\ Y^2 + A(10, K)\ X^0\ Y^3$

$X = RB(IJ) \qquad Y = RB(IJ) \times VRH(IJ)$

2. $TREF = F(0) + F(1)\ VREF + F(2)(VREF)^2 + F(3)(VREF)^3$

3. $TCIJ = G(0) + G(1)\ EMF + G(2)(EMF)^2 + G(3)(EMF)^3 + G(4)(EMG)^4$

4. $EMF = H(0) + H(1)(TREF) + H(2)(TREF)^2 + H(3)(TREF)^3 + H(4)(TREF)^4$

5. $VREF = P(0) + P(1)\left(\frac{N_2-N_4}{N_1-N_3}\right) + P(2)\left(\frac{N_2-N_4}{N_1-N_3}\right) + P(3)\left(\frac{N_2-N_4}{N_1-N_3}\right)^3$

ONSTANTS INDEPENDENT OF PROBE AND SECTION
COEFFICITNES OF THE POLYNOMIAL (P) USED TO CALCULATE THE REFRENCE TEMPERATURE
-0.1009786E-04
0.1068218E 00
-0.1113908E-02
-0.9881476E-05
OFFICIENTS OF THE POLYNOMIAL (F) USED IN THE REFRENCE TEMPERATURE CALCULATION
0.2731534E 03
0.5035033E 03
0.5305088E 03
0.7589066E 03
COFFICIENTS OF THE POLYNOMIAL (G) USED IN THE THERMOCOUPLE CALCULATION
0.272798E 03
0.171559E 05
-0.199535E 06
0.138173E 08
-0.377338E 10
OFFICIENTS OF THE POLYNOMIAL (H) USED IN THE THERMOCOUPLE CALCULATION
-0.994125E-02
0.564034E-05
0.151562E-06
-0.168125E-09
0.934759E-13
S
.1098719E 04
C19
1.8153529E-02
R
2.0109999E 05

ONSTANTS FOR PROBE 1 UPPER SECTION
KH-GRADIENT BRIDGE
5.4412999E-03
KL-GRADIENT BRIDGE
2.0013999E 01
CKT-GRADIENT BRIDGE
2.7223999E-03
KH-RING BRIDGE
5.4407999E-03
CKT-RING BRIDGE
2.7223999E-03
L-GRADIENT BRIDGE
1.0863659E 03
L-RING BRIDGE
1.1252769E 03
OFFSET (DELT) FOR RING SENSOR TEMPERATURE MEASUREMENT
0.42
FFSET (DELDT) FOR RING SENSOR TEMPERATURE DIFFERENCE MEASUREMENT
0.013
COFFICIENTS OF POLYNOMIAL (A) TO CALCULATE DT (GRADIENT BRIDGE)
-0.266611E-09
0.197734E-06
-0.179790E-06
-0.280342E-05
0.319800E-03
0.151150E-07
-0.122003E-01
-0.887667E 00
-0.845143E-05
-0.293055E-07
OFFICIENTS OF POLYNOMIAL (B) TO CALCULATE T (GRADIENT BRIDGE).
-0.311852E-07
0.820543E-04
-0.106858E-06
0.442780E 00
0.941846E-04
-0.999205E-07
0.338416E 02
-0.205678E-01
0.843699E-04
-0.164700E-06
OFFICIENTS OF POLYNOMIAL (A) TO CALCULATE DT (RING BRIDGE)
-0.311319E-09
0.301770E-06
-0.288730E-06
-0.788840E-04
0.406890E-03
-0.323312E-08
0.156298E-01
0.871178E 00
-0.488865E-05
-0.100458E-06
COFFICIENTS OF POLYNOMIAL (B) TO CALCULATE T (RING BRIDGE)
-0.672863E-07
0.127310E-03
-0.222470E-06
0.424425E 00
0.185863E-03
-0.193652E-06
0.362192E 02
-0.381612E-01
0.128124E-03
-0.577336E-07

CONSTANTS FOR PROBE 1 LOWER SECTION
CKH-GRADIENT BRIDGE
5.4407999E-03
CKL-GRADIENT BRIDGE
2.0014999E 01
CKT-GRADIENT BRIDGE
2.7222999E-03
CKH-RING BRIDGE
5.4409999E-03
CKT-RING BRIDGE
2.7224999E-03
RL-GRADIENT BRIDGE
1.0852649E 03
RL-RING BRIDGE
1.1151639E 03
COFFICIENTS OF POLYNOMIAL (A) TO CALCULATE DT (GRADIENT BRIDGE)
-0.979433E-09
0.804358E-06
-0.177329E-06
-0.323272E-03
0.318565E-03
0.122310E-07
0.276256E-01
0.888993E 00
-0.719786E-05
-0.498331E-07
OFFSET (DELT) FOR RING SENSOR TEMPERATURE MEASUREMENT
0.43
OFFSET (DELDT) FOR RING SENSOR TEMPERATURE DIFFERENCE MEASUREMENT
0.002
COFFICIENTS OF POLYNOMIAL (B) TO CALCULATE T (GRADIENT BRIDGE).
-0.293987E-07
0.801089E-04
-0.111504E-06
0.444086E 00
0.952909E-04
-0.994985E-07
0.337309E 02
-0.202479E-01
0.859163E-04
-0.207970E-07
COFFICIENTS OF POLYNOMIAL (A) TO CALCULATE DT (RING BRIDGE)
-0.115781E-09
-0.641674E-07
-0.230547E-06
0.143433E-03
0.361760E-03
-0.425779E-08
-0.433145E-01
0.879956E 00
-0.361284E-05
-0.821537E-07
COFFICIENTS OF POLYNOMIAL (B) TO CALCULATE T (RING BRIDGE)
-0.320674E-07
0.839119E-04
-0.120889E-06
0.442156E 00
0.960771E-04
-0.105135E-06
0.338265E 02
-0.189357E-01
0.921830E-04
-0.620094E-07

ONSTANTS FOR PROBE 2 UPPER SECTION
KH-GRADIENT BRIDGE
5.4416999E-03
KL-GRADIENT BRIDGE
2.0012999E 01
CKT-GRADIENT BRIDGE
2.7224999E-03
KH-RING BRIDGE
5.4407999E-03
CKT-RING BRIDGE
2.7224999E-03
L-GRADIENT BRIDGE
1.1526379E 03
L-RING BRIDGE
1.1911879E 03
OFFSET (DELT) FOR RING SENSOR TEMPERATURE MEASUREMENT
0.44
FFSET (DELDT) FOR RING SENSOR TEMPERATURE DIFFERENCE MEASUREMENT
0.075
COFFICIENTS OF POLYNOMIAL (A) TO CALCULATE DT (GRADIENT BRIDGE)
-0.713456E-09
0.585882E-06
-0.178331E-06
-0.183267E-03
0.318679E-03
0.113276E-07
0.664210E-02
0.888245E 00
-0.731774E-05
-0.542548E-07
OFFICIENTS OF POLYNOMIAL (B) TO CALCULATE T (GRADIENT BRIDGE)
-0.379122E-07
0.905694E-04
-0.137705E-06
0.439389E 00
0.115400E-03
-0.131060E-06
0.343261E 02
-0.240102E-01
0.995450E-04
-0.845763E-07
OFFICIENTS OF POLYNOMIAL (A) TO CALCULATE DT (RING BRIDGE)
-0.393423E-09
0.480838E-06
-0.138068E-06
-0.183168E-03
0.288045E-03
-0.401717E-08
-0.180119E-01
0.894535E 00
-0.173705E-05
-0.514405E-07
COFFICIENTS OF POLYNOMIAL (B) TO CALCULATE T (RING BRIDGE)
-0.438101E-07
0.986520E-04
-0.156807E-06
0.436061E 00
0.128361E-03
-0.143882E-06
0.346491E 02
-0.260400E-01
0.108307E-03
-0.769807E-07

```
CONSTANTS FOR PROBE 2 LOWER SECTION
CKH-GRADIENT BRIDGE
  5.4409999E-03
CKL-GRADIENT BRIDGE
  2.0014999E 01
CKT-GRADIENT BRIDGE
  2.7222999E-03
CKH-RING BRIDGE
  5.4401999E-03
CKT-RING BRIDGE
  2.7223999E-03
RL-GRADIENT BRIDGE
  1.1627679E 03
RL-RING BRIDGE
  1.1850689E 03
OFFSET (DELT) FOR RING SENSOR TEMPERATURE MEASUREMENT
 0.43
OFFSET (DELDT) FOR RING SENSOR TEMPERATURE DIFFERENCE MEASUREMENT
 0.014
COFFICIENTS OF POLYNOMIAL (A) TO CALCULATE DT  (GRADIENT BRIDGE)
 -0.519676E-09
  0.519439E-06
 -0.173038E-06
 -0.189586E-03
  0.313782E-03
  0.144434E-07
  0.157517E-01
  0.889129E 00
 -0.792534E-05
 -0.523338E-07
COFFICIENTS OF POLYNOMIAL (B) TO CALCULATE  T  (GRADIENT BRIDGE)
 -0.346705E-07
  0.863719E-04
 -0.118910E-06
  0.441090E 00
  0.102698E-03
 -0.110149E-06
  0.340914E 02
 -0.219537E-01
  0.878969E-04
 -0.198182E-06
COFFICIENTS OF POLYNOMIAL (A) TO CALCULATE DT  (RING BRIDGE)
 -0.499832E-10
  0.756820E 08
 -0.218375E-06
  0.149796E-04
  0.352170E-03
 -0.310824E-08
 -0.228220E-01
  0.881985E 00
 -0.360373E-05
 -0.754563E-07
COFFICIENTS OF POLYNOMIAL (B) TO CALCULATE  T  (RING BRIDGE)
 -0.272979E-07
  0.783620E-04
 -0.104056E-06
  0.444380E 00
  0.872501E-04
 -0.104719E-06
  0.335556E 02
 -0.177555E-01
  0.923802E-04
 -0.564468E-07
```

Outline of

DATA REDUCTION PROCEDURE

FOR THE ALSEP LUNAR CONDUCTIVITY EXPERIMENT

August 18, 1969

Lamont-Doherty Geological Observatory
of Columbia University
Palisades, New York

This document is a supplement to the L-DGO document "Real Time Data Requirements for the ALSEP Lunar Heat Flow Experiment."

SUMMARY OF REAL TIME REDUCTION OF LUNAR HEAT FLOW EXPERIMENT CONDUCTIVITY MEASUREMENTS IN MODE 2

TREND ANALYSIS

High sensitivity temperature difference measurements, and the times of their occurrence, constitute the input data for the trend analysis program. A function of time, F(TIME), based on the theory of equilibration of the probe with the lunar medium is used to predict the values of the temperature difference at future times. This function is equation (1) in the appendix.

The coefficients A(K) of the function F(TIME) are determined by applying least squares techniques to a set of previously measured temperature differences. The procedure for determining a satisfactory set of A(K) is given below. (See appendix 1 for definitions of terms used.)

The first 40 values of DTEM(I) and TIME(I) out of a set of 50 values in the interval TPRES — TSW are used to calculate A(K). TIME(I) has incremental values separated by 1 hour of real time. The coefficients are then used to calculate PRDT(I) for all 50 values of TIME(I). The last 10 values of PRDT(I) are predictions of temperature difference beyond the region of fit (TEND — TSW). The deviations, DIFF(I) = DTEM(I) — PRDT(I), are calculated. If the root mean square of the last 10 DIFF(I) is greater than 0.001°C another 10 hours of data are accumulated and the procedure repeated. When the root mean square of DIFF(I) is less than or equal to 0.001°C, the last values of A(K) are saved to be used to predict undisturbed temperatures during the Mode 2 conductivity measurement. This procedure is outlined in block diagram form in figure (1).

CONDUCTIVITY CALCULATION IN MODE 2

The input data to the reduction program shown in block diagram form in figure (2) are; the ambient temperature at the heater location of interest, T(N, L), and the gradient bridge temperature difference DTH(N, L), where N refers to the heater location (N = 1—4) and the index L refers to one of eight discrete times after turn on of the heater. (See table 1.) The values of T(N, L) and DTH(N, L) are determined by manually averaging the data in the vicinity of the time corresponding to L. To facilitate the determination of these parameters, T(N, L) and DTH(N, L) will be graphed versus time by the principal investigator team.

The time TIME(L) corresponding to DTH(N, L) and T(N, L), and coefficients A(K) from the Mode 2 trend analysis are used in equation (1) to calculate a predicted undisturbed temperature difference PRDT(L). This predicted temperature difference is subtracted from DTH(N, L) to yield corrected temperature differences DTHST(N, L).

DTHST(N, L) and T(N, L) are inserted in equation (2) to calculate the $\log_{10}$[COND(L)]. The terms B(N, L, K) in equation (2) are coefficients that will be supplied by the principal investigator. There are 32 sets of these coefficients corresponding to 4 locations and eight different times. Each set consists of 6 coefficients bringing the total to 192. The best estimate of the lunar conductivity, COND(L), is then obtained by taking the antilog of the result.

The calculations outlined in Figure (2) yield successive values of lunar conductivity which will in general improve with increasing time. These results will be monitored by maintaining a plot of computed conductivity values versus time. This plot will reveal trends in successive calculations and the scatter of the calculated values about the mean. On the basis of this information a judgement can be made as to when to terminate the conductivity experiment.

SUMMARY OF REAL TIME REDUCTION OF LUNAR HEAT FLOW EXPERIMENT CONDUCTIVITY MEASUREMENTS IN MODE 3

TREND ANALYSIS

Following completion of the Mode 2 trend analysis procedure 10 hours of ring bridge temperature difference data, RDTEM(I), are accumulated. These data are fitted to a function of the form in equation (1) to determine coefficients AR(K), K=1,6. Residuals RDIFF(I) are calculated using the input data as in the Mode 2 procedure. If the root mean square of the residuals is greater than 0.001°C an additional 10 hours of data are accumulated and new coefficients are calculated. If the root mean square of RDIFF(I) is less than 0.001°C the final set of AR(I) is saved to predict undisturbed ring bridge temperature differences during the Mode 3 conductivity experiment.

This procedure is illustrated by flow chart in figure (3).

CONDUCTIVITY CALCULATIONS IN MODE 3

The input data required to perform the calculation of conductivity in Mode 3 are the ring bridge temperature differences DTR(N,I) where N refers to the location index 1-4, at times, TIME(I). A flow chart of this calculation is presented in Figure (4).

All data are plotted manually by the principal investigator team. At discrete times after heater turn on five DTR(N,I) and TIME(I) are selected. These points must be symmetrical in time around the point at time corresponding to index L. (SEE TABLE 1) The five TIME(I) are used to calculate predicted undisturbed temperature differences RPRDT(I). The coefficients AR(K) from the Mode 3 trend analysis are used in a function of the form of equation (1) appendix (1) to make this computation. Corrected ring bridge temperature differences, DTRST(N,I), are determined by subtracting the RPRDT(I) from the DTR(N,I). The five values of DTRST(N,I) are combined with the five corresponding times, TIME(I), and

fitted by least squares to a function of the form given in equation (3) in the appendix. The coefficient S(L), where L is the time index, is the slope of a plot of log temperature difference versus log time. This slope is the basic parameter needed to calculate the lunar conductivity COND(L).

The conductivity is calculated directly by use of equation (4) given in the appendix. The 64 coefficients BR(N, L, K) are provided by the principal investigator. Only two sets of BR's are required for all heater locations. One set is for locations 1, 2, and 3; and another for location 4. Therefore; BR(1, L, K) = BR(2, L, K) = BR(3, L, K) $\neq$ BR(4, L, K).

The calculations outlined in Figure (4) yield values of COND(L) at successively longer times after heater turn on. These results will be plotted by the principal investigator team to monitor trends and determine when the experiment should be switched to the decay mode.

APPENDIX 1 — DEFINITIONS

Mode 2 Trend Analysis

DTEM(I)	Hourly samples of gradient bridge temperature difference on the probe section where the conductivity experiment is to be run.
TIME(I)	time of DTEM(I) measurement in milliseconds after HFE turn on.
KAPPA	estimated diffusivity of lunar soil (1×10^{-4})
OMEGA	2π/ (period of lunation) (2.5×10^{-6} sec^{-1})
TRAD(I)	OMEGA x TIME(I) / 1000.0
TAU(I)	KAPPA x TIME(I) / 1000.0
TPRES	time of last recorded measurement
TSW	time at start of sample interval
TEND	time at end of sample interval
PRDT(I)	predicted temperature difference
DIFF(I)	DTEM(I) — PRDT(I)
A(K)	coefficients of equation (1) determined by least squares

Mode 2 Conductivity calculation

COND(L)	calculated lunar conductivity at time L
T(N, L)	ambient temperature at location N, time L
DTH(N, L)	temperature difference at gradient bridge at location N, time L
DTHST(N, L)	gradient bridge temperature difference minus the predicted undisturbed temperature difference.
B(N, L, K)	coefficients of the second order polynomial used to calculate $\log_{10}$[COND(L)]

APPENDIX 1 (continued)

Mode 3 Trend analysis

RDTEM(N, I)	hourly samples of ring bridge temperature difference on the probe section where the conductivity experiment is to be run
AR(K)	coefficients of equation (1) fitted by least squares
RPRDT(I)	predicted temperature difference
RDIFF(I)	RDTEM(I) — RPRDT(I)

Mode 3 Conductivity Calculation

DTR(N, I)	temperature difference at ring bridge, location N, time I
DTRST(N, I)	gradient bridge temperature difference minus the predicted undisturbed temperature difference
S(L)	coefficient S in equation (3)
BR(N, L, K)	coefficients of equation (4) used to calculate COND(L)

Table 1: Definition of time index L

Index (L)	time in hours after turn on of heater	
	Mode 2	Mode 3
1	2	3
2	4	4
3	8	5
4	12	6
5	20	7
6	28	8
7	36	9
8	42	10

Equations:

(1) $$F(TIME) = A(1) + A(2)/\,TAU(I) + A(3)/\,[TAU(I)]^2 + A(4) \times Ln[TIME(I)/1000.0]/[TAU(I)]^2 + A(5) \times TRAD(I) + A(6) \times [TRAD(I)]^3$$

(2) $$Log_{10}[COND(L)] = B(N,L,1) + B(N,L,2)\,U + B(N,L,3)\,V + B(N,L,4)\,UV + B(N,L,5)\,U^2 + B(N,L,6)\,V^2$$

where $U = DTHST(N,L)$ and $V = T(N,L)$

APPENDIX 1 (continued)

Equations (continued)

(3) $\text{Log}_{10}[\text{DTRST}(N,I)] = M + S(L) \times \text{Log}_{10}\left([\text{TIME}(I)]/1000.0\right)$

(4) $\text{COND}(L) = \text{BR}(N,L,1) + \text{BR}(N,L,2) \times S(L) + \text{BR}(N,L,3) \times [S(L)]^2 + \text{BR}(N,L,4) \times [S(L)]^3$

APPENDIX 2 Outline of lunar heat flow conductivity measurement procedure

The following is a step by step procedure for running the first conductivity experiment.

(1) Sample DTH(11), DTH(12), DTH(21), and DTH(22) at hourly intervals during the first 100 hours after the HFE is turned on. The experiment is in Mode 1 full sequence.

(2) Perform trend analysis on DTH(11) until predictions are valid.

(3) Accumulate an additional 10 hours of data and sample DTR(11) every hour by switching to Mode 3 with the heater off.

(4) Perform Mode 3 trend analysis and determine AR(K)'s. Calculate the final set of coefficients, A(K), using the Mode 2 trend analysis.

(5) Initiate heater 11 in Mode 2 and compute estimates of lunar conductivity, COND(L), corresponding to 2 and 4 hours. If COND(L) is greater than 5×10^{-4} watts/cm°C, go to step 6; otherwise go to step 9.

(6) Switch to Mode 3 operation and calculate successive COND(L) using Mode 3 procedures. (NOTE: After switching to Mode 3, time is kept relative to Mode 3 turn on).

(7) Terminate Mode 3 operation on principal investigators approval and run decay mode sequence.

(8) Return to Mode 1 and obtain 10 hours of DTH data at bridge 21. Switch to Mode 3 at hourly intervals and accumulate 10 hours of DTR(21) data. Go to step 12.

(9) Continue in Mode 2 with full sequence. Calculate COND(L) using Mode 2 procedures.

(10) Terminate Mode 2 experiment.

APPENDIX 2 (continued)

(11) Accumulate 10 additional hours of DTH(21) and DTR(21) data in Mode 1 and Mode 3 with heaters off.

(12) Perform trend analysis on all bridge (21) data. When prediction is valid, initiate experiment at heater location 21 in Mode 2 and repeat steps 5—11.

(13) Continue until all 10 conductivity experiments have been performed.

MODE 2 TREND ANALYSIS

1. DETERMINATION OF ADJUSTED TIMES:

TIME(I) → KAPPA · TIME (I)/1000 → TAU (I) (SAVE)

TIME(I) → OMEGA · TIME (I)/1000 → TRAD (I) (SAVE)

2. DETERMINATION OF ANALYSIS INTERVAL:

TPRES → TPRES — 50 HOURS → TSW (SAVE)

TPRES → TPRES — 10 HOURS → TEND (SAVE)

3. DETERMINATION OF COEFFICIENTS A(K): K=1-6

DTEM(I) →
TIME (I) →
TAU (I) →
TRAD (I) →

DTEM (I) = F(TIME(I))
TIME (I) =
TSW, TSW + 1HR, .. TEND

→ A(K) (SAVE)

4. VALIDATE CLOSENESS OF FIT

A(K) →
TIME (I) → F(TIME (I)) → PRDT(I) → DTEM(I) − PRDT(I) → DIFF(I) → CONTINUE ON THE NEXT LINE

TIME (I) = TSW, TSW + 1HR, ... TPRES

DIFF(I) → IF $\left(\sqrt{\frac{\Sigma[DIFF(I)]^2}{10}}\right) - .001$

→ TSW = TSW + 10 HRS.
TEND = TEND + 10HRS.
RETURN TO STEP 3

→ 0 or { GO TO MODE 3 TREND ANALYSIS }

TIME(I) = TEND + 1HR, ... TPRES

MODE 2 CONDUCTIVITY CALCULATION

1. DETERMINATION OF $T(N,L_s)$ AND DTH(N,L)

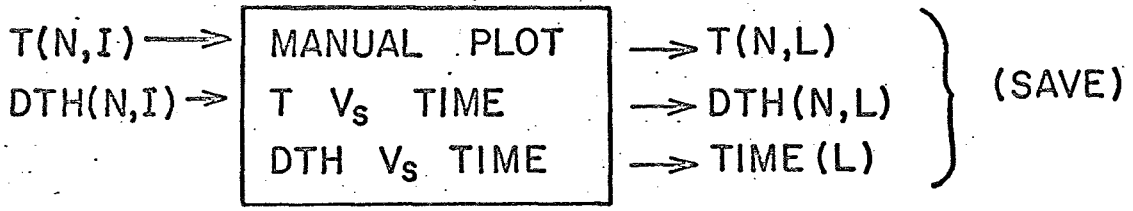

2. PREDICT UNDISTURBED TEMPERATURE DIFFERENCE AND CORRECT DTH(N,L)

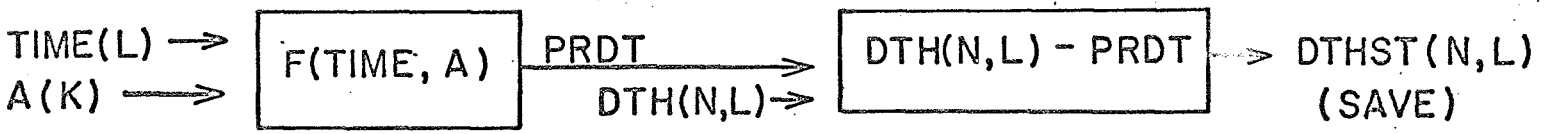

3. CALCULATE CONDUCTIVITY

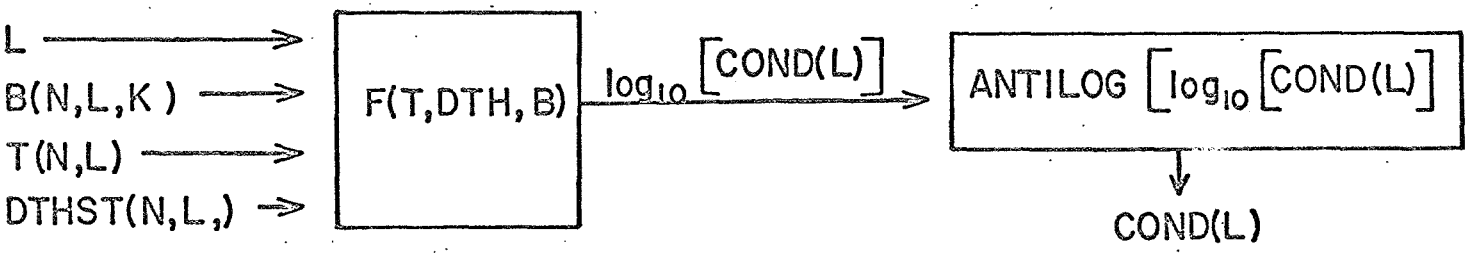

MODE 3 TREND ANALYSIS

1. DETERMINATION OF COEFFICIENTS A(K): K=1-6

RDTEM(I) →
TIME(I) →
TAU(I) →
TRAD(I) →

LEAST SQUARE FIT
RDTEM(I) = F(TIME)
TIME(I) = TEND+1,.... TPRES

→ AR(K) (SAVE)

2. VALIDATE CLOSENESS OF FIT:

AR(K) →
TIME(I) →

F(TIME(I)) → RPRDT(I) / RDTEM(I) → RDTEM(I) - RPRDT(I) → RDIFF(I) (SAVE)

RDIFF(I) → IF $\left[\sqrt{\frac{\Sigma(RDIFF(I))^2}{10}} - .001\right]$

+ → TEND = TEND + 10 HRS
TPRES = TPRES + 10 HRS
{ RETURN TO STEP 1 }

− / 0 → GO TO CONDUCTIVITY ANALYSIS

MODE 3 CONDUCTIVITY CALCULATION

1. DETERMINATION OF DTR(N,L)'S

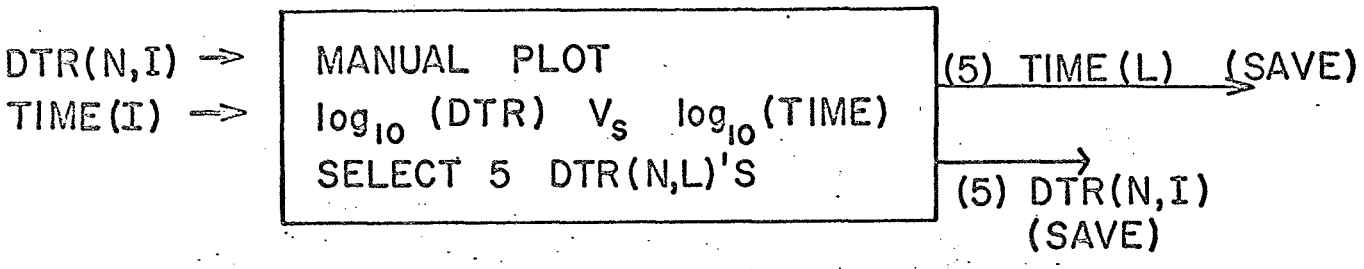

2. PREDICT UNDISTURBED TEMPERATURE DIFFERENCES
   CALCULATE DTRST(N,L)

3. CALCULATE SLOPE OF $\log_{10}$ DTR V_s $\log_{10}$ TIME

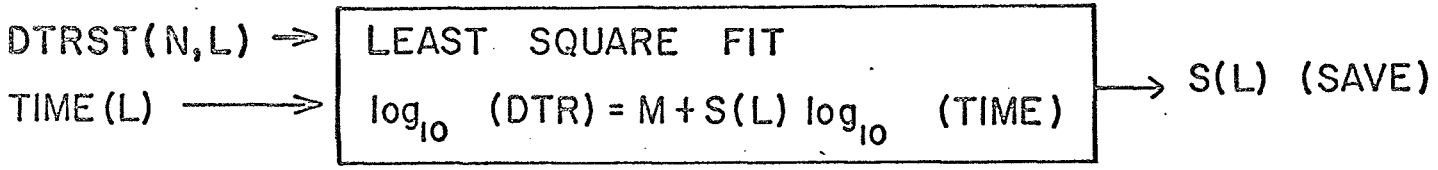

4. CALCULATE CONDUCTIVITY

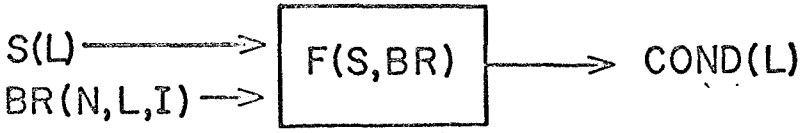

APPENDIX A

THERMAL CONDUCTIVITY MEASUREMENTS OF BORON-REINFORCED FIBERGLASS TUBE

I. INTRODUCTION

The ALSEP Heat Flow Experiment will use two heat flow probes each emplaced in a 3 meter borehole in the lunar surface. The borehole will be cased with a boron-reinforced filament-wound fiberglass tube used as the drill stem. The temperature gradient and thermal conductivity measurements made by the heat flow probes are influenced by the thermal properties of the borehole casing. To provide data needed in estimating the effects of the casing on the probe's measurements, we measured the thermal conductivity of a typical section of the borehole casing.

II. METHOD AND APPARATUS

The longitudinal heat flow method was used to evaluate the thermal conductivity of a prototype section of boron-reinforced fiberglass tube, 15 1/2 inches long. After carefully measuring the tube dimensions, fourteen 0.003" diameter chromel-constantan thermocouples were cemented in small holes drilled into the tube. Most of the thermocouples were located in the boron layer of the tube; others were located in the outer fiberglass layer. A 1000 ohm wire wound resistance heater was placed inside the tube at its midpoint and cemented to the tube with Dow Corning 340 epoxy. Copper end plugs, with cooling coils, were fixed to each end of the tube. The void space within the tube was filled with open cell urethane foam of approximately 2 lb/ft^3 density. The foam conductance is very much lower than that of the sample and can be neglected. The outside surface of the tube was insulated with approximately 12 layers of multilayer insulation -- each containing an aluminized mylar shield and a woven fiberglass cloth spacer. The insulation was applied in a continuous wrap; the thermocouple wires were led out from the casing sample tube within the insulation. A schematic diagram of the apparatus is shown in Figure 1.

The boron-reinforced tube, together with thermocouples, end plugs, heater and insulation were placed on a laboratory vacuum table and covered with a bell jar. The assembly was evacuated to 10^{-5} Torr or less. A constant temperature fluid was circulated through the coils of the end plugs; electric power was applied to the heater using a controlled dc power supply. An experimental measurement consisted of: 1) providing a controlled temperature fluid in the end plugs; 2) applying a constant electric power to the heater; 3) waiting a sufficient period (8-24 hrs) for a steady state temperature distribution to be established in the tube; 4) recording the thermocouple emfs (using a L&N type K-3 potentiometer and null meter) and the heater current and voltage. Measurements were made at three temperature levels: room temperature, 230°K and 330°K. Temperature measurements were accurate to about $\pm$ .25°C. Several heater power levels were used. During the measurements program, when it was determined that radial heat losses were extensive, an additional layer of fiberglass insulation, approximately 1/2" thick, was added to the outside of the already insulated bore tube.

III. RESULTS AND DISCUSSION

The original concept of the measurements required that the radial heat interchange between the tube and its surroundings be small so that one dimensional heat flow in the bore tube would result. Under these conditions, the temperature distribution in the tube should be linear and the conductance of the tube (the conductivity-area product) could be evaluated from the heater power and slope of the temperature - distance curve. Because of the low conductance of the tube, its relatively high surface area, and the low insulating effectiveness of the insulation applied to the tube, radial heat flow was significant in almost all tests and an alternate method of analysis had to be adopted.

Figure 2 shows typical temperature profiles for several tests at room temperature. Note the linearity for tests 6 and 23 and the curvature for test 5. High and low temperature test data are shown in Figures 4 and 5. For these tests, the large radial heat flow made it difficult, if not impossible, to derive reliable values of conductance at low and high temperatures; however from tests at room temperature, particularly those where several power levels were used, reliable values of conductance can be determined.

A. Room Temperature Results

Test runs 6, 7, 14, 19 and 23 were conducted at room temperature with a relatively low power spplied to the heater. Because of the small difference between the temperature of the boretube and the surroundings, radiation losses were small and the temperature gradient along the tube was almost linear. If we assume negligible heat losses, the conductivity-area product can be calculated from the equation:

$$kA_x = \frac{q}{\Delta T/L} \qquad (1)$$

where q is half of the electric power applied to the heater (one half flows in each direction), and $\Delta T/L$ is the temperature gradient. The results are shown below:

Test	Heater Power (watt)	Average Temperature (°K)	kA_x (watt cm/°K)
6	.0079	300	0.012
7	.0075	300	0.012
14	.0031	296	0.013
19	.0077	299	0.015
23	.0079	301	0.013

and indicate that the conductance is probably 0.013 ± 0.001 watt cm/°K.

However, careful examination of the temperature-distance plots show some curvature, particularly for those tests at higher heater power and at locations near the center of the tube. This is expected if heat is lost from the tube to the surroundings.

As an alternate method of evaluating conductance, we assumed that the heat losses were proportional to the difference between the average tube temperature, T_m, and the ambient temperature, T_o. Then the electrical power dissipation can be related to the losses and the heat flow in the tube as follows:

$$q_h = \frac{kA_x}{L} (T_1 - T_2) + h\pi DL (T_m - T_o) \qquad (2)$$

where T_1 and T_2 are the heater temperature and heat sink temperature, D is the tube diameter, L the tube length between the heater and the heat sink, and h is the heat transfer coefficient. Equation 2 can be rearranged as follows:

$$\frac{q_h}{(T_m - T_o)} = \frac{kA_x (T_1 - T_2)}{L (T_m - T_o)} + h\pi DL \qquad (3)$$

For an almost linear gradient in the tube $T_m \approx \frac{T_1 + T_2}{2}$.

A plot of $q_h/(T_m - T_o)$ versus $(T_1 - T_2)/(T_m - T_o)$ should give a straight line of slope kA_x/L and intercept $h\pi DL$, thus providing a means for estimating kA_x/L and h. Figure 3 shows such a plot for the room temperature data, including the points where losses may be significant. In drawing the line through the data, the results of test 17 were weighted only slightly because of the small temperature drop along the tube (0.45°C) and small difference between the ambient temperature and the tube temperature. Similarly, in test 5, the data point was discounted since the heat losses were the greatest and the temperature-distance curve was decidedly nonlinear. From the slope of the plot of all other data points from tests at about 300°K, the value of kA_x is found to be approximately 0.011 watt cm/°K -- slightly lower than that assuming no heat losses. From the intercept, we find that $h = 2.1 \times 10^{-6}$ watt/cm^2°K.

The radiation heat losses during the tests can also be estimated using an analytical model where a cylindrical fin of length L has its ends held at temperatures T_1 and T_2 and is radiating to surroundings at T_o. The temperature distribution in the tube is:

$$T - T_o = \frac{(T_1 - T_o) \sinh m(L-X) + (T_2 - T_o) \sinh mx}{\sinh(mL)} \qquad (3)$$

where $T_1 + T_2$ are the temperatures at x=0 and at x=L, respectively. By matching theoretical and experimental temperature profiles, the value of mL can be estimated, where:

$$mL = \sqrt{\frac{h\pi D}{kA_x}}\, L \qquad (4)$$

or

$$h = \frac{kA_x}{\pi D}\left(\frac{mL}{L}\right)^2 \simeq 4\sigma F_\varepsilon F_A T^3 \qquad (5)$$

In Figure 2, theoretical curves are shown for mL = 1.0 and mL = 1.2. The best match is obtained at about mL = 1.3 which corresponds to a value of

$$h = \frac{(.011)}{\pi(2.5)}\left(\frac{1.3}{17.1}\right)^2 = 8 \times 10^{-6} \text{ watt/cm}^2\text{°K} \qquad (6)$$

This test was conducted before the 1/2" fiberglass insulation was installed and represents the effect of 12 wraps of multilayer insulation. The equivalent emittance factor would have a value of $F_e \simeq .013$. The theoretical factor for 12 ideal wraps having an emissivity of .025 per surface would be about .001. The actual insulation performance is less good than anticipated, although the ideal value could not be achieved in practice because of effects such as 1) the conductance through the spacer 2) the spiral wrap (instead of floating concentric shields) 3) presence of thermocouple leads 4) slightly tight wrap.

Tests following #16 were run with additional insulation installed outside the multilayers. One might expect to see in Figure 3 a displacement between data from tests 5, 6, 7, 14 and from tests 17, 19, 23 which would indicate different values of the intercept or equivalent loss coefficient, h. Test 5 may reflect this effect. However, tests 6, 7 and 14 all had "cold end" temperatures below room temperature so that heat could be lost to the surroundings near the warm end and gained near the cold end. Net losses would be small for these tests and would not give a realistic estimate of h. Close examination of the temperature profile for Test 6 (figure 2) shows this effect since the data actually indicate an S-shaped curve around the straight line drawn. The slope decreases slightly with distance from the heater at the warm end indicating a heat loss. The opposite effect can be detected near the cold end.

B. High Temperature Results

Data at about 330°K were obtained by controlling end temperatures at about 65°C. Data from a typical test are shown in Figure 4. This test was conducted at a high power level and the shape of the curve is indicative of substantial heat losses. In earlier tests with no power and with low power, the heater temperature was actually lower than the controlled end temperatures since the system was losing heat to surroundings at about 22°K.

The same fin model described in the previous section (equation 3) again is applicable and allows an estimate of losses to be made using eqs. 4 and 5. For test 51 shown in Figure 4 and for the q = 0 test, the best match was obtained using mL = 0.6. This corresponds to

$$h = \frac{.011}{\pi(2.5)} \left(\frac{0.6}{17.1}\right)^2 = 1.7 \times 10^{-6} \quad \frac{\text{watts}}{\text{cm}^2\ ^\circ\text{K}} \tag{7}$$

or

$$F_e = \frac{1.7 \times 10^{-6}}{4(5.67 \times 10^{-12})\ (350)^3} = .002 \tag{8}$$

This is for the system after addition of fiberglass insulation over the multilayer wrap. The magnitude of this value seems reasonable and is in agreement with the value of h obtained from the intercept of Figure 3.

C. Low Temperature Results

Figure 5 presents the temperature profile for a typical low temperature test. In these tests, the coolant temperature was controlled at about -65°C. Since the surroundings were at about 22°C, in these tests heat was flowing through the insulation into the test section. The shape of the profile in Figure 5 shows this effect.

The fin analysis indicates that mL $\simeq$ 0.7 for the low temperature tests. The equivalent value of h is about 2.3×10^{-6} watts/cm^2°K. This represents radiation from about a 300°K temperature level and would result in an estimate of $F_a F_e \simeq .004$. However, since the outer insulation is now the heat source, the effective area factor F_a is likely to be greater than unity.

IV. CONCLUSIONS

1. The measured conductance of the boron-reinforced epoxy - fiberglass casing at 300°K is about 0.011 watt cm/°K. This value has an accuracy of about $\pm$ 10%.

2. Tests at 230°K and 330°K temperature levels give results consistent with the room temperature tube conductance and reasonable losses or gains of heat through the sample insulation. These results are not sufficiently accurate to allow an experimental determination of the conductance variation with temperature level.

3. Previous predictions for casing conductance based on geometry and literature values for boron, tungsten and epoxy-fiberglass indicated values of kA = .025 watt cm/°K at 200°K and = .020 watt cm/°K at 300°K. The difference in predicted and measured conductances probably is due to uncertainty in the conductance of the boron fibers which represent 75% of the casing conductance. No data for boron fibers were located, so literature values for boron crystals (1) were used in the calculations. Deviation from a pure crystalline form would lower conductance, therefore the measured values are consistent with expectations based on the predicted values. The 10% decrease in conductance between

200°K and 300°K reported in the literature is probably applicable to the experimental data.

V. RECOMMENDATIONS

The following values should be used as axial thermal conductances for the HFE drill casing:

$$kA_x = .011 \pm .001 \text{ watt cm/°K at } 300°K$$

$$kA_x = .012 \pm .002 \text{ watt cm/°K at } 200°K$$

(1) Thompson, J.C. and W. J. McDonald, "Low Temperature Thermal Conductivity of Boron" in Gavle, "Boron," Vol. 2 Plenum (1965)

ARTHUR D. LITTLE, INC.
CAMBRIDGE, MASS.

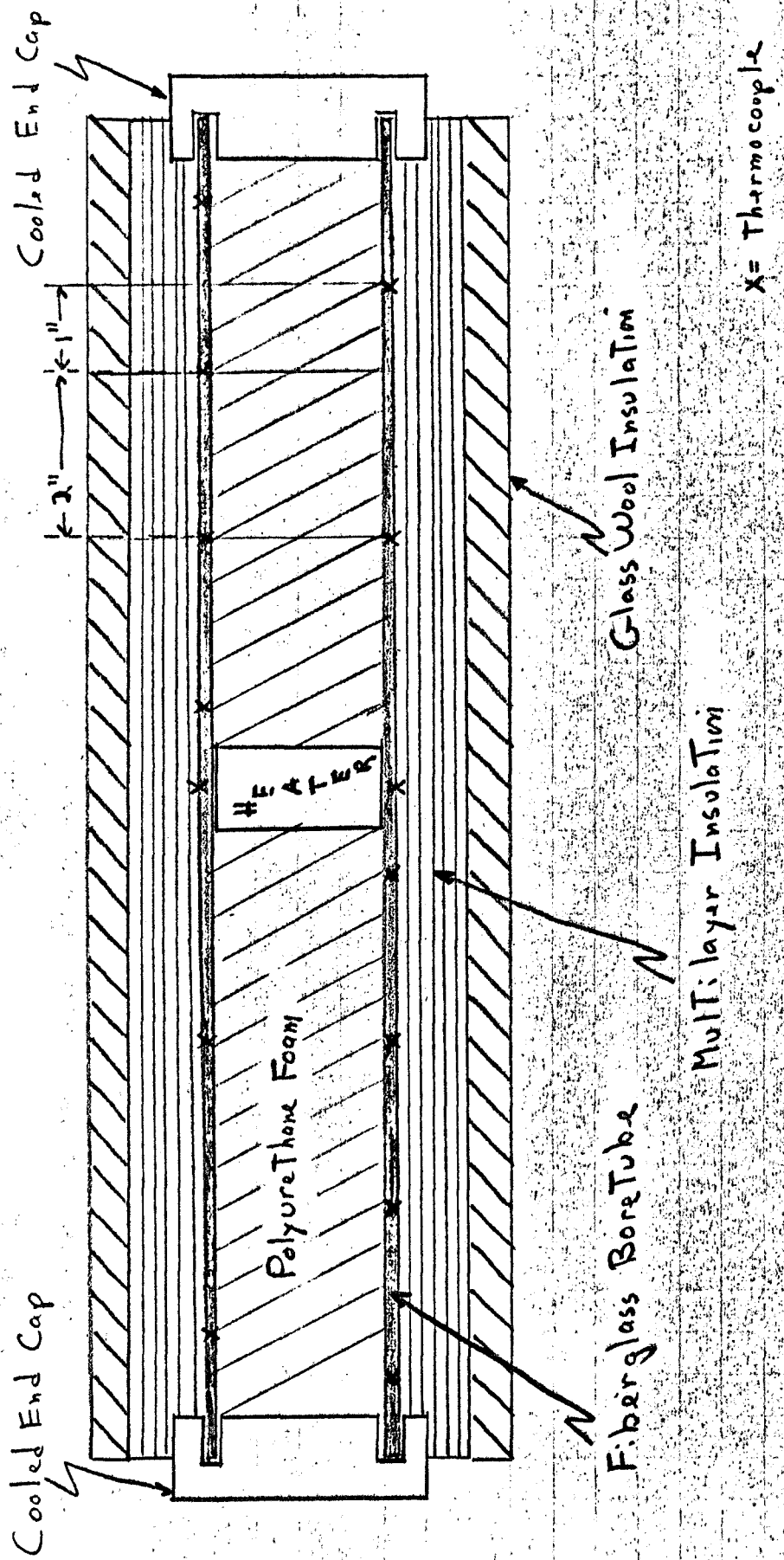

Figure 1 Schematic Diagram of Apparatus

KEUFFEL & ESSER CO. 250 14G

Figure 2 Temperature Profile in Boron Reinforced Tube - Room Temperature

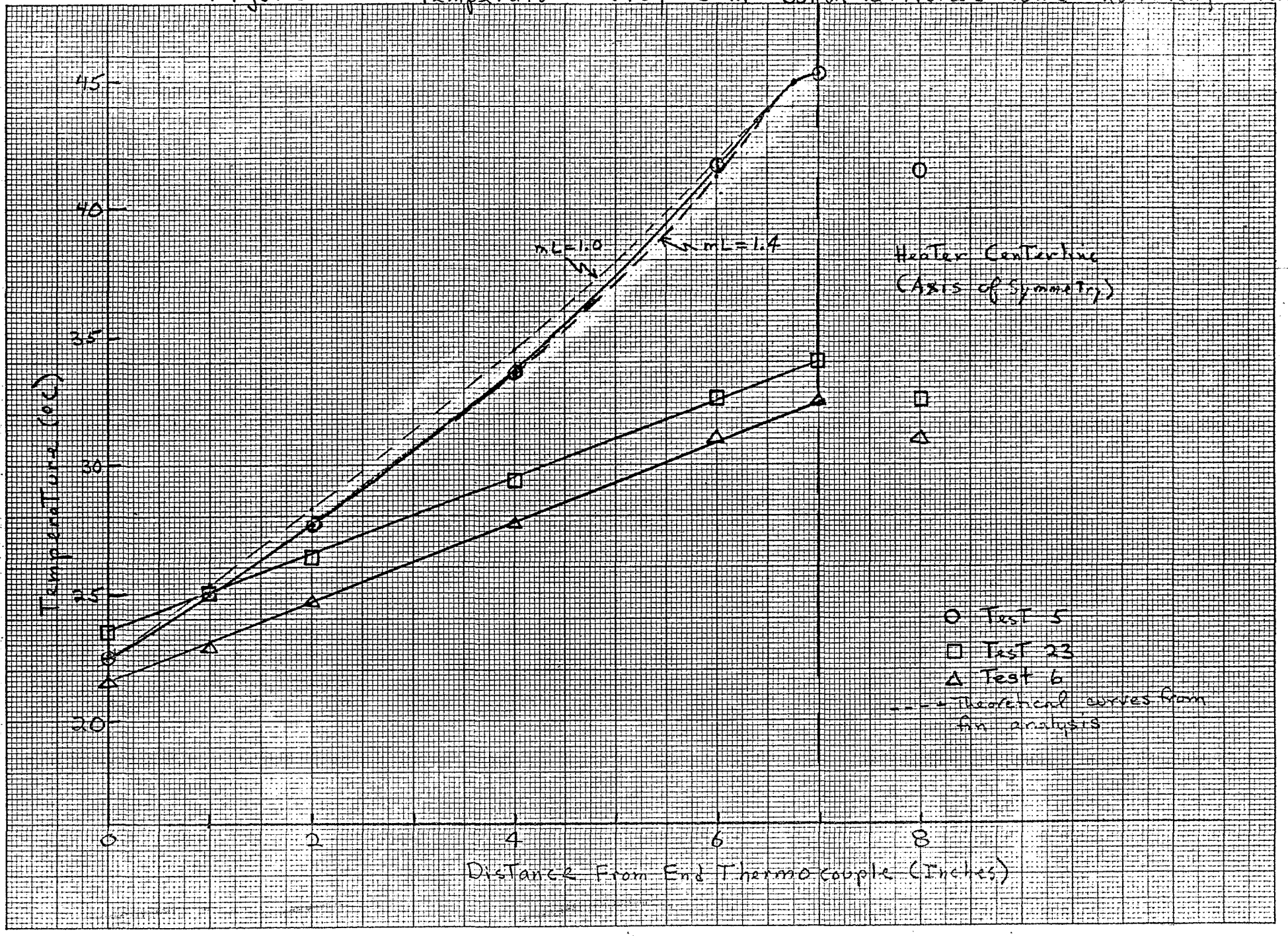

Fig 3.

Estimate of Casing Conductance

From Room Temperature Data.

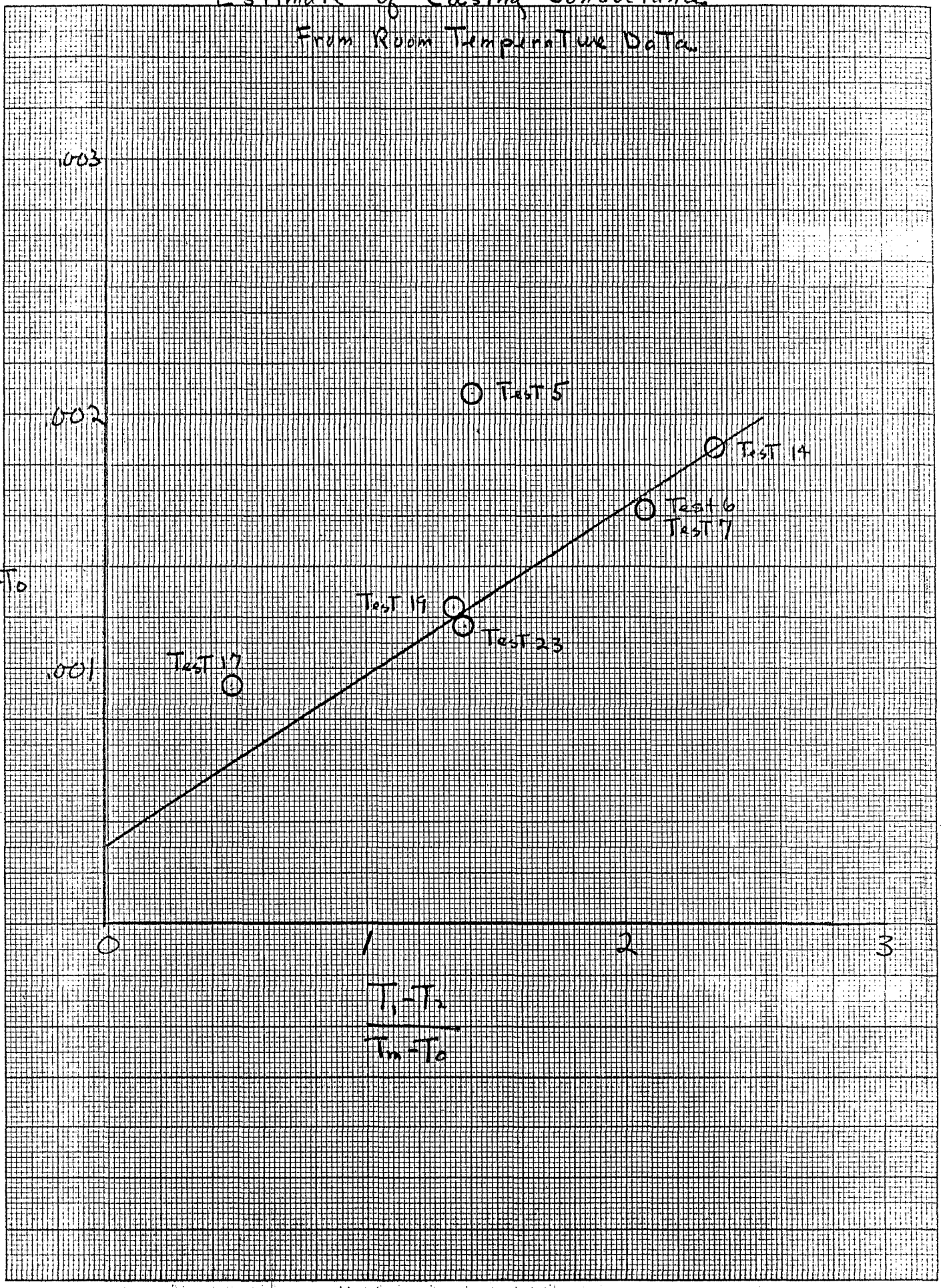

NO. 319-C. MILLIMETERS. 180 BY 250 DIVISIONS.
PRINTED IN U. S. A.

Figure 4 Temperature Profile in Boron Reinforced Tube - 330 °K

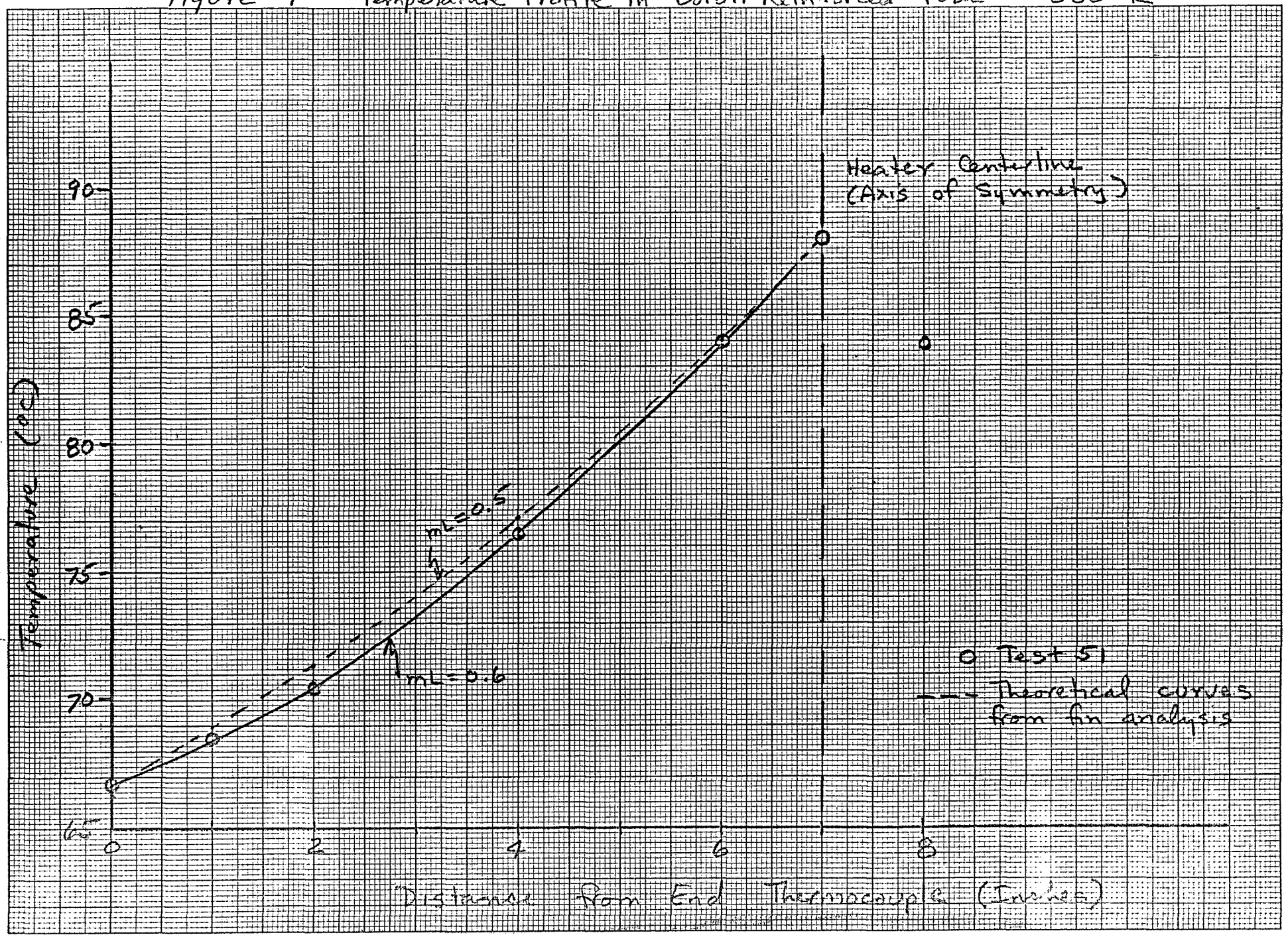

Figure 5 Temperature Profile in Boron Reinforced Tube - 230°K

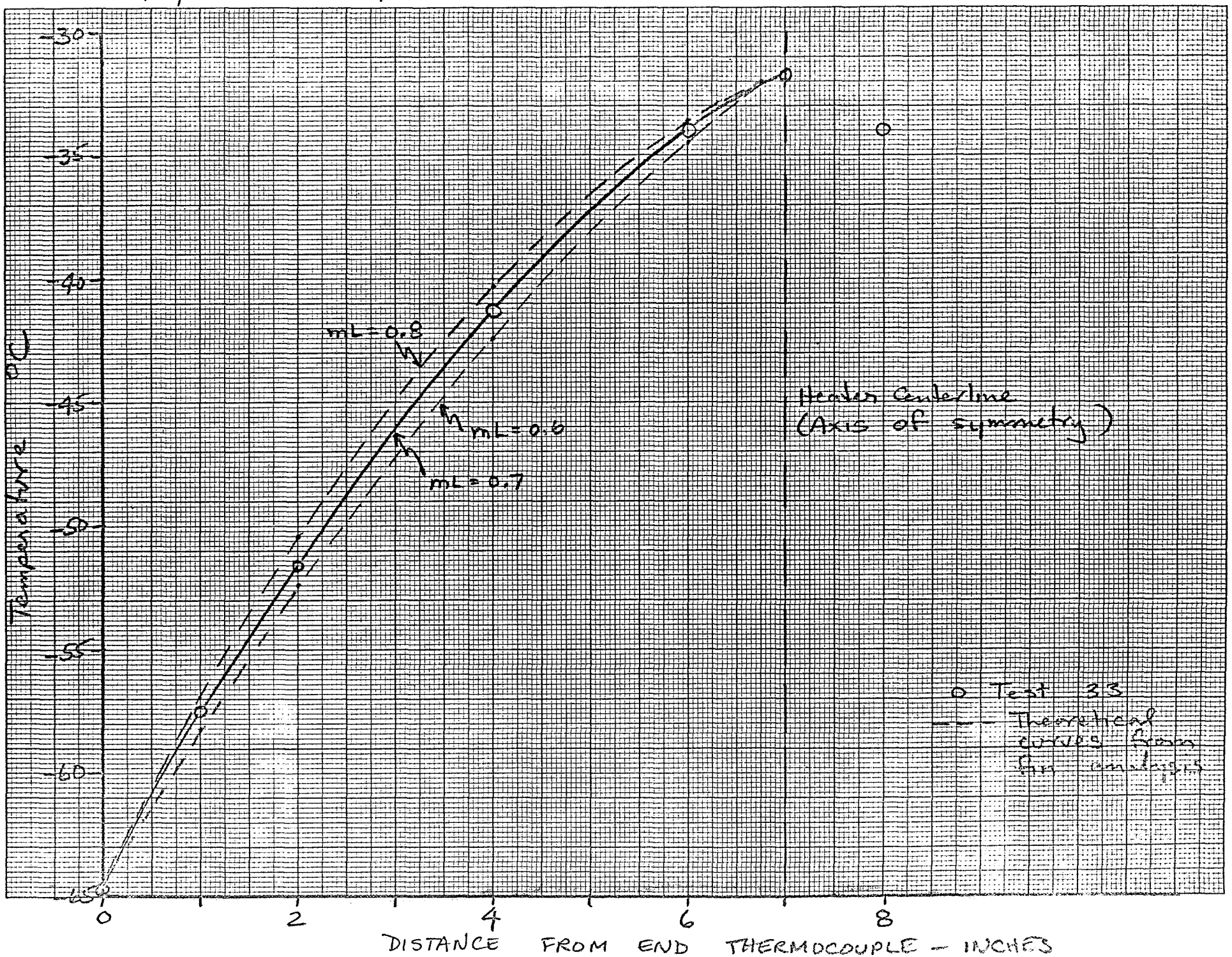

APPENDIX B

HFE PROGRAM

LAMONT-DOHERTY SC 7

CASE 71470

HEAT FLOW PROBE

THERMAL CONDUCTIVITY TESTS

MONTHLY PROGRESS REPORT NO. 3

AUGUST 25, 1969

Prepared Under

SUBCONTRACT SC 7

for

LAMONT-DOHERTY GEOLOGICAL OBSERVATORY

COLUMBIA UNIVERSITY

PALISADES, NEW YORK

ARTHUR D. LITTLE, INC.

CAMBRIDGE, MASSACHUSETTS

I. INTRODUCTION

This report summarizes the work accomplished by Arthur D. Little, Inc., under Subcontract SC 7 during the period 1 July 1969 to 1 August 1969. During this period we carried out portions of the following tasks:

A. Prepared plans and procedures for conduct of the test program.

B. Conducted tests with HFE Qualification Model Spare Probes No. 1 and No. 2 and the electronics.

C. Performed maintenance on test apparatus for calibration tests.

D. Reduced and analyzed the data and summarized the test results.

In the section that follows, we describe the progress made under each task, we indicate current problems which have occurred and corrective actions taken, and we discuss the work to be performed during the next monthly reporting period.

II. SUMMARY OF PROGRESS

A. Plans and Preparations

During the week of July 28, we submitted for approval our Test Procedures No. 0501, Part IV, Paragraph 9.0 for performing the Group IV tests. These are procedures for the tests to be performed with the Qualification Model Spare, Probe No. 1 to obtain data at the same temperature level and thermal conductivity value using both the Mode 2 and Mode 3 thermal conductivity measuring modes. The procedures are based on the development tests results performed with System Qualification Model Spare Probe No. 2 in thermal conductivity apparatus No. 2 during June and July. Test results are discussed in Section D of this report.

B. Test Program

Both the Group II and Group III tests were completed in this report period. The results of these tests are summarized in Section D of this report. As noted there, the 48-hour long, low thermal conductivity test using Heater H11 (Test K19D) produced anomalous results. This test will be repeated.

We plan to initiate Group IV tests when approval of the procedures is received. We expect that these will be completed prior to September 1.

C. Test Facility and Maintenance

In July, we performed routine maintenance on the HFE test facility. The Joseph Kaye thermocouple reference temperature instrument used with the thermal conductivity apparatus for absolute temperature measurements was replaced in July when the in-service unit failed.

D. Summary of Test Results

1. Group II Series

Figure 1 presents gradient sensor temperature rise data as a function of time for the four Group II (Mode 2) tests conducted during June and July. These tests with SQS-1 (SN 3, probe 1) are for heater positions 11, 13, and 14 at a nominal temperature level of 225°K, and heater position 12 at 205°K.

Observation of the results indicates an unusually high rate of temperature rise at long times in the H11 test. A more detailed evaluation of slope data suggests that a perturbation due to the test equipment probably caused this anomalous behavior and plans have been made to repeat this test. A malfunction in an ice point reference bath used in the temperature control system was discovered after this test was completed and is the probable cause of the equipment transient.

A test at H12 and 225°K was not included in the present Mode 2 series because this was one of the original acceptance test conditions for SQS-1. In the earlier test, the temperature rise after 18 hours was 0.391°K producing a curve which would fall between those plotted for H13 and H14 in Figure 1. However, this test was conducted to acceptance test standards which were somewhat less stringent than Group II test requirements. Because the present tests are to be used for detailed scientific evaluation of Mode 2 performance, vacuum levels in the test tank have been held below the 1μ level. The H12 acceptance test was run with an 8μ vacuum level which may result in a slight increase in the effective thermal conductivity of the bead bed due to residual gas conduction. It would be desirable to repeat this test at a low vacuum level to obtain results more directly comparable to the Group II tests.

2. Group III Series

Figure 2 shows Mode 3 ring sensor temperature rise data as a function of time for the four Group III tests with probe SQS-1 (SN 3) at heater

position H12. Test conditions include two absolute temperature levels - 205°K and 225°K - at each of two thermal conductivity values corresponding to helium-filled and nitrogen-filled glass beads.

Group III Test Conditions

Gas	Temperature (°K)	$K\left(\frac{\text{watts}}{\text{cm °K}}\right)$*
Helium	205°	4.95×10^{-3}
	225°	4.95×10^{-3}
Nitrogen	205°	1.54×10^{-3}
	225°	1.72×10^{-3}

The Group III temperature response curves (Figure 2) show an initial rise which is primarily a function of absolute temperature level. After about 100 minutes, the helium test curves level out more rapidly than do the nitrogen test curves. This behavior can be seen more clearly in Figure 3 which presents the first derivative or rate of temperature rise as a function of time for these tests. A clear distinction is made in the rate data between the helium and nitrogen test conditions after about 150 minutes; by 300 minutes, the effect of absolute temperature level has disappeared from the helium test data, and nearly disappeared from the nitrogen test data. In fact, the nitrogen results may be reflecting the 10 percent decrease in thermal conductivity of the nitrogen-filled bead bed between 225 and 205°K. The conductivity of helium-filled beads is almost independent of temperature in this range. These Mode 3 results are consistent with theoretical performance predictions. About a three-fold change in test bed conductivity is reflected in a 2.5-fold change

*From ADL measurements in guarded cold plate apparatus under BxA contract 0242.

in the value of the rate of temperature rise at 300 minutes after initiation of a Mode 3 experiment.

Further information will be extracted from the Group III experiments when temperature decay data are reduced for all sensor locations near the heater.

3. Preliminary Tests at 50μ Bead Pressure

Group IV tests are planned to simulate an intermediate value of thermal conductivity in the K Apparatus by operating at a partial vacuum. Mode 2 and Mode 3 experiments will be run at this controlled intermediate condition which should be selected to fall within the range where Mode 2 and Mode 3 ranges overlap.

Preliminary tests have been run to find a satisfactory operating point. These tests are for a 50μ nitrogen pressure level and were run using probe 2 in the K-2 Apparatus to avoid interference with the regular test series. Also, the Mode 2 procedure development test was performed at 205°K absolute temperature level although both of the official Group IV tests are to be run at 225°K.

Results from the Mode 2 test at H22 are shown in Figure 4. Dashed lines show equivalent response curves for H12 Mode 2 tests at 205°K both in the ΔT Apparatus ($K \approx \infty$) and in the K Apparatus with vacuum level below 1μ. If differences between probe 1 and probe 2 are ignored, the spread of the curves in Figure 4 indicate that the 50μ pressure level corresponds to about $K = 1.5 \times 10^{-4}$ watts/cm°K.

Figure 5 presents data from a Mode 3 test run at the same 50μ bead pressure at at 205°K. The rate of temperature rise for this test is shown in Figure 6. Dotted lines show similar 225°K data for H12 during tests with nitrogen-and helium-filled beads. At 300 minutes into the Mode 3 test, the ratios of the rise rates are 1:2.5:7.1. If we use the helium and nitrogen tests to determine a relationship between slope at 300 minutes and thermal

conductivity, we find a proportionality between thermal conductivity and the -1.25 power of the slope. Scaling on this crude basis, the estimated thermal conductivity for the 50μ test condition would be about 4.5×10^{-4} watts/cm°K. Because of the longer time constant for the 50μ test, the slope at 300 minutes is still being affected by short term effects and scaling of results in the above manner is not justified. If longer term data were available, the response curve would be levelling out so that a lower value of thermal conductivity would actually be predicted. To properly interpret these data, the Mode 3 computer model presently being developed under Subcontract No. 8 should be employed.

For present purposes, however, these tests indicate that 50μ provides a good intermediate thermal conductivity operating point. Much lower pressures would create problems in Mode 3 because the 2°K range of the ring sensor would be exceeded before short term effects had dissipated. For control purposes, Group IV tests will be conducted at 45μ pressure since the vacuum gage undergoes a scale change at 50μ.

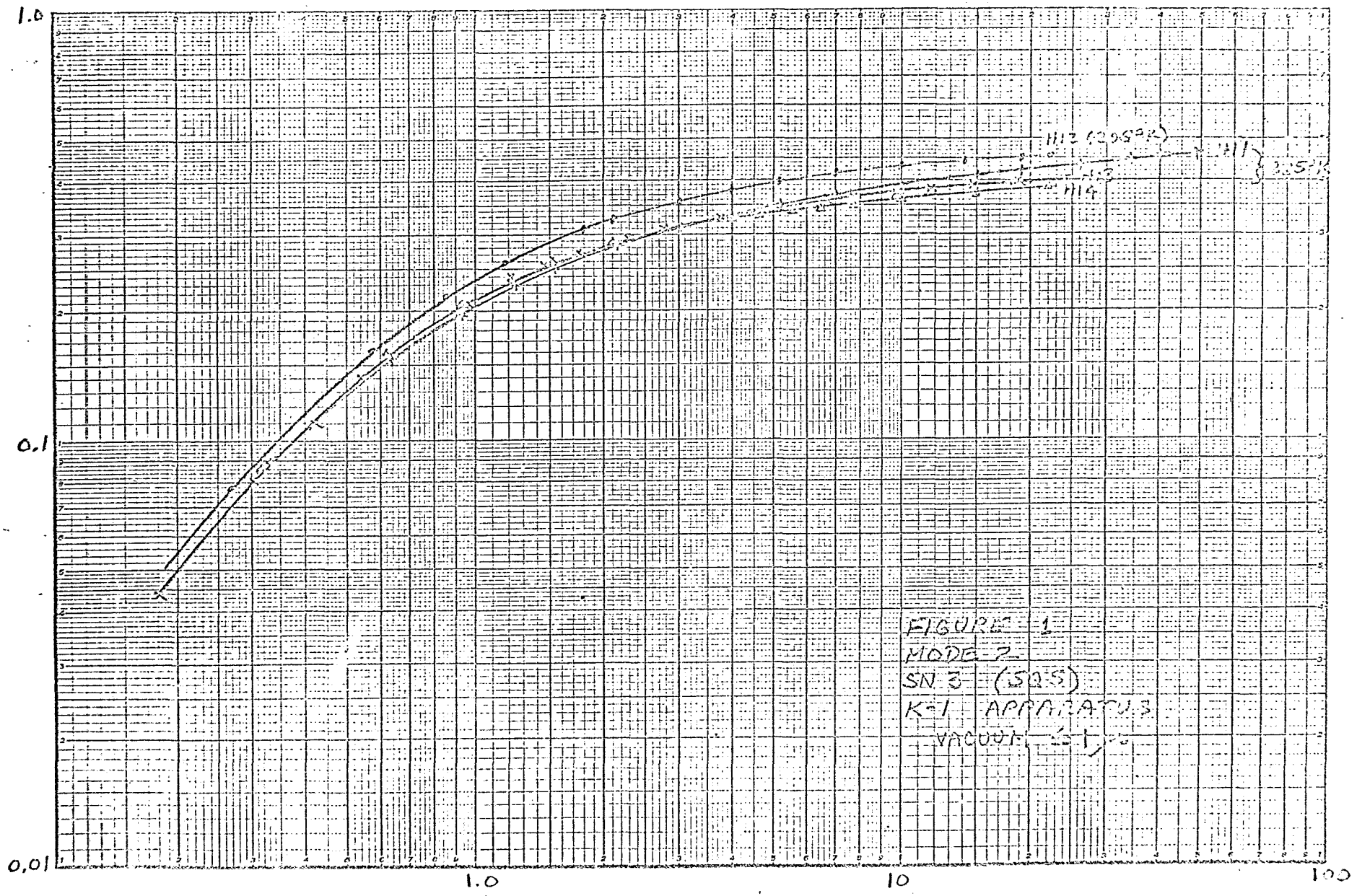
GRADIENT SENSOR TEMPERATURE RISE °K
1.0
0.1
0.01
1.0
10
100
TIME FROM START OF HEATING - HOURS
H12 (295°K)
H11
H14
FIGURE 1
MODE 2
SN 3 (295°K)
K-1 APPARATUS
VACUUM 5-1

Figure 1

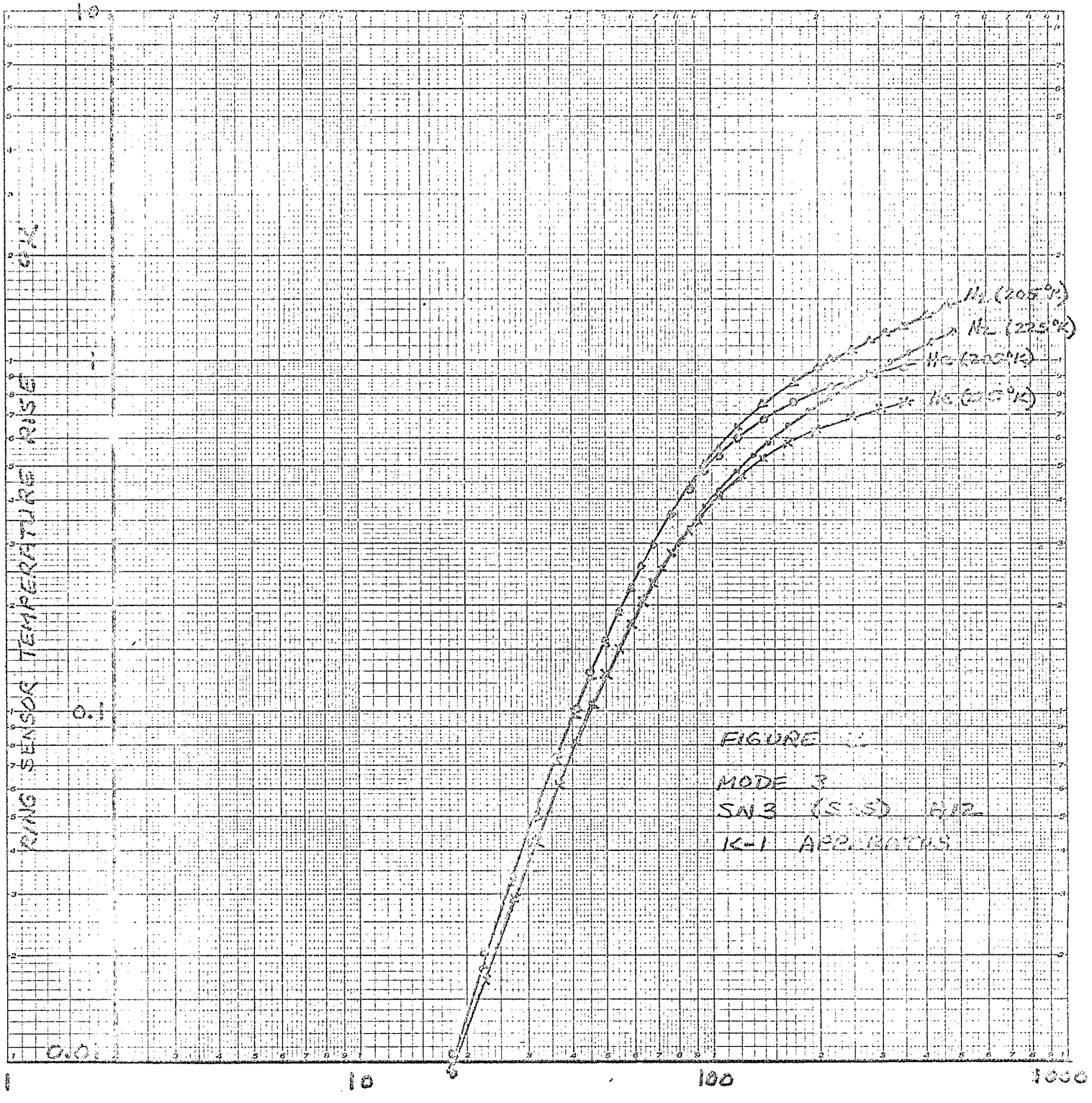

TIME FROM THE START OF HEATING - MINUTES

Figure 2

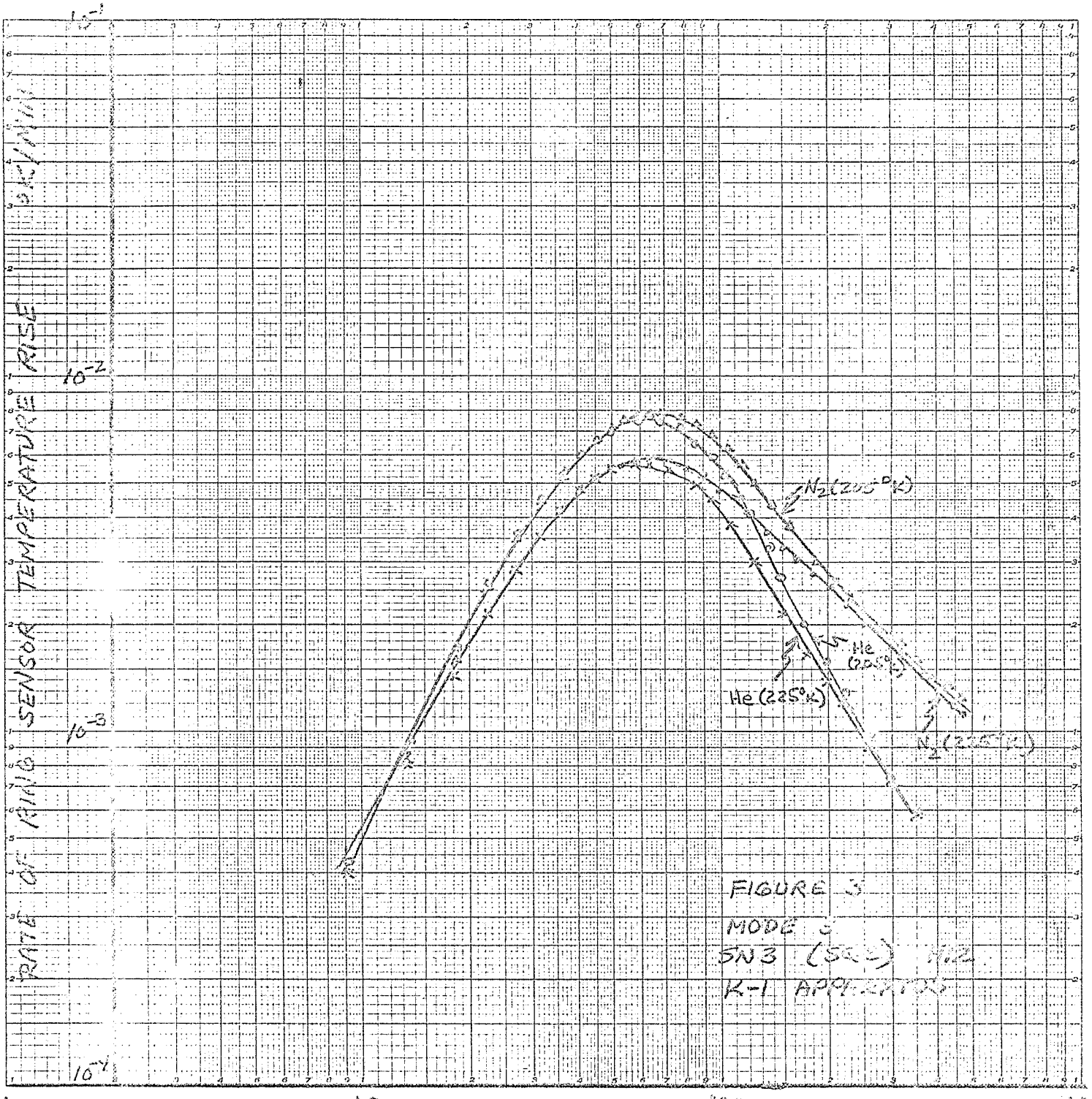

FIGURE 3
MODE 3
SN3 (SC-1) N-2
K-1 APPARATUS

TIME FROM THE START OF HEATING - MINUTES

Figure 3

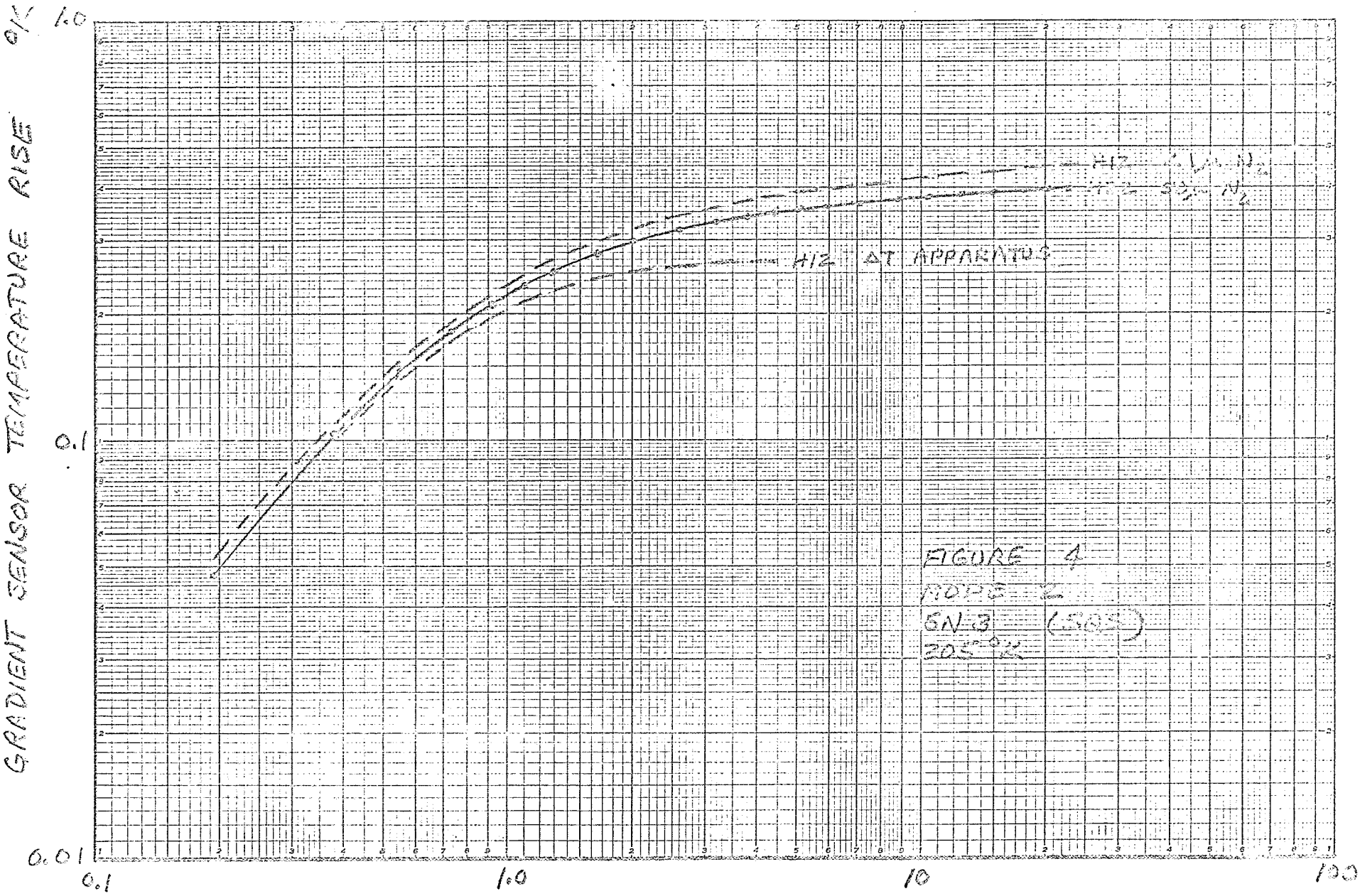
GRADIENT SENSOR MOUNTED IMMERSION RISE
1.0
0.1
0.01
0.1
1.0
10
100
TIME FROM START OF HEATING - HOURS
FIGURE 4

Figure 4

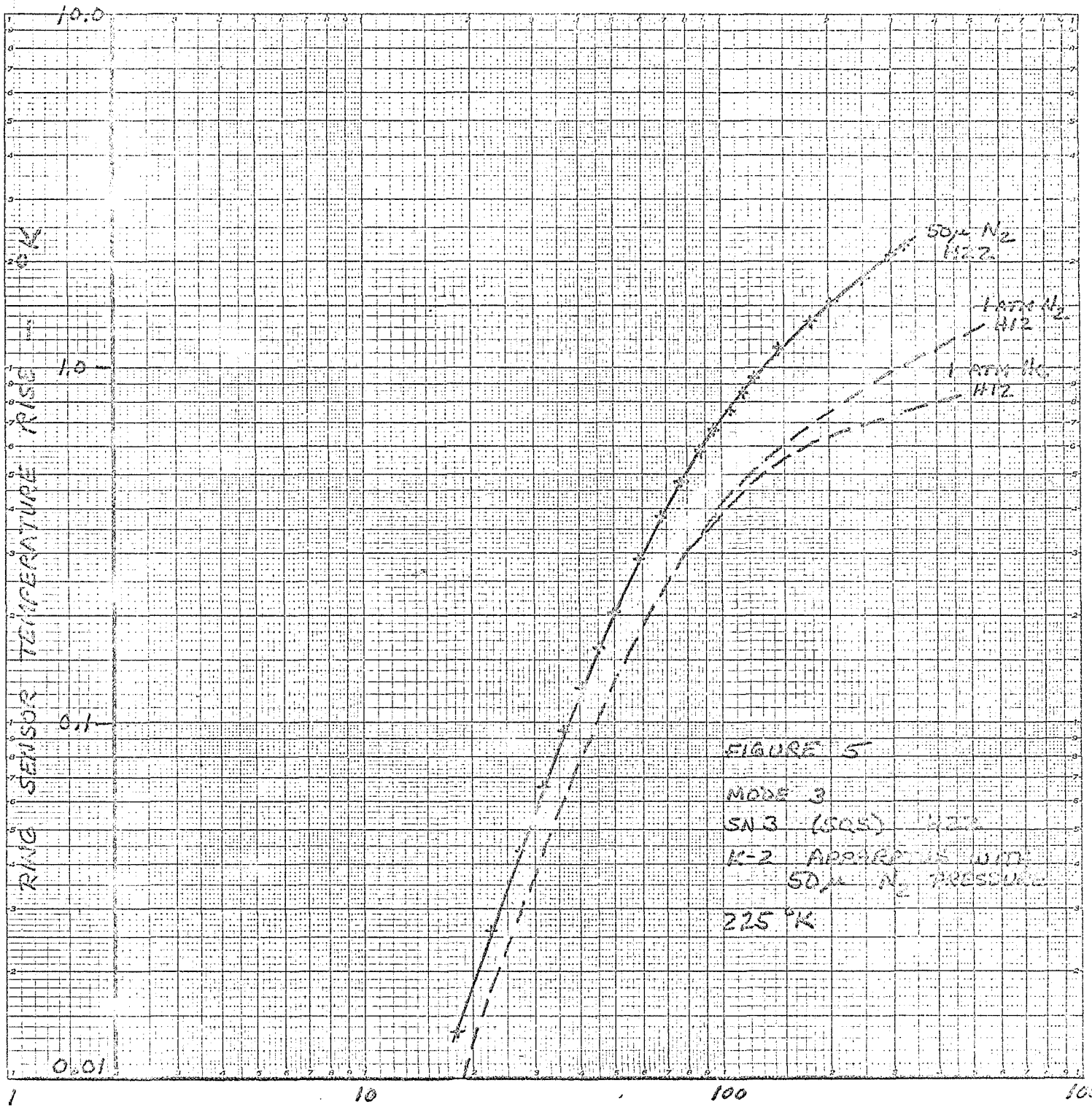
10.0
1.0
0.1
0.01
RING SENSOR TEMPERATURE RISE °K
50% N2 H2
1 ATM N2 H2
1 ATM H2
1
10
100
1000
TIME FROM START OF HEATING - MINUTES
FIGURE 5
MODE 3
SN 3 (SOAS)
K-2 APPARATUS
50% N2 PRESSURE
225 °K

Figure 5

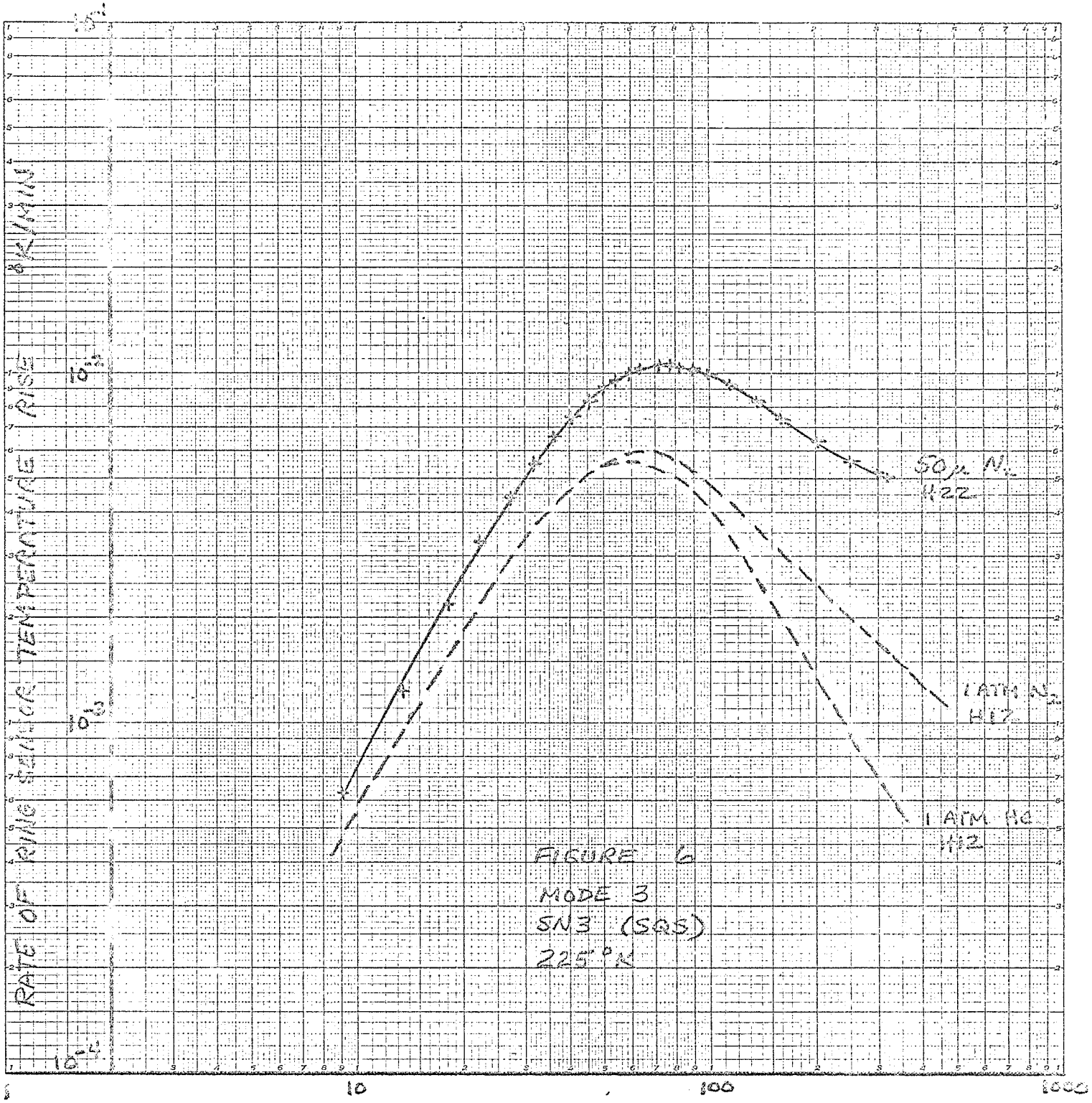
RATE OF RING SENSOR TEMPERATURE RISE °K/MIN
10^{0}
10^{-1}
10
100
1000
50 μ N₂ H2Z
1 ATM N₂ H2Z
1 ATM N₂ H1Z
FIGURE 6
MODE 3
SN3 (SQS)
225°K
TIME FROM THE START OF HEATING - MINUTES

Figure 6

APPENDIX C

Technical Memorandum No. 1

Preliminary Thermal Analysis of Heat Flow Probe and Lunar Medium

prepared for

Lamont Geological Observatory
Palisades, New York

Under Subcontract No. 8 of
Prime Contract No. NAS9-6037
with Columbia University

by

D. Nathanson
R. Merriam

Arthur D. Little, Inc.
Cambridge, Massachusetts 02140

May 29, 1969

C-71424

TABLE OF CONTENTS

Arthur D. Little, Inc.

LIST OF FIGURES

LIST OF TABLES

Arthur D. Little, Inc.

I. SUMMARY AND CONCLUSIONS

A preliminary analytical study was performed to determine the requirements for an accurate computer thermal model of a heat flow probe and the feasibility of obtaining an accurate model of the surrounding lunar medium. In both instances, heat flow equations were written in finite-difference form using the Zone Method of Strong and Emslie* and solutions were obtained using a generalized thermal analyzer program (ADLGTA).

The lunar medium was modeled by many layers of concentric annuli whose thickness was chosen to vary with distance from the probe location. A procedure was developed for numbering the nodes and for generating the input data to the thermal analyzer program. Solutions for the temperature distribution arising from a point heat source were obtained and were compared with exact solutions. The agreement between exact and computed temperature distributions was found to be adequate, demonstrating that this approach is suitable for computer modeling the lunar medium in our Phase II effort. For a lunar model containing nearly 200 nodal points, the computing time was less than one second per time step on a CDC 6600 computer.

Calculations of temperatures and temperature differences were made for a low-conductance probe sheath 50 cm long surrounded by a drill casing, which was, in turn, surrounded by a medium with a specified temperature gradient of 0.04°K/cm (2°K ΔT over 50 cm). The number of finite-difference subdivisions was varied until the computed ΔT over both the probe sheath and drill casing was not influenced by a further increase in the number of subdivisions. The results showed that a requirement of a maximum vertical subdivision size of 2 cm in the probe sheath, drill casing and lunar medium is adequate for an accurate description of heat flow along the probe sheath. This requirement will be observed when we prepare detailed computer models of experiment locations during our Phase II effort.

---

* Strong, P. F. and Emslie, A. E., "The Method of Zones for the Calculation of Temperature Distribution," Paper 65 WA/HT-47, 1965, American Society of Mechanical Engineers.

II. THERMAL MODEL OF LUNAR MEDIUM

A. Introduction

The primary goals of the Phase I analysis of the lunar medium can be summarized as follows:

a. Development of finite-difference models for lunar medium.

b. Development of computer routines to set up model and solve equations.

c. Investigation of computer running time required to solve equations.

Within the following sections, the work performed to meet these goals will be described.

B. Finite-Difference Model

The lunar medium was modeled as a series of layers of concentric annuli of varying thicknesses. Heat flow equations are written for each surface of an individual element in accordance with the Method of Zones' technique, and solved using an existing Generalized Thermal Analyzer (ADLGTA).

Figure 1 illustrates a typical element. Shown in the figure are the coordinate system and the dimensions of the ring. Within each element a parabolic temperature distribution is assumed and expressions for the net heat flow from faces 1 through 4 are found in terms of the average surface temperatures, T_1 through T_4 and the mean temperature of the element, T_m:

$$Q_1 = \frac{2\pi k \ell a}{b - a}\left(6T_m - \frac{3b + 5a}{b + a}T_1 - \frac{3b + a}{b + a}T_2\right) \quad (1)$$

$$Q_2 = \frac{2\pi k \ell b}{b - a}\left(6T_m - \frac{5b + 3a}{b + a}T_2 - \frac{b + 3a}{b + a}T_1\right) \quad (2)$$

$$Q_3 = \frac{k\pi(b^2 - a^2)}{\ell}\left(6T_m - 4T_3 - 2T_4\right) \quad (3)$$

$$Q_4 = \frac{k\pi(b^2 - a^2)}{\ell}\left(6T_m - 4T_4 - 2T_3\right) \quad (4)$$

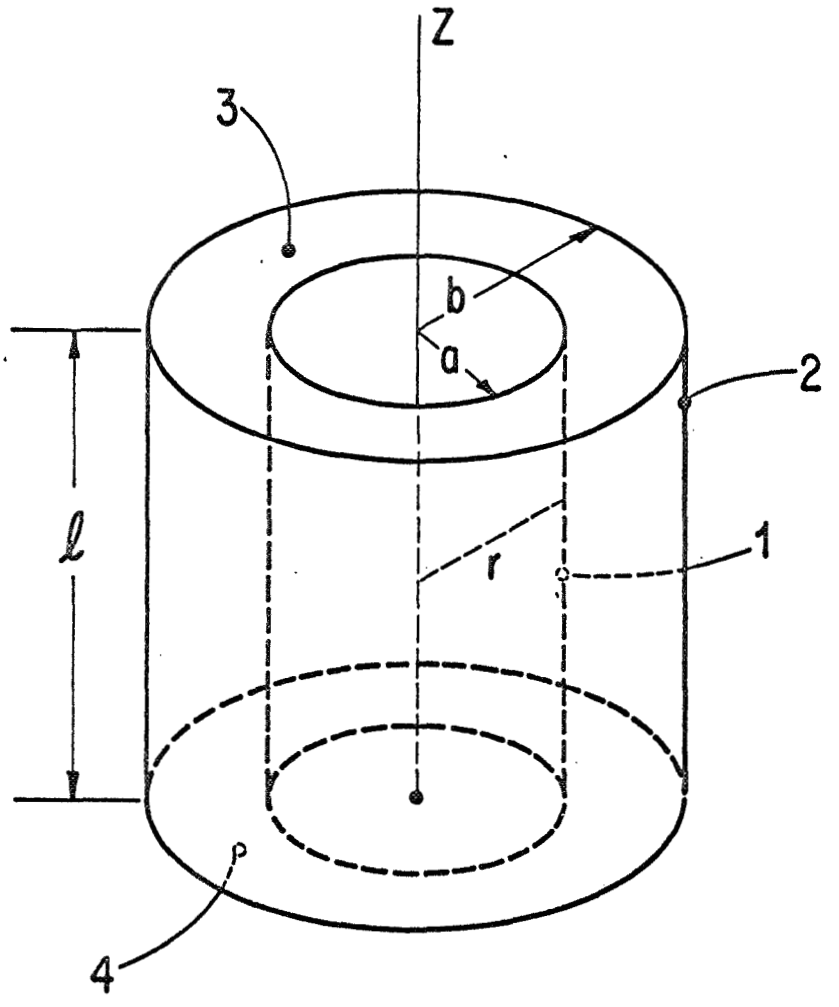

FIGURE 1 ANNULAR CYLINDER ELEMENT OF LUNAR MEDIUM

The equation for the mean temperature of the zone is described by Equation (5):

$$Q_1 + Q_2 + Q_3 + Q_4 + \rho \pi (b^2 - a^2) \ell C_p \frac{dT_m}{dt} = 0 \qquad (5)$$

where ρ is the density and C_p is the specific heat of the lunar medium.

Thermal connection between the zones is made by way of the net heat flows at the zone surfaces. For example, the heat flow from the outer surface of an element (surface 2 in Figure 1) is equal to the negative of the heat flow from the inside surface (1) of the surrounding annular ring. Special boundary conditions are applied at the outermost - or boundary - surfaces. The method of treating these faces will be discussed below.

The vertical height, ℓ, of each element was chosen to be a constant whose value depends on the properties of the medium and the mode of probe operation. On the other hand, because of the rapid attenuation of a thermal wave within the medium, the thickness of each zone varies with the radial distance, r. Since the temperature distribution from a point heat source - as well as from a spherical surface heat source - varies approximately as 1/r, the thickness, and hence the ratio of outer to inner radii b/a, was chosen to vary as r. That is,

$$b \equiv c_2 a$$

where c_2 is a parameter. The lunar medium is then composed of M vertical layers of N concentric annuli whose height are ℓ and whose outer to inner radii have ratio c_2.

At the boundaries, the heat flow from the surfaces are matched with the form of solution predicted for a point heat source or a spherical surface heat source:

$$Q'' = \frac{k}{R^*} T (R^*, t) - \frac{k}{R^*} T_\infty + f (Q_o, R^*, t) \qquad (6)$$

where

R^* = distance from center of source

Q_o = strength of heat source

T_∞ = initial temperature of lunar medium

The function f (Q_o, R^*, t) is nearly zero for short times.

C. Method of Solution

The finite-difference equations resulting from the thermal model described above are solved with ADLGTA. This digital computer program allows the equations to be written in implicit form (with respect to time) so that time steps taken in the solution may be chosen independent of numerical stability limitations.

To obtain an accurate thermal model of the lunar medium, a large number of zones is required. Associated with each zone are 4 surfaces. If there are M vertical and N radial subdivisions, the total number of equations required to describe the medium is 3 M N + M + N. For the present problem, the average number of input data cards associated with each equation is approximately 8-10. Hence, for 11 vertical and 5 radial subdivisions the total number of equations is 181 corresponding to nearly 1,500 data cards.

To assist in the preparation of this enormous number of data cards, a program was written. Input to the program are the lunar soil properties, strength of heat source, probe dimensions and number of subdivisions desired.

In the preparation of input cards, an automatic numbering system was adopted. Figure 2 illustrates this system. Each zone is identified by the constants I and J where the maximum value of J (M) is an odd number so that the cylindrical heat source (surrounding the gradient sensor) makes up the innermost element of the central layer. In Figure 2 the plus signs schematically represent the mean temperature node, while the dots represent the surfaces shown as 1 through 4 in Figure 1.

In addition, a program was written to determine the distance of each temperature location from the center of the heat source and the local transient temperatures. The program is useful for checking the thermal model against available solutions as well as in aiding in the choice in the size of the subdivisions.

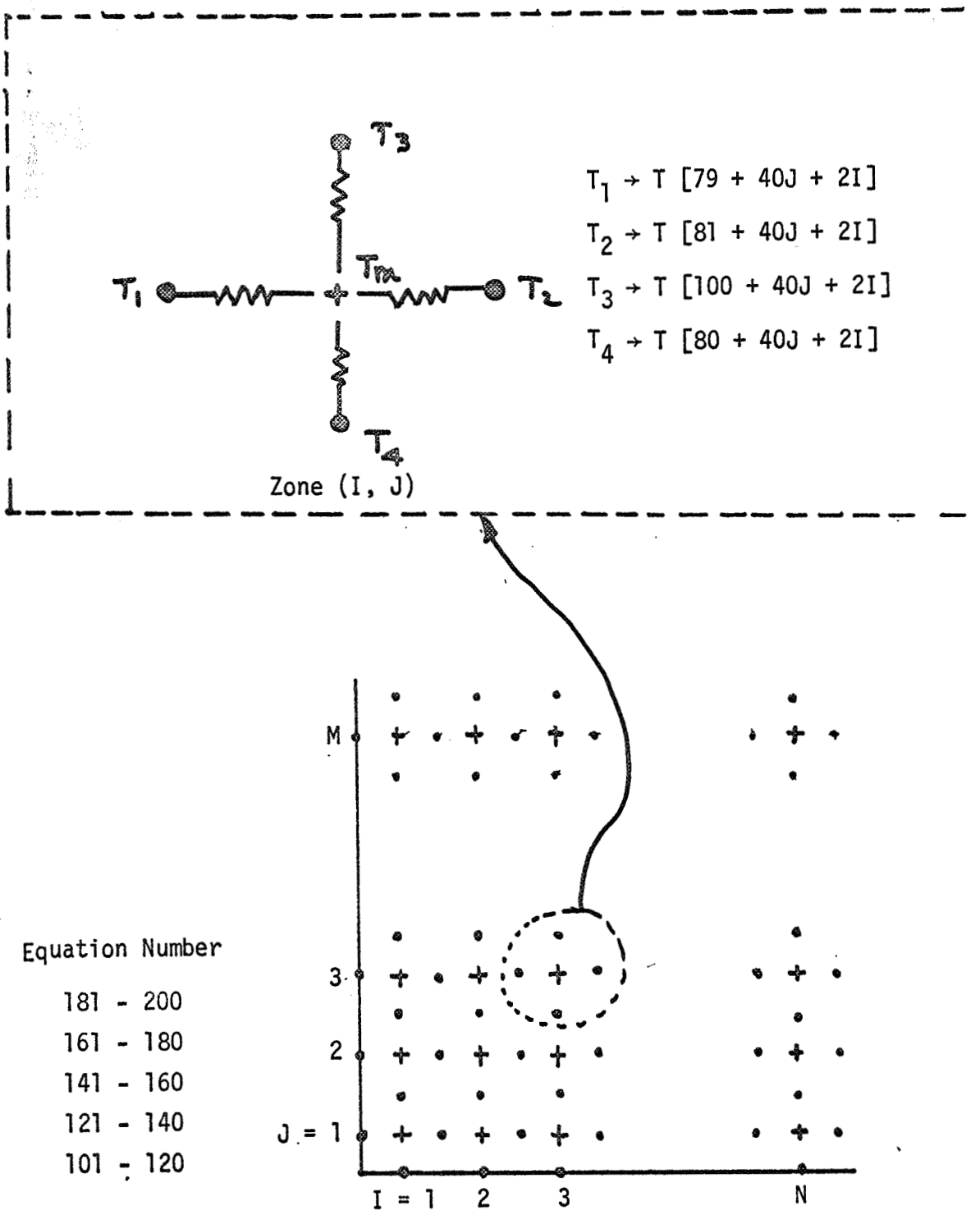

FIGURE 2 NUMBERING PATTERN FOR TEMPERATURE LOCATIONS (See Text)

D. Results

Solutions were obtained for a point heat source within an infinite medium of various thermal conductivities. For these cases, the probe was replaced by cylindrical elements of lunar material where the central element has a source of heat Q_o.

As a result of preliminary studies, several modifications were made to the thermal analysis program. The most important change was a doubling of the field length for the input of thermal conductances. To obtain accurate heat balances at each node point, the thermal couplings must be specified to nine significant digits.

Furthermore, a change was made in the method of treating the boundary conditions. It appears that the accuracy of the numerical solutions can be improved by retaining only the first two terms on the right-hand side of Equation (6). The reason for this is not clear and is being investigated more closely.

A comparison between some computed local temperatures and exact solutions is given in Table 1. The lunar medium was assumed to be initially uniform at 230°K; the temperatures listed in Table 1 are the increases over the initial temperature (°K). Each zone is identified by the indices (I, J) as defined in Figure 2 and by the distance from the source R^* (cm). The heat source Q_o and thermal conductivity k are in units of watts and watts/cm-°K, respectively. Cases A and B correspond to Mode 2 operation and Mode 3 operation, respectively.

The agreement between computed and exact values of local temperatures is adequate and encouraging, indicating that the above approach is suitable for computer modeling the lunar medium in our Phase II effort. Since these results were obtained early in our program with limited experience gained in applying the thermal model, we believe the agreement will improve when we do further work in preparing models of the lunar medium for our Phase II work.

The computing time required to obtain these solutions is very short - less than one second per time step. Total time required to compute the local temperatures (at about 200 temperature locations) at a time of 300 minutes was less than 30 seconds in each case.

TABLE 1

NUMERICAL SOLUTIONS FOR HEAT FLOW FROM POINT SOURCE

IN INFINITE LUNAR MEDIUM

		CASE A			CASE B		
TIME	(I, J)	R^*	T_{NODAL}	T_{EXACT}	R^*	T_{NODAL}	T_{EXACT}
150.0 min.	(1, 3)	2.877	6.5773	6.9961	2.522	0.0138	0.0258
	(3, 3)	4.303	1.7397	1.6139	2.908	0.0070	0.0098
	(1, 5)	1.777	23.0459	21.4920	1.562	0.2318	0.2124
	(3, 5)	3.660	3.4109	3.1710	2.129	0.0[illegible]4	0.0636
	(5, 5)	8.076	-0.0109	0.0129	2.980	0.0114	0.0081
300.0 min.	(1, 3)	2.877	11.4510	11.4108	2.522	0.0649	0.0803
	(3, 3)	4.303	4.4951	4.0769	2.908	0.0403	0.0429
	(1, 5)	1.777	29.2959	27.4299	1.562	0.3804	0.3518
	(3, 5)	3.660	6.9042	6.4637	2.129	0.1676	0.1480
	(5, [illegible]	[illegible]076	0.1799	0.2113	2.980	0.0576	0.0381

CASE A: $Q_o = 0.5$, $k = 0.0005$, $\rho_c = 1.5$, $T_\infty = 230.0$

CASE B: $Q_o = 0.002$, $k = 0.0001$, $\rho_c = 1.5$, $T_\infty = 230.0$

Arthur D. Little, Inc.

In summary, because of the relatively short time required to solve the finite-difference equations and the adequate agreement between computed and exact temperature distributions, the proposed techniques for modeling the lunar medium is very promising.

III. SUBDIVISION REQUIREMENTS FOR LUNAR PROBE

A. Introduction

The selection of a finite-difference subdivision of the lunar heat flow probe is dependent on: 1) the subdivision necessary to accurately describe the characteristics of the probe assembly including construction details in the gradient and ring sensors, and 2) the size of the vertical subdivisions in the low-conductance probe sheath necessary to render an accurate description of the heat flow between sensor locations. The following discussion describes numerical experiments performed to determine the requirements for vertical subdivisions in the low-conductance probe sheath and the drill casing. The results of this study will also serve as a guide for vertically subdividing the lunar medium which communicates with the drill casing by radiation.

B. Thermal Models

Two thermal models, shown schematically in Figure 3, were used to examine the relationship between the number of subdivisions in the probe and the accuracy of the temperature predictions. Model A considers an epoxy-fiber-glass probe sheath 50-cm long separated from a surrounding medium by a radiation gap. The surrounding medium has a specified temperature difference of 2°K; the temperature varies linearly from 240°K at the lower end to 238°K at the top end. The emittances of the outer surface of the probe sheath and the internal surface surrounding medium are taken as unity. The heat flow in the probe sheath is governed by radiation on its outer surface and conduction along its length. In this physical model, the internal surface of the sheath and its ends are adiabatic. Model B considers a similar arrangement with a drill casing (lunar drill string) interposed between the probe sheath and the surrounding

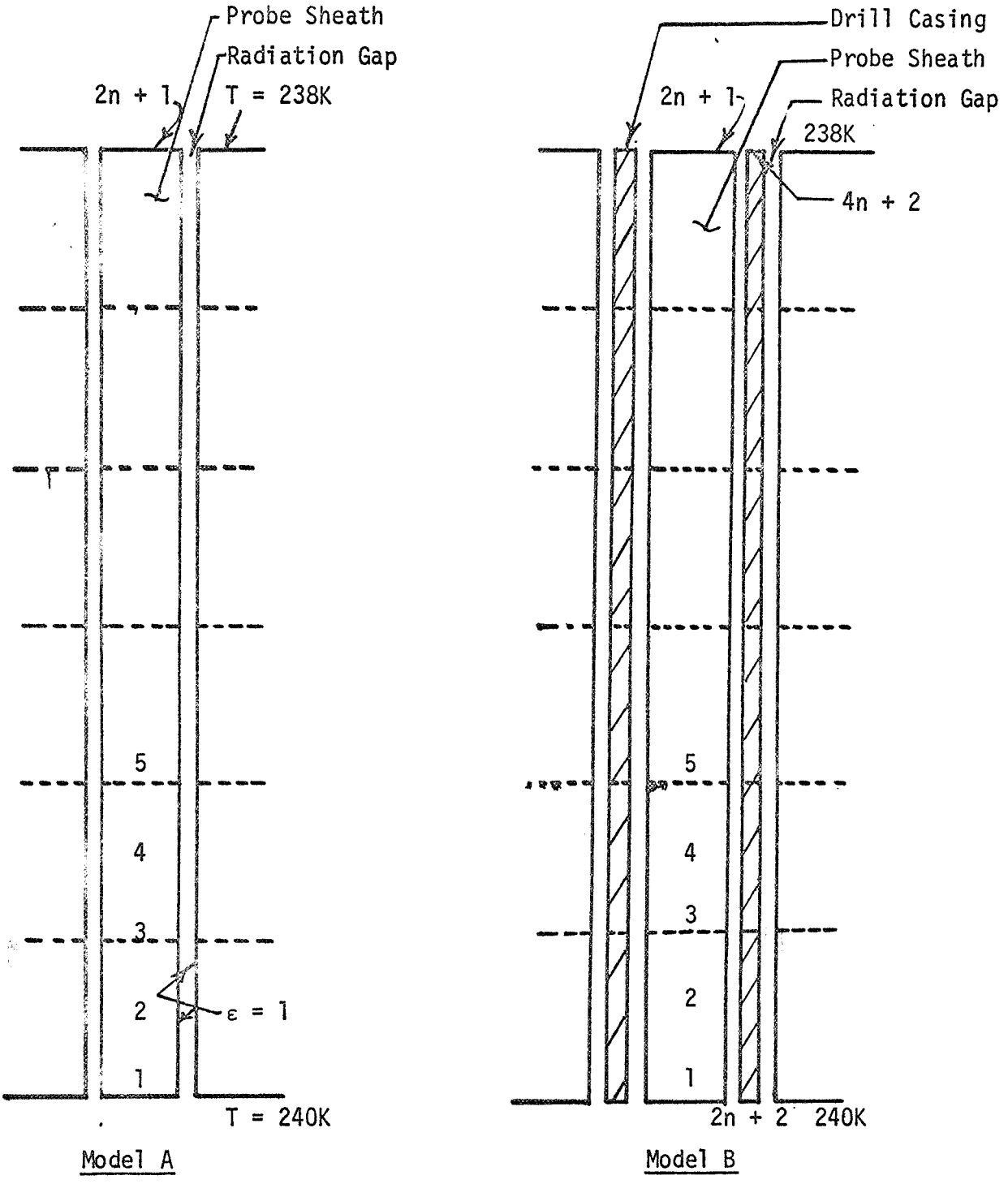

NOTE: Dotted line denotes finite-difference subdivision

$\Delta T_{probe} = T_1 - T_{2n+1}$

FIGURE 3 THERMAL MODELS FOR STUDY OF SUBDIVISION REQUIREMENTS IN LUNAR PROBE

Arthur D. Little, Inc.

medium. This drill casing radiates internally to the probe sheath and externally to the surrounding medium having a specified 2°K ΔT over 50 cm.

The thermal properties and dimensions used in setting up the thermal models are summarized below:

Description	Thermal Conductivity (w/cm°K)	Thickness (cm)
Probe sheath (Models A and B)	5×10^{-3}	0.0317
Drill casing (Model B)	7.62×10^{-3}	(0.292 effective)

The thermal conductivity of the drill casing has not been measured experimentally to date. Thermal properties shown above for the drill casing are based on an effective conductivity-area product (KA) of 17.6×10^{-3} w/cm°K which was calculated analytically. We expect that the measured values of casing thermal conductance will exceed those used in our preliminary calculations. Therefore, the estimated values of conductance describe a conservative condition for the evaluation of subdivision size required for accurate temperature predictions. That is, in systems governed by radiation and conduction (radiating fin effect), the subdivision size for accurate calculations is proportional to the thermal conductance of the radiating object.

The number of equal-length subdivisions in the probe sheath (and both the probe sheath and drill casing for Model B) was varied from a minimum of 2 to a maximum of 40. Because of the large amount of data preparation for this study, input data for ADLGTA was prepared by computer routines.

C. Results

The results of the study of subdivision size in the probe sheath are shown graphically in Figure 4 where the end-to-end ΔT in the probe is plotted as a function of the number of equal subdivisions (and subdivision size). For Model A, which considers the probe sheath directly exposed to

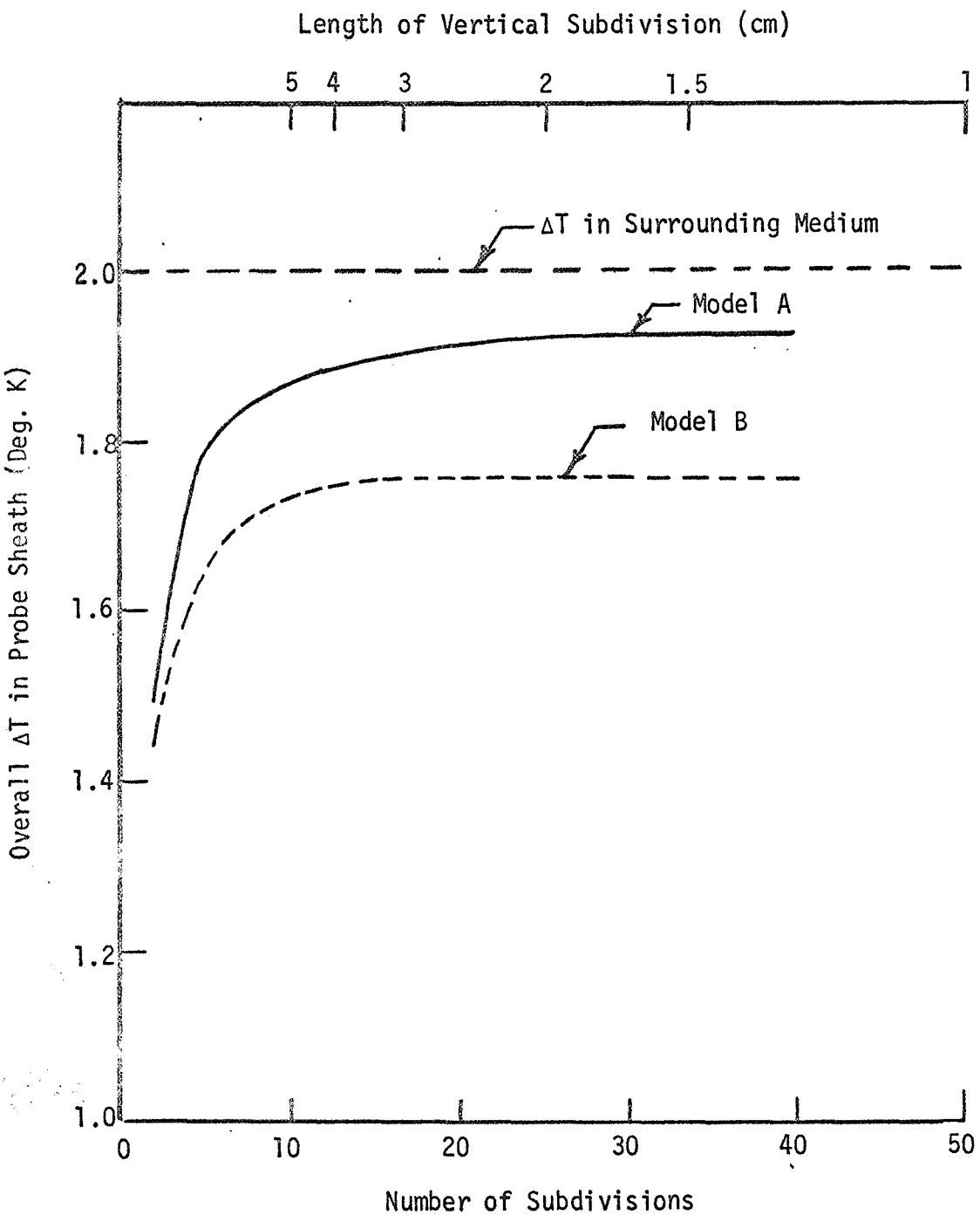

FIGURE 4 COMPUTED VERTICAL TEMPERATURE DIFFERENCE IN PROBE SHEATH VERSUS NUMBER OF SUBDIVISIONS

the environment, the dependence on "n", the number of subdivisions drops off at approximately 30 subdivisions. Increasing "n" from 30 to 40 increases the computed ΔT by less than 0.01°K. The calculations for Model B show that a subdivision length of 2 cm (n = 25) is adequate for the probe when the drill casing is considered in the calculation. Here, increasing "n" from 20 to 30 changes the computed ΔT in the sheath by less than 0.005°K. It can also be noted that the consideration of the drill casing caused a reduction in the ΔT measured over the probe sheath. The ΔT changes from 1.94°K for Model A to 1.77 for Model B.

In summary, in formulating detailed thermal models of the lunar heat flow probe in the regions of the gradient and ring sensor, the length of vertical subdivision should not exceed 2 cm. This requirement also applies to thermal modeling of the drill casing and lunar medium in the same region.

Progress Report

Prepared for

Lamont-Doherty Geological Observatory
of Columbia University
Palisades, New York

Contract:

Thermal Analysis of the Heat Flow Experiment
Subcontract No. 8
of Prime Contract No. NAS9-6037
with Columbia University

Reporting Period:

1 May 1969 to 1 August 1969

Prepared by:

Arthur D. Little, Inc.
Cambridge, Massachusetts

1 August 1969

C-71424

Arthur D Little Inc.

I. INTRODUCTION

Our work and progress on the thermal analysis of the Heat Flow Experiment were comprehensively covered during an oral presentation at Arthur D. Little, Inc., on July 10 and 11, 1969. L-DGO representatives attending this meeting were Drs. Marcus G. Langseth, Jr., and John Chutte, and Mr. Steven Khein.

In this report we intend to summarize our progress and document a condensed version of our oral presentation. Consequently, we have organized this report in two sections. One section, contained in the body of the report presents a brief discussion of the tasks completed during the reporting period. Another section, included as an appendix, describes our progress on the development of two-dimensional, finite-difference models of the lunar medium.

II. PROGRAM PROGRESS

A. Phase I - Preliminary Analysis

In late May we issued Technical Memorandum No. 1, "Preliminary Thermal Analysis of Heat Flow Probe and Lunar Medium." This memorandum described the technical approach for preparing a finite-difference subdivision of the lunar medium and the requirements for an accurate finite-difference subdivision of the lunar probe.

B. Phase II - Analysis of Thermal Conductivity Experiments

1. Modeling Studies on Lunar Medium

Using the technical approach evolved during our Phase I effort, work continued on the development of thermal models of the lunar medium. Parametric studies were made using the two-dimensional model of the lunar medium (layers of concentric annuli in the radial direction and equally spaced subdivisions in the vertical direction) having a solid, cylindrical heat source. The effects of the following variables on the accuracy of solutions were examined: a) number of radial subdivisions, b) number of

vertical subdivisions, and c) numerical parameters involved in the computer solution, i.e., integration parameter, α, tolerance, and time step.

In order to check the mesh size or number of subdivisions in the radial direction for accurate predictions of temperature at regions close to the heat source (important to the Mode 2 operation), we conducted further studies using a one-dimensional problem of a thin, cylindrical heat source in a medium composed of annular concentric rings. As before, the ratio of outer to inner radii was taken to vary as r. The results of our study were presented in detail during a meeting with Lamont at ADL on July 10 and 11, 1969; and three sets of graphical plots of computed results and comparisons with corresponding exact solutions were furnished to Lamont.

In summary, computer-modeling procedures have been developed for the lunar medium which are accurate and which can be used to comprehensively analyze the conductivity experiments in the two modes of operation. The attached appendix briefly summarizes the approach and findings of this work.

2. Modeling of the Lunar Heat Flow Probe

We are presently near completion in the development of detailed mathematical models of typical ring sensor and gradient sensor locations in the heat flow probe. Approximately 50 equations describe the details of the ring sensor, split inner tube, end sheath and outer sheath contained within the two split annular spacers above and below the ring sensor. This model description accounts for such important heat transfer modes as: radiation heat transfer between the ring sensor and drill casing; radiant heat transmitted along the annular space between the end sheath and the outer sheath; and conduction heat transfer along the end sheath, filler sleeve, outer sheath, and wire harnesses.

Approximately 40 equations are used to describe the heat flow in the region of the gradient sensor location. The majority of thermal conductances are well defined in terms of lengths and probe thermal properties. The most important parameters which determine the thermal behavior in the gradient sensor region are the emittances of the inner and outer surfaces of the sensor, and the thermal masses of the sensor and heater.

The next step in our work will be to check out these models and perform calculations in an environment simulating the Group I series of tests in the ΔT apparatus. Parametric calculations will be made for three temperatures of the aluminum test sleeve (T = 205.4, 224.4 and 244.5°K). Temperature histories of the sensor and steady-state temperature rise will be computed and compared with measurements from the Group I tests.

APPENDIX

Summary of Thermal Analysis of Lunar Medium

I. INTRODUCTION

In our early studies using the two-dimensional model of the lunar medium, the accuracy of calculations was examined by comparing computer predictions with an available exact solution. The exact solution was for the problem of a spherical surface heat source in an infinite medium, while the finite-difference model described a solid, cylindrical heat source centered in a lunar medium.

The preliminary results reported in our Technical Memorandum No. 1 indicated that the modeling approach was reasonable in terms of the projections for the required number of equations necessary and the computer time for a transient solution. However, further studies were required to improve the agreement of exact and numerical results. Also, the preliminary calculations reported in Technical Memorandum No. 1 indicated that the accuracy of the numerical solution could be improved when only the first two terms of the following equation (describing the heat flow at the boundaries of the finite-difference model) were retained, a result having no logical explanation:

$$Q'' = \frac{K}{R^*} T\ (R^*,\ t) - \frac{K}{R^*} T_o + f\ (Q_o,\ R^*,\ t) \qquad (1)$$

where R^* = distance from center of source,

Q_o = strength of heat source, and

T_o = initial temperature of the lunar medium.

Our further analytical studies yielded significant improvements in the agreement between exact and finite-difference models--when all terms of Equation (1) were retained in the description of the boundary conditions. However, agreement between the exact and computer models was poorer at regions close to the source than for regions far from the source (a distance corresponding to the distance between the gradient sensor (heat source) and

Arthur D Little Inc

ring sensor locations). Further numerical studies were made using a one-dimensional physical problem to determine whether the poor agreement near the source was due to differences between the source geometries in the exact and finite-difference models (sphere and right circular cylinders, respectively) or inadequacies in the finite-difference model. Our work on the one-dimensional model will be described below, followed by a discussion of further work on the two-dimensional model.

A. One-Dimensional (Line Source) Problem

Finite-difference models were set up for the problem of a thin, cylindrical heat source surrounded by a medium composed of concentric annular rings. Numerical calculations were compared with exact solutions for the problem of a line heat source in an infinite medium. The motivation for this study was to examine the adequacy of the radial subdivision used in our 2-dimensional model for predicting temperatures in the lunar medium near the source of heat. For the one-dimensional problem, the heat source geometries for the finite-difference model can be made to closely resemble the source of heat in the exact model. This was not true in our work on the two-dimensional problem because exact solutions for the problem of a finite cylindrical heat source in an infinite medium are not available.

Figure 1 schematically illustrates the radial subdivision in the finite-difference model which simulates the line source problem. Pertinent information relating to the exact solution and specification of parameters are presented in Figure 2. As shown in Figure 2, due to the differences in heat source power, thermal conductivity levels and important locations in the lunar medium, two finite-difference models were selected--one appropriate to each mode of operation.

In the Mode 2 operation, accurate temperature predictions at locations near the source (i.e., near the heater at a gradient sensor location) are important. In the Mode 3 operation, accurate temperature predictions at remote locations from the source (i.e., near a ring sensor location) are important. Consequently, in the following discussion comparisons between exact and numerical solutions will be important at a

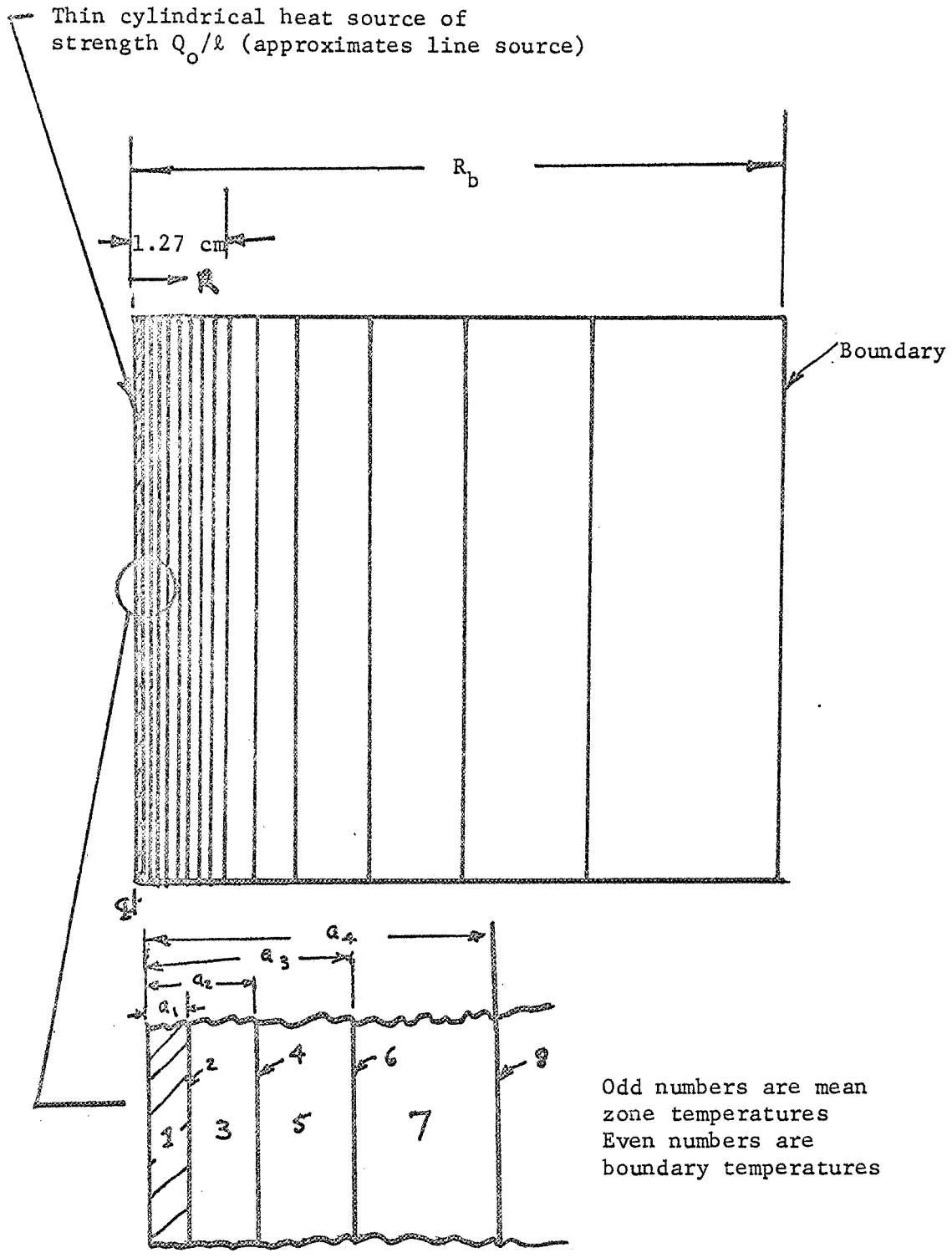

Note: Further details given on Figure 2

FIGURE 1 SCHEMATIC DIAGRAM OF FINITE-DIFFERENCE MODEL FOR LINE SOURCE PROBLEM

Arthur D Little Inc.

Nomenclature:

a_1 = radius of cylindrical heat source (typically 0.02 cm)

R_b = radius at boundary

K = number of radial subdivisions in the region $a_1 \leq R \leq 1.27$ cm

N = number of radial subdivisions in the region 1.27 cm $\leq R \leq R_b$ (same as considered in 2-dimensional finite-difference model of lunar medium)

$a_j = c_2 a_{j-1}$, where c_2 is a parameter which depends upon N

$$E_1(t) = \int_1^\infty \frac{e^{-tx}}{x}\, dx$$

k = thermal conductivity

α = thermal diffusivity

Q_o/ℓ = strength of line source

T_o = initial temperature of lunar medium

Exact Solution for Line Source of Strength Q_o/ℓ in an Infinite Medium:

$$T(r,t) = T_o + \frac{Q_o/\ell}{4\pi k} E_1 (r^2/4\alpha t)$$

Heat Flow Boundary Condition on Outer Surface of Last Annular Ring:

$$q_{boundary} = Q_o e^{-R_b^2/4\alpha t}$$

Model for Mode 2 Experiment:

R_b = 6 cm; a_1 = 0.02 cm; Q/ℓ = 0.002 watt; and

K = 1×10^{-4} watt/cm°K

Model for Mode 3 Experiment:

R_b = 15 cm; a_1 = 0.020 cm; Q_o/ℓ = 0.3 watt; and

K = 1×10^{-3} watt/cm°K

FIGURE 2 DETAILS ON FINITE-DIFFERENCE MODEL FOR LINE SOURCE PROBLEM

radius of approximately 1.27 cm for the Mode 2 operation and at a radius of approximately 10 cm for the Mode 3 operation.

1. Results

Figure 3 illustrates a comparison of temperature rise versus time for the Mode 2 finite-difference model and the exact model of the line source problem. The solid line is the exact solution at a radial location of 1.274 cm, and the circled symbols denote the values predicted with our computer program. Increasing the number of radial subdivisions in the region $1.27 \leq R \leq R_b$, N, and making the associated changes in K, the number of subdivisions in the region $a_1 \leq R \leq 1.27$ produced no change in the agreement between the two models. The close agreement between exact and finite-difference models for N = 5 suggests that the discrepancies noted near the source in our 2-D model for Mode 2 operation can be attributed to differences in the geometry of the heat source (spherical surface source versus cylindrical pill-shaped source in finite-difference model).

Although agreement for the 2-dimensional, finite-difference model of the lunar medium was good at locations approximately 10 cm from the center of the source, we also examined the radial subdivision in the lunar medium for Mode 3 operation using the line source model. Figure 4, which was shown during our July 10 meeting, presents the computed temperature rise at R = 10.0 cm for the Mode 3 finite-difference model of the line source and illustrates good agreement with the exact solution. Also shown on Figure 4 is the temperature rise at R = 1.28. Here, the agreement is also good; but the plot indicates that the computer results begin to deviate slightly from the exact solution at times of approximately 500 minutes. In order to investigate this tendency further and determine if a deviation would also occur at R = 10.0 cm at longer times, the computer calculation was repeated and carried out to 800 minutes. Figure 5 shows a comparison of computer and exact results for the same problem up to a time of 800 minutes. The computed temperature rise at R = 10.0 continues to agree very well with the exact solution; the deviation between the computed and exact results at R = 1.28 beyond 500 minutes does not increase but remains steady at a value of approximately 2.5%.

Arthur D Little Inc.

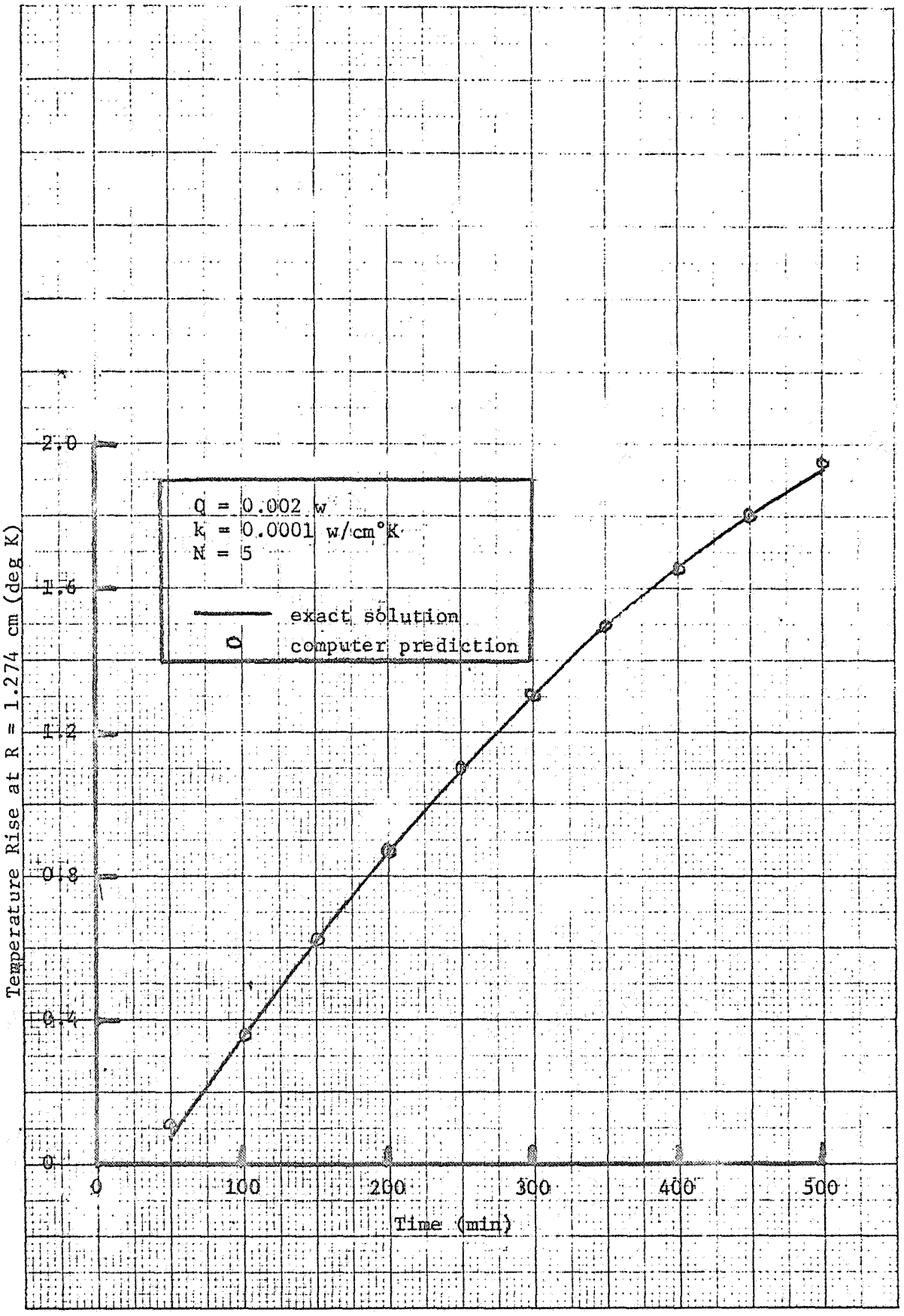

FIGURE 3 TEMPERATURE RISE VERSUS TIME FOR MODE 2 MODEL OF LINE SOURCE PROBLEM

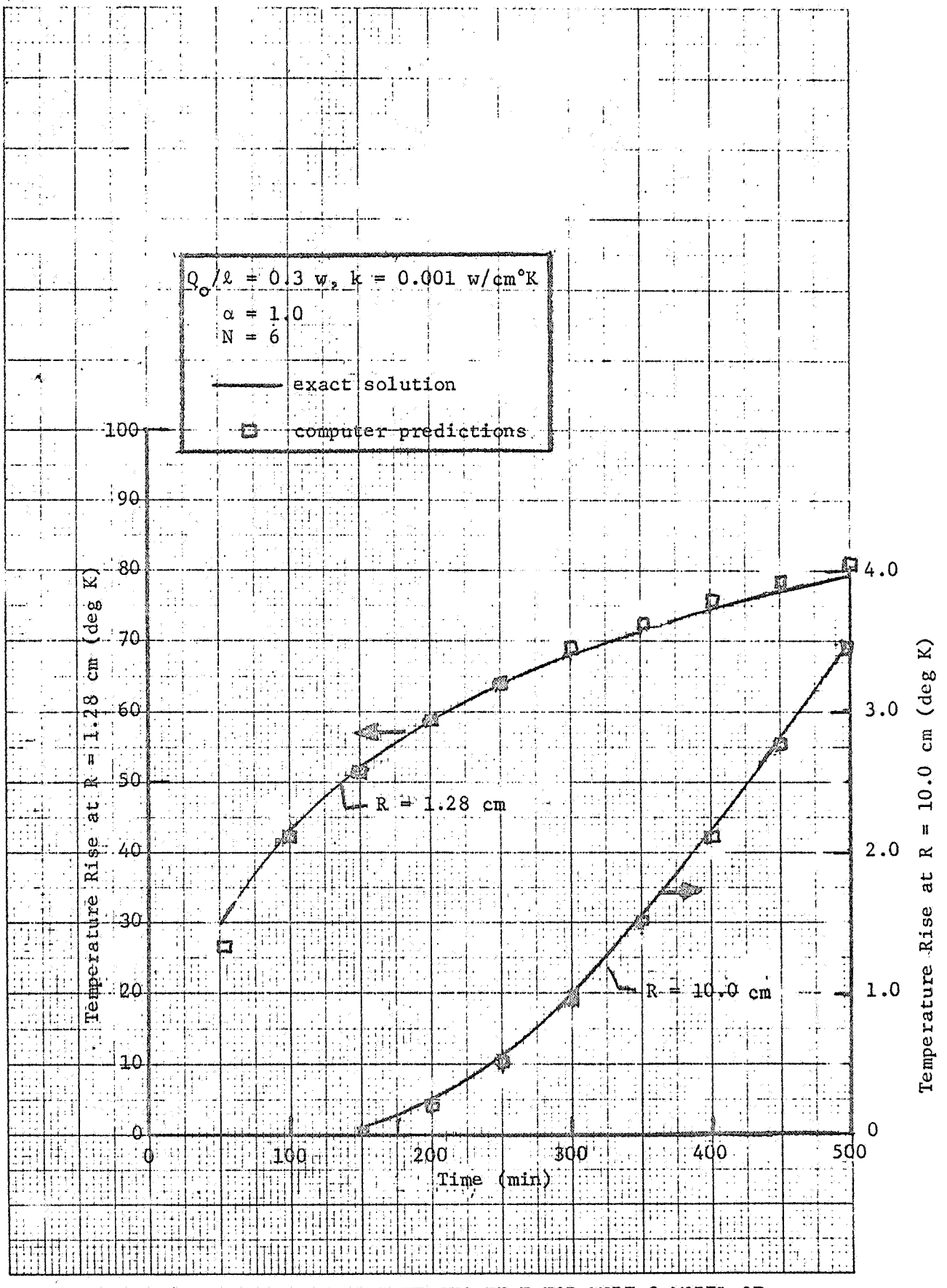

FIGURE 4 TEMPERATURE RISE VERSUS TIME FOR MODE 3 MODEL OF LINE SOURCE PROBLEM

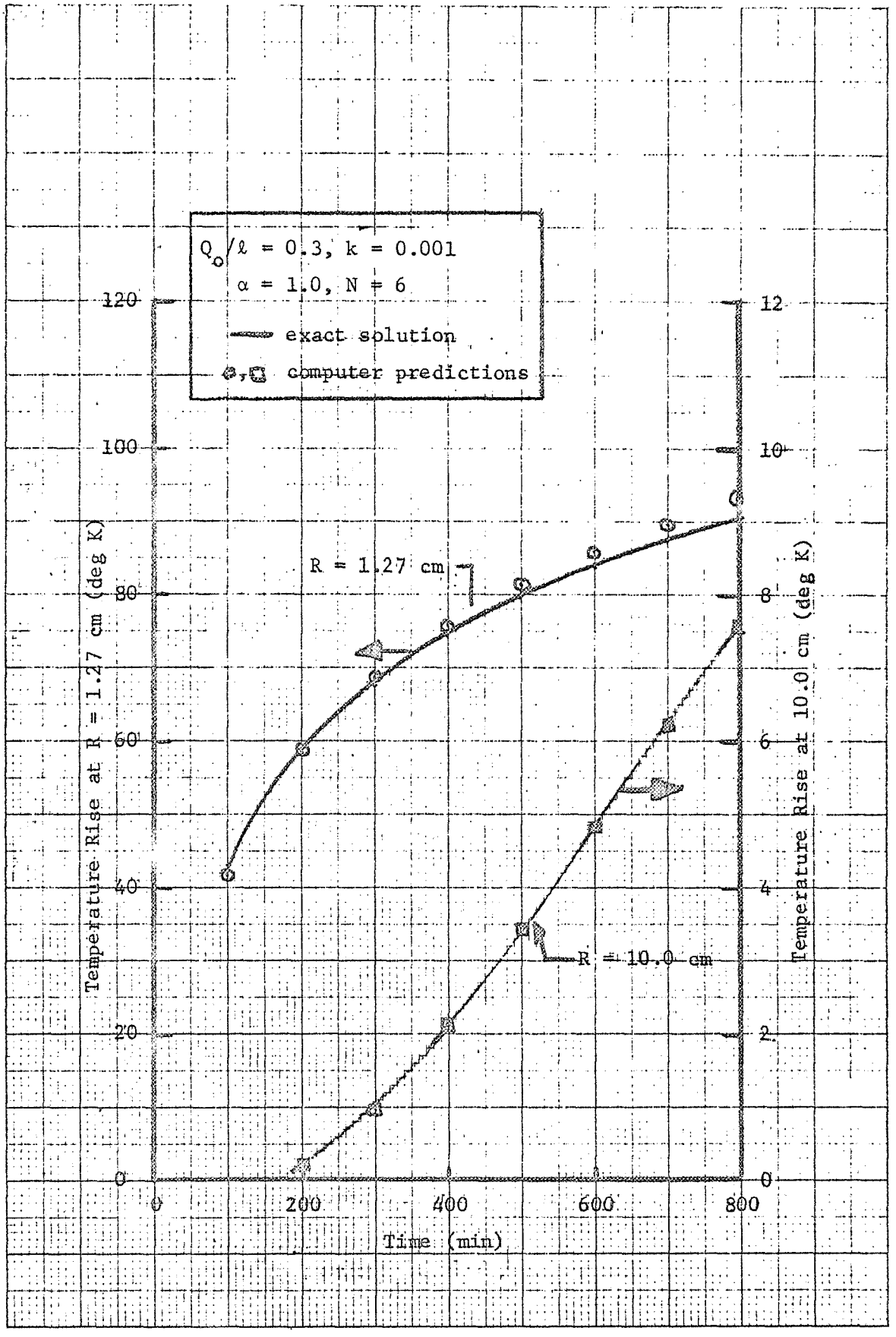

FIGURE 5 TEMPERATURE RISE VERSUS TIME FOR MODE 3 MODEL OF LINE SOURCE PROBLEM

Although we do not believe that the deviation noted at the location near the source (R = 1.27 cm) has an impact on our work or the validity of the computer models of the lunar medium, we have investigated various possible explanations for this effect. For example, we have maintained the radius of the source a_1 and doubled the number of subdivisions in the region $a_1 \leq R \leq 1.27$ cm (increased K from 10 to 20) and obtained results identical to those shown in Figure 5. We have also performed calculations considering the source as a cylindrical surface source and observed no difference in computed results. We expect that the small deviation (2.5%) noted at R = 1.27 cm can be related to the fact that the analytical model has a line source and the finite-difference model has a finite cylindrical source. We will examine this possibility in the near future.

2. Conclusions

Our studies of the line source have enabled us to check the requirements for radial subdivisions in the lunar medium for accurate predictions close to the source for the Mode 2 operation and remote from the source for the Mode 3 operation. Pertinent conclusions from this study are summarized below:

1) In the Mode 2 model, accurate solutions are obtained with 5 radial subdivisions in the region 1.27 cm $\leq R \leq R_b$.

2) In the Mode 3 model, accurate solutions are obtained with 6 radial subdivisions in the region 1.27 cm $\leq R \leq R_b$.

3) Best numerical solutions are obtained when the integration parameter (α) in our thermal analysis computer program is specified as 1.0.

B. Two-Dimensional Model of Lunar Medium

Our approach for describing a 2-dimensional, finite-difference model of the lunar medium for use in our thermal analysis of the lunar medium

Arthur D Little Inc

was described in Reference 1. The approach will be briefly reviewed here, followed by a discussion of our more recent results and conclusions.

The lunar medium was modeled as a series of concentric annuli of varying thickness in the radial direction and equally spaced subdivisions in the vertical direction as illustrated in Figure 6. The homogeneous medium contains an inner core ($0 \leq R \leq 1.27$ cm), so that computed results can be compared with exact solutions. In an analysis of the conductivity experiments, this inner core will be removed and replaced by the heat flow probe, drill casing, and appropriate thermal couplings between the drill casing and the lunar medium. Parameters involved in the model and pertinent information relating to the boundary conditions are shown in Figure 7. At the boundaries, the heat flow from the surfaces are matched with the form of solution shown in Figure 7 for a spherical-surface source.

1. Results

In reviewing comparisons here between the computed results and the exact solution, it is important to consider the following:

1) In the finite-difference model, the heat source has the shape of a solid circular cylinder, while the exact solution applies to a spherical surface source. This difference should be most important at regions in the lunar medium close to the heat source. It is important to note, however, that checks on the subdivision close to the source were made in the work described above for a one-dimensional problem, where the geometrical difference between exact and finite-difference source is small.

2) Comparisons between exact and finite-difference models are made as a function of R, the distance from the center of the source to the location of interest in the lunar medium. We calculate R in the finite-difference model as the

Arthur D Little, Inc.

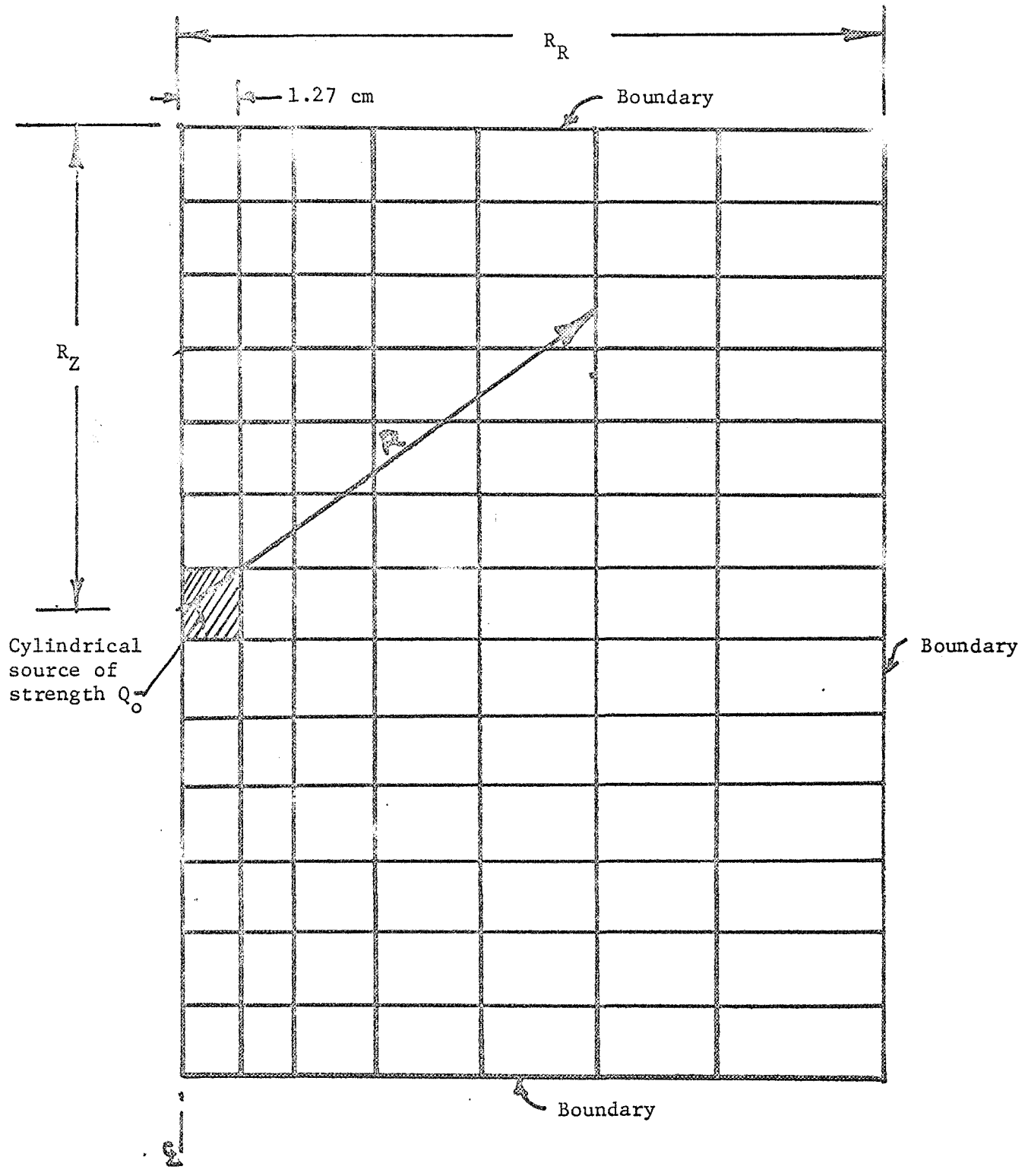

Note: Further details given on Figure 7

FIGURE 6 SCHEMATIC DIAGRAM OF FINITE-DIFFERENCE MODEL FOR 2-DIMENSIONAL MODEL OF LUNAR MEDIUM

Nomenclature:

R = radial distance to boundary of annular cylindrical zones

R_R = distance from origin to boundary in the radial direction

R_Z = distance from origin to boundary in the vertical direction

N = number of radial subdivisions in the region $1.27 \text{ cm} \leq R \leq R_R$

M = number of equally-spaced vertical subdivisions

Q_o = strength of heat source

T_o = initial temperature of lunar medium

k = thermal conductivity of lunar medium

α = thermal diffusivity

t = time

Heat Flow Boundary Condition on Outer Boundary of Lunar Medium: (from analysis of spherical surface source)

$$Q_{boundary} = \frac{k}{R_b} T(R_b, t) - \frac{k}{R_b} T_o + f(Q_o, R_b, \alpha t)$$

Model for Mode 2 Experiment:

$R_R = 6$ cm; $R_Z = 6$ cm; $Q_o = 0.002$ watt; $k = 1 \times 10^{-4}$ watt/cm°K

Model for Mode 3 Experiment:

$R_R = 15$ cm; $R_Z = 12$ cm; $Q_o = 0.5$ watt; $k = 2 \times 10^{-3}$ watt/cm°K

FIGURE 7 DETAILS ON 2-DIMENSIONAL FINITE-DIFFERENCE MODEL OF LUNAR MEDIUM

distance from the center of the source to the center of a radial boundary of an annular cylindrical zone. The computed temperature of this surface is the temperature averaged over the surface and is not necessarily equal to the center temperature of the surface.

Since the heat flows at the boundaries are determined as a function of the absolute distance from a spherical surface source, it is of interest to examine the computed results from the standpoint of radial symmetry. Figure 8 shows the radial temperature distribution in the lunar medium for a Mode 3 Model (i.e., Q_o = 0.5 watts, K = 2 x 10^{-3} watt/cm°K, R_r = 15 cm) at a time of 500 minutes. The circled X symbol corresponds to the values computed from the exact solution; the dotted symbols correspond to the values computed using the finite-difference model; and the plotted curve is a fit to all the plotted points. Values obtained from computer solution apply to position vectors originating at the center of the source and extending in various angular directions to locations in the lunar medium. The close agreement between exact and computed values and the plotted curve indicates that the Mode 3 model is accurate (at the time of 500 minutes) and that the 2-dimensional, finite-difference model of the lunar medium preserves radial symmetry.

Figure 9 shows a comparison of exact and computed temperature rise at R = 8.811 cm, as a function of time up to 1,000 minutes. The computed values shown on this curve were obtained for several values of N, the number of radial subdivisions in the region 1.27 cm $\leq$ R $\leq$ 15 cm.

The agreement is good up to times of 500 minutes. As time increases, the computed results begin to have a small deviation from the exact solution. At a time of a thousand minutes (approximately 8 hours), the deviation is 5%. It is believed that the deviation can be accounted for by a difference in the source geometries discussed earlier. Our confidence in the mathematical model for the Mode 3 operation is reinforced by our results from the one-dimensional problem, where we used the same radial subdivision in the region 1.27 $\leq$ R $\leq$ $R_{boundary}$ and obtained

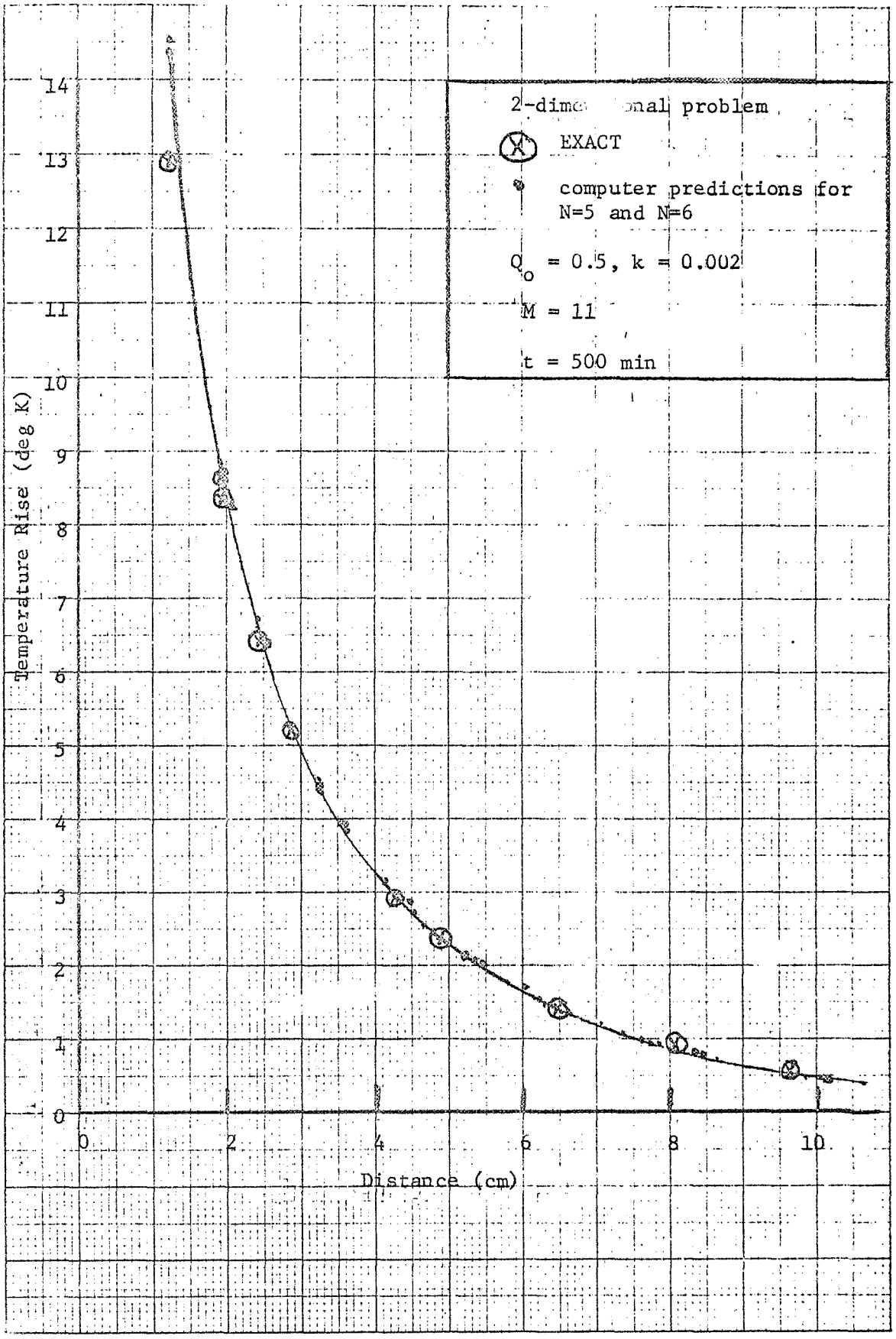

FIGURE 8 TEMPERATURE DISTRIBUTION IN MODE 3 MODEL OF LUNAR MEDIUM

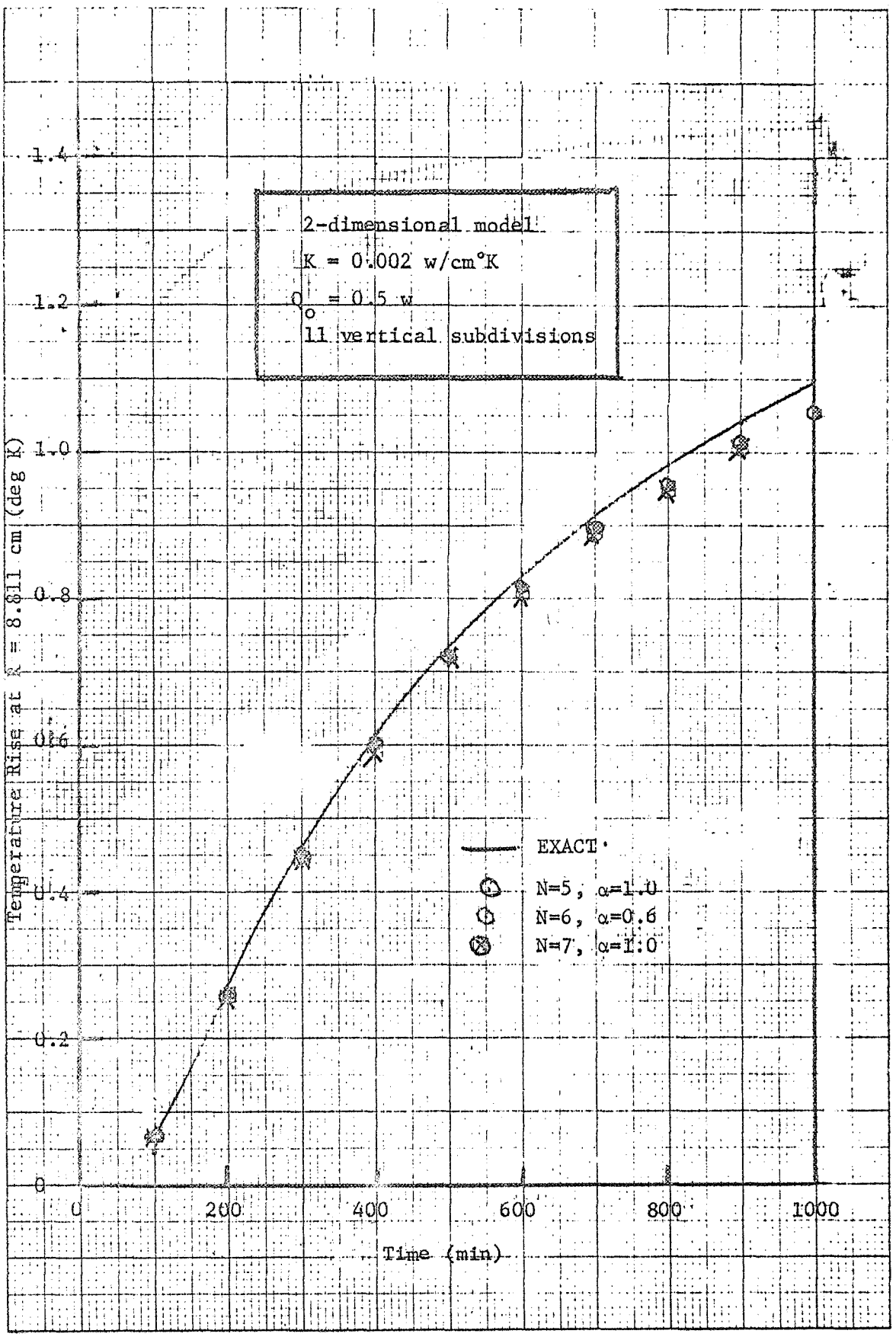

FIGURE 9 TEMPERATURE RISE VERSUS TIME FOR MODE 3 MODEL OF LUNAR MEDIUM

computed results essentially identical to the exact solution. The uncertainties which arise because of the deviation we described are believed to be small compared to other uncertainties which can arise when analyzing the entire experiment. Nevertheless, we remain interested in the problem of the lunar medium and will evaluate approaches which have potential for improving our understanding of the problem.

2. Conclusions

Conclusions obtained from our numerical experiments performed with 2-dimensional model of the lunar medium are summarized below:

1) Radial symmetry observed in 2-dimensional model justifies the approach for subdividing the lunar medium and specifying the heat flow boundary conditions.

2) Accurate results can be obtained with reasonable numbers of radial subdivisions, vertical subdivisions, and heat-balance equations as shown below:

	Mode 2 Operation	Mode 3 Operation
Number of radial subdivisions	5	6
Number of vertical subdivisions	11	13
Number of equations for model shown in Figure 6	181	253

3) Best numerical results are obtained when the integration parameter (α) in our thermal analysis computer program is specified as 1.0.

REFERENCES

1. D. Nathanson and R. Merriam, "Preliminary Thermal Analysis of Heat Flow Probe and Lunar Medium," Technical Memorandum No. 1, May 29, 1969.

2. P. F. Strong, and A. G. Emslie, "The Method of Zones for the Calculation of Temperature Distribution," Arthur D. Little, Inc., July 1963.